

Polarization microscopy for visualizing FRET between identical fluorophores

Monitoring receptor clustering in live cells

By Rick Krabbendam

Master of Science in Applied Physics Report

October 2012

Nanobiophysics Group
University of Twente
The Netherlands

Graduation committee:

Prof. Dr. V. Subramaniam

Dr. Ir. J.S. Kanger

Dr. C. Otto

Ir. P.J. Bosch

1 Contents

1	Abstract	7
2	Introduction.....	9
2.1	Research context and relevance	9
2.2	Task definition	9
2.3	Report outline.....	10
3	Theory.....	11
3.1	Physical properties of fluorescent molecules	11
3.1.1	Fluorescence.....	11
3.1.2	Radiative and non-radiative decay.....	11
3.1.3	Förster resonance energy transfer.....	12
3.1.4	Homo-FRET	15
3.1.5	Anisotropy	15
3.1.6	Effect of resonance energy transfer on anisotropy.....	18
3.1.7	Effect of Homo-FRET on the fluorescence lifetime of the donor	19
3.1.8	Fluorescence lifetime imaging microscopy	21
3.2	Epidermal growth factor receptor.....	23
3.2.1	ErbB family of receptors.....	23
3.2.2	Structure of the epidermal growth factor receptor	23
3.3	Oligomerization of the EGF-receptor	24
4	Modeling the effect of homo-FRET on the anisotropy.....	27
4.1	Mathematical and physical background for anisotropy simulations	27
4.2	Effect of homo-FRET on anisotropy for different fluorophore densities	31
4.3	Effect of homo-FRET between two fluorophores on anisotropy	32
4.4	Outlook.....	35
4.5	Limitations	35
5	Experimental setup	37
5.1	Experimental setup	37
5.2	Implementation of polarization microscope.....	38
5.3	Calibration procedures and setup verification.....	39
5.3.1	Image alignment of the two cameras.....	39
5.3.2	Background correction	41
5.3.3	Calibration with a reference dye	41

5.3.4	Gain calibration	43
5.3.5	Polarizer alignment.....	44
5.3.6	Effect of numerical aperture on measured anisotropy.....	46
5.3.7	Anisotropy of EGFP in glycerol	46
6	HeLa cells expressing mCitrine and mCitrine-mCitrine Proteins.....	49
6.1	Photobleaching of fluorescent protein dimers	49
6.2	Experimental procedure.....	51
6.2.1	Sample preparation.....	51
6.2.2	Fluorescence lifetime imaging.....	51
6.2.3	Fluorescence anisotropy imaging.....	51
6.3	Results and discussion.....	52
6.3.1	Effect of homo-FRET on the measured fluorescence lifetime	52
6.3.2	Effect of homo-FRET on the measured fluorescence anisotropy.....	54
7	MCF-7 cells expressing EGFR-mCherry fusion proteins	61
7.1	The fluorescent protein mCherry	61
7.2	Selection of cell type	61
7.3	Experimental procedure.....	62
7.3.1	Sample preparation.....	62
7.3.2	Fluorescence anisotropy imaging.....	62
7.4	Results and discussion.....	62
8	Visualizing EGFR clustering using SNAP-EGFR Fusion Proteins	65
8.1	The SNAP-tag.....	65
8.2	Artificially induced dimerization.....	66
8.3	Selection of fluorescent dyes	66
8.4	Experimental procedure.....	67
8.4.1	Sample preparation.....	67
8.4.2	SNAP-tag labeling with fluorescent dyes.....	67
8.4.3	Fluorescence anisotropy imaging.....	68
8.4.4	Outline of experimental settings.....	68
8.5	Results and discussion.....	70
8.5.1	NIH-3T3 cells expressing SNAP-EGFR labeled with Alexa-647	70
8.5.2	NIH-3T3 cells expressing SNAP-TMD-Fv labeled with alexa-647.....	71
9	EGF-receptor clustering after addition of antibodies against EGFR.....	75
9.1	Experimental procedure.....	75

9.1.1	Sample preparation	75
9.1.2	Fluorescence anisotropy imaging	75
9.2	Results and discussion	75
9.2.1	MCF-7 cells expressing EGFR-mCitrine and addition of Cetuximab	76
9.2.2	MCF-7 cells expressing EGFR-mCitrine stimulated with EGF	79
10	Conclusions and Recommendations	83
10.1	Fluorescence polarization microscopy setup	83
10.2	Anisotropy simulations.....	83
10.3	Homo-FRET anisotropy and lifetime	84
10.4	Cells expressing protein-SNAP-tag fusions.....	84
10.5	Cells expressing EGFR-fluorescent protein fusions	84
11	References	87
12	Appendix.....	91

1 Abstract

Clustering behavior of plasma membrane receptors such as the epidermal growth factor receptor (EGFR) is intensively investigated. Learning about this clustering behavior provides information about the biological role and function of the EGF-receptor in general and possibly about its role in the development of cancer. We investigated the clustering behavior of EGFR using fluorescent probes. Förster resonance energy transfer between identical fluorescent probes (homo-FRET) in an EGFR cluster can be visualized by its effect on the fluorescence anisotropy. In order to do so a fluorescence polarization microscope was implemented in a wide-field fluorescence microscope. The possibility to observe homo-FRET in live cells by a decrease in anisotropy using this microscope was verified with a model protein consisting of two closely spaced fluorescent proteins connected by an amino acid linker. In this model protein, homo-FRET can occur. It was also verified that homo-FRET cannot be observed by a decrease in the fluorescence lifetime of the donor.

The effect of homo-FRET on the fluorescence anisotropy is simulated based on equations describing photophysical properties of fluorescent molecules. Results from these simulations show that the maximum decrease in anisotropy due to homo-FRET between a single donor and a single acceptor is 0.20 for randomly orientated non-rotating fluorophores. When there is a small angle between the absorption and emission transition moment in a single fluorophore, the anisotropy decrease due to homo-FRET is smaller.

Then the polarization microscope was used to obtain anisotropy images of EGF receptor and model systems. The clustering behavior of the receptor was altered by addition of its ligand EGF or the addition of antibodies against EGFR which may induce dimerization. This experiment uses MCF-7 and NIH-3T3 cells expressing EGFR protein fusions consisting of EGFR and a fluorescent protein and protein fusions consisting of EGFR and a fluorescently labeled SNAP-tag. No change in anisotropy was found after the addition of EGF or antibodies compared to before. The anisotropy did also not depend on the intensity. Also in cells expressing SNAP-TMD-Fv, a model system that can be dimerized upon addition of a dimerizer molecule (AP20187), no significant change in anisotropy was found within five minutes after addition of this dimerizer molecule. In literature can be found that TMD-Fv protein domains and EGFR protein domains dimerize within five minutes after addition of AP20187 and EGF respectively, therefore we conclude that the used fluorescent probes are too far away from each other for homo-FRET to occur.

2 Introduction

The use of fluorescent probes in biological applications has enabled direct microscopy of biomolecules and has led to a wealth of knowledge on biological processes. In this report these fluorescent probes are used to study the clustering behavior of the plasma membrane protein called the epidermal growth factor receptor (EGFR). In this introduction the reason why membrane proteins are studied and which techniques can be used to do so will be discussed first. Then the objectives of this project will be given. The last part covers the outline of this report.

2.1 Research context and relevance

Clustering behavior of proteins on the plasma membrane of cells is an intensely studied subject. The clustering behavior of membrane proteins provides information on the biological role and functioning of the proteins. This clustering can be completely different in the presence or absence of certain external factors such as ligands or therapeutic drugs, leading to changes in the biological functioning of the membrane proteins, which is why this subject is important to study. Since some diseases are related to structural changes of certain membrane proteins, it is important to obtain more understanding of the behavior of these proteins on a molecular scale. Several techniques exist to study the clustering behavior of membrane proteins. A large part of these techniques uses fluorescent labels. Techniques using fluorescence are for example fluorescence lifetime imaging, fluorescence anisotropy imaging, single molecule tracking, fluorescence recovery after photobleaching (FRAP). Fluorescence lifetime and anisotropy imaging can both be used to detect Förster resonance energy transfer (FRET) between different fluorophores (hetero-FRET) and between identical fluorophores (homo-FRET), respectively. FRET occurs when fluorescent probes are close together with a distance between them not more than 5-7 nm. Examples of fluorescent probes that can be used in techniques using fluorescence are fluorescent proteins and organic dyes.

2.2 Task definition

The goal of this research is to study whether the clustering behavior of the epidermal growth factor receptor (EGFR) in live cells can be visualized by detecting homo-FRET. Since in these clusters small distances between the individual receptors are expected, using a technique that can visualize FRET between fluorophores attached to these receptors could be a good way to study this clustering behavior. Detection of hetero-FRET can for example be performed with fluorescence lifetime measurements. However, designing an experiment that visualizes clustering of the EGF-receptor with hetero-FRET has several disadvantages. A disadvantage of using FRET between two different fluorophores over FRET between identical fluorescent proteins is that the results are influenced by the relative amount of donor fluorescent molecules with respect to acceptor fluorescent molecules. Another disadvantage is that only approximately half of the present fluorophores (all donors) can absorb excitation light in hetero-FRET experiments. In homo-FRET experiments all fluorophores can absorb excitation light. Finally, in hetero-FRET experiments, FRET can only be detected when a donor that absorbed excitation light transfers energy to an acceptor. Since approximately half of the present fluorescent molecules is an acceptor, the probability that an excited donor transfers energy to an acceptor in the same cluster of EGF-receptors is relatively low compared to homo-FRET. Because of these drawbacks of hetero-FRET, homo-FRET could be a better tool to investigate EGFR clustering behavior.

Detection of homo-FRET cannot be done with fluorescence lifetime experiments or by detecting a change in emission color. Homo-FRET can be detected by measuring the anisotropy. To measure

anisotropy in live cells at high spatial and time resolution, a fluorescence polarization microscope is implemented in an existing wide-field fluorescence microscope. Using this microscope, proof of principle experiments will be performed to verify that homo-FRET can be observed with this setup.

2.3 Report outline

Chapter 3 describes the theoretical background on fluorescence, anisotropy and on the EGF-receptor. Chapter 4 discusses simulations that are performed to give more insight into the relation between homo-FRET and anisotropy. The used fluorescence wide-field microscope will be discussed in chapter 5. This chapter also covers the implemented fluorescence polarization microscope and the calibration procedures that are necessary to perform fluorescence anisotropy experiments. In chapter 6 an experiment is performed that shows that homo-FRET can be measured with the implemented polarization microscope. Also fluorescence lifetime experiments are performed here to show that homo-FRET cannot be detected by observing a change in the fluorescence lifetime of the donor. Chapter 7, 8 and 9 focuses on the effect of addition of EGF and antibodies against EGFR on the clustering behavior of the EGF-receptor in live cells. In these chapters different labeling techniques are used to fluorescently label the EGF-receptors. Finally the conclusions and recommendations are presented in the last chapter.

3 Theory

This chapter reviews a part of the physics of fluorescence, Förster resonance energy transfer (FRET), and anisotropy measurements. See the book “Principles of Fluorescence Spectroscopy”¹, written by J. R. Lakowicz, for additional details. This chapter also discusses the structure and function of the EGF-receptor. This is followed by a summary of previously done research on the EGF-receptor to show that the properties of fluorescent molecules can be used to learn about the clustering behavior of the EGF-receptor.

3.1 Physical properties of fluorescent molecules

This part of the chapter covers the physical properties of fluorescent molecules. Firstly the fluorescence processes in the absence of FRET will be discussed. Secondly, the fluorescence energy transfer rate and its effect on the fluorescence processes will be discussed. Then the theoretical background on fluorescence anisotropy measurements and the effect of homo-FRET on anisotropy values will be discussed. Finally the effect of homo-FRET on the fluorescence lifetime is theoretically investigated. Also the theory on fluorescence lifetime measurements in the frequency domain will shortly be explained here.

3.1.1 Fluorescence

Fluorescence can occur when a fluorescent molecule absorbs light. This absorption will transfer an electron in the fluorescent molecule from the electronic ground state (S_0) to the first (S_1) or second (S_2) electronic state. This is shown in the Jablonski diagram in figure 3.1. Each electronic state has several vibrational states. After light absorption, internal conversion occurs, which means that the electron relaxes to the lowest vibrational state of the first electronic state. This process takes place under the release of heat. After this process, fluorescence may occur, which is the emission of light when the electron returns to the ground state from the first electronic state (green arrow in figure 3.1). Internal conversion usually occurs within 10^{-12} s, whereas fluorescence occurs after times in the order of 10^{-8} s, which is the cause for the fact that fluorescence decay happens from the lowest vibrational state of the first electronic state.

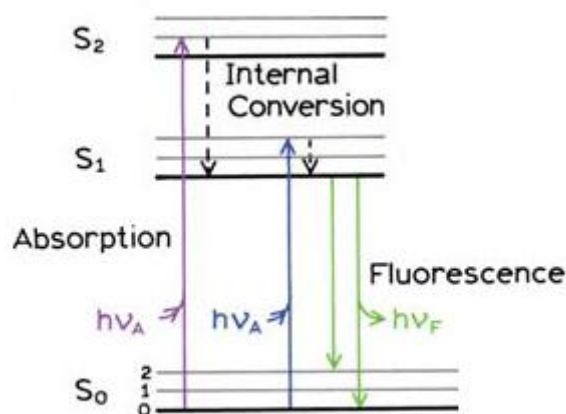


figure 3.1: Jablonski diagram that shows the principles of excitation and fluorescence decay

3.1.2 Radiative and non-radiative decay

The efficiency of fluorescence is described by the quantum yield (Q) and the time in which fluorescence occurs is described by the fluorescence lifetime (τ) of this specific fluorophore. The quantum yield is defined as the ratio between the radiative decay rate and sum of all decay rates (radiative and non-radiative):

$$Q = \frac{K_F}{K_F + K_{nr}} \quad \text{eq. 3.1}$$

In this equation K_F is the radiative decay rate and K_{nr} is the non-radiative decay rate. The quantum yield can also be written as the ratio between the emitted photons and absorbed photons by fluorescent molecules. From this definition it is clear that the quantum yield cannot exceed 1. The lifetime is defined as the average time a fluorophore remains in the excited state and is given by:

$$\tau = \frac{1}{K_F + K_{nr}} \quad \text{eq. 3.2}$$

When the lifetime and quantum yield of a fluorophore are known, both the radiative and non-radiative decay rate can be calculated with the equations above.

If at a time $t=0$ a certain amount of fluorophores can be found in the excited state (N), and no absorption takes place by fluorophores in the ground state, the amount of fluorophores that can be found in the excited state at a certain time t is given by:

$$N(t) = N(0) e^{-\frac{t}{\tau}} \quad \text{eq. 3.3}$$

The probability that a single fluorophore excited at $t=0$ emits a fluorescence photon at time t is given by:

$$P(t) = \frac{1}{\tau} e^{-\frac{t}{\tau}} \quad \text{eq. 3.4}$$

3.1.3 Förster resonance energy transfer

When there is an overlap between the emission spectrum of a certain excited fluorophore (donor) and the absorption spectrum of a non-excited fluorophore (acceptor), energy transfer from the donor to the acceptor can occur. This energy transfer is called Förster resonance energy transfer (FRET). After excitation of the donor fluorescent molecule, there is a probability that this molecule will transfer its energy to an acceptor molecule. If this acceptor molecule emits light with a different wavelength than the donor molecule, the energy transfer could be measured by detecting the emission spectrum of the donor or acceptor. Energy transfer then decreases the emission of the donor and increases the emission of the acceptor. FRET occurs only when the distance between donor and acceptor is sufficiently small. In this paragraph it will be discussed how the FRET efficiency is related to several physical parameters.

Applications for FRET are mainly detecting whether two molecules are close to each other or not. Normal optical microscopy can only discriminate between two molecules when they are separated

more than the diffraction limit. When the occurrence of FRET is detected, this proves that two fluorescent molecules capable of transferring energy from one fluorescent molecule to the other are separated from each other by a distance not more than 5 to 10 nm.

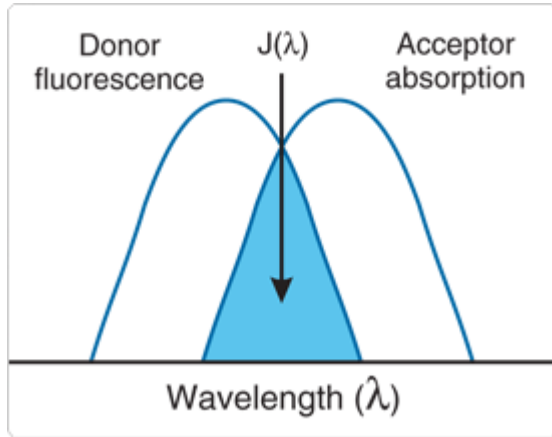


figure 3.2: Schematic representation of overlap integral between emission spectrum of the donor and absorption spectrum of the acceptor. Image taken from [2]

A measure for the amount of FRET between two fluorescent molecules is the resonance energy transfer rate (k_{ET}). This rate depends for example on the distance r between both molecules. The efficiency (E) of energy transfer is defined as follows:

$$E = \frac{K_{ET}}{K_F + K_{nr} + K_{ET}} \quad \text{eq. 3.5}$$

At a certain distance the efficiency of energy transfer from donor to acceptor is 0.5, which means that at this distance the energy transfer rate equals the sum of all other decay rates. This distance is called the Förster distance and is often in the range from 2 to 7 nm. The energy transfer rate of FRET from donor to acceptor is described as:

$$K_{ET} = \tau_D^{-1} \left(\frac{R_0}{r} \right)^6 \quad \text{eq. 3.6}$$

where τ_D is the fluorescence lifetime of the donor in the absence of the acceptor. R_0 is the Förster distance and r is the distance between donor and acceptor. In this equation R_0 is given by:

$$R_0 = 0.0211 \left(\frac{\kappa^2 \phi_D}{n^4} J(\lambda) \right)^{1/6} \quad \text{eq. 3.7}$$

with R_0 in nm. Here κ^2 is the orientation factor between the transition dipoles of the donor and acceptor, ϕ_D is the quantum yield of the donor, n is the refractive index of the medium (1.384 ± 0.0018 for HeLa cells)³ and $J(\lambda)$ is the overlap integral between donor emission and acceptor absorption spectra (see figure 3.2). $J(\lambda)$, (in $M^{-1}cm^{-1}nm^4$), is given by:

$$J(\lambda) = \int_0^{\infty} F_d(\lambda) \varepsilon_A(\lambda) \lambda^4 d\lambda \quad \text{eq. 3.8}$$

here $F_d(\lambda)$ is the normalized wavelength dependent fluorescence intensity of the donor, with the total area under the curve normalized to unity. $\varepsilon_A(\lambda)$ is the wavelength dependent extinction coefficient of the acceptor in $\text{M}^{-1}\text{cm}^{-1}$.

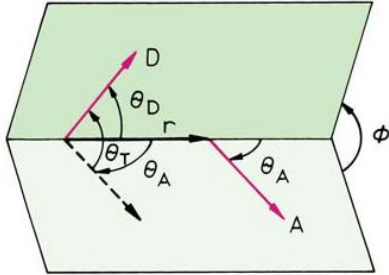


figure 3.3: Orientation of emission dipole of the donor with respect to the absorption dipole of the acceptor. Image taken from [1]

The orientation factor κ^2 (see figure 3.3) is given by:

$$\kappa^2 = (\cos(\theta_T) - 3 \cos(\theta_D) \cos(\theta_A))^2 \quad \text{eq. 3.9}$$

Here θ_D is the angle between the donor emission transition dipole and the direction vector r between the donor and acceptor molecule. The angle θ_A is the angle between this direction vector r and the absorption transition moment in the acceptor. θ_T is the angle between the donor emission transition dipole and acceptor absorption transition moment. κ^2 values range from 0 to 4, but when R_0 is given in the literature, often a κ^2 value of $2/3$ is assumed, which corresponds to the average orientation factor in an ensemble of molecules which can undergo completely isotropic motion. In figure 3.4 the dependence of the Förster radius as a function of the orientation factor is shown. This relation was calculated using the physical properties of Atto-532.

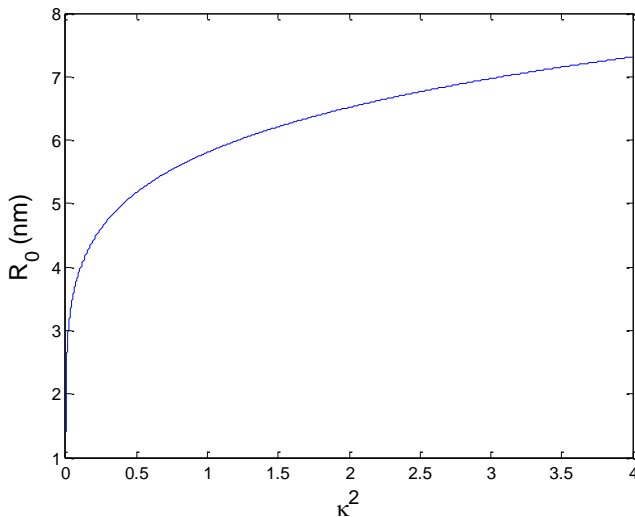


figure 3.4: Förster radius as a function of the orientation factor

When FRET occurs, the expression for the fluorescence lifetime of the donor (eq. 3.2) changes to:

$$\tau_D = \frac{1}{K_F + K_{nr} + k_{ET}} \quad \text{eq. 3.10}$$

Thus, in the presence of FRET, the fluorescence lifetime of the donor molecule decreases.

3.1.4 Homo-FRET

FRET between different fluorophores (hetero-FRET) can occur when there is an overlap between the emission spectrum of the donor and the absorption spectrum of the acceptor. However, when there is an overlap between the absorption and emission spectrum of a single fluorophore, this fluorophore, when excited, can also transfer energy to an identical fluorophore. FRET between identical fluorophores is called homo-FRET. Because the emission of the donor and acceptor are exactly the same in this case, homo-FRET cannot be detected by a change in emission color, but it can be by anisotropy measurements. This will be explained later in this chapter, but first the theory on anisotropy measurements will be discussed. Because hetero-FRET can also be detected by observing a change in the fluorescence lifetime of the donor, we also investigated whether homo-FRET can be detected with lifetime measurements.

3.1.5 Anisotropy

Fluorescence anisotropy is measured by exciting fluorophores with polarized light. This light only excites fluorophores that have a component of the absorption transition moment parallel to the polarization of the excitation light. These fluorophores then emit light that contains a fraction of parallel polarized light (I_{\parallel}) and a fraction of perpendicular polarized light (I_{\perp}). Parallel here means that the polarization direction of the emitted light is equal to that of the excitation light. When I_{\parallel} and I_{\perp} are measured, the anisotropy r can be determined with:

$$r = \frac{I_{\parallel} - I_{\perp}}{I_{\parallel} + 2I_{\perp}} \quad \text{eq. 3.11}$$

Using this equation the maximum anisotropy that can be measured in a solution with fluorescent molecules can be determined. This maximum anisotropy value holds for anisotropy measurements on fluorescent molecules that have parallel emission and absorption transition moments and do not rotate during the excited state lifetime. This value also only holds when all molecules are completely randomly orientated and when a sufficient amount of molecules is measured.

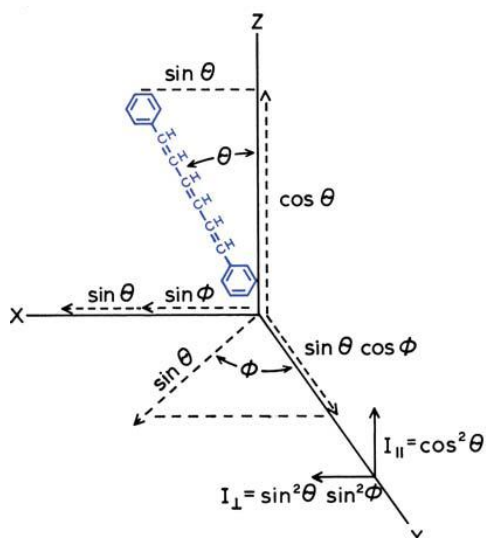


figure 3.5: Representation of the orientation of the absorption transition moment of a fluorescent molecule with respect to the fixed reference system composed of the x, y and z axes. The absorption transition moment in this case is collinear with the line connecting the five carbon atoms shown. Image taken from [1]

In figure 3.5 the orientation of a single molecule is shown with respect to the three axes x, y and z. These three axes form a fixed coordinate system with which the orientation of the molecule is described. For anisotropy measurements the excitation light is polarized. For convenience, the polarization direction of the light that excites this molecule is chosen to be in the direction of the z-axis. The intensity that is emitted with polarization also in direction of the z-axis by this molecule can be calculated for a given angle θ between the emission transition moment and the z-axis. This intensity is given by:

$$I_{\parallel}^{mol}(\theta) = \cos^2(\theta) * I_T^{mol} \quad \text{eq. 3.12}$$

with I_T^{mol} the total amount of light emitted by the fluorophore shown in figure 3.5. The angle φ also defines the position of the molecule with respect to the fixed reference system. With this angle φ and the previously mentioned angle θ the intensity emitted by the fluorophore with polarization perpendicular to the polarization of the excitation light (so the polarization direction is in the direction of the x) can be calculated:

$$I_{\perp,x}^{mol}(\theta, \varphi) = \sin^2(\theta) \sin^2(\varphi) * I_T^{mol} \quad \text{eq. 3.13}$$

Since there are two axes (x and y) for which the light intensity with polarization direction in these axes is perpendicular to the excitation light polarization, the total intensity emitted by the fluorophore is given by:

$$I_T^{mol} = I_{\parallel}^{mol} + I_{\perp,x}^{mol} + I_{\perp,y}^{mol} \quad \text{eq. 3.14}$$

From this it can be seen that the anisotropy r in eq. 3.11 is defined as the difference between measured parallel polarized intensity and perpendicular polarized intensity, divided by the total intensity. To calculate the maximum anisotropy when averaged over a lot of randomly orientated molecules, the expressions in eq. 3.12 and eq. 3.13 should be integrated over all possible orientations of the molecule. For simplicity, the total intensity emitted by a fluorophore is set to 1. Each molecule with an emission transition moment that makes a given angle θ with the z-axis has equal probability to emit light with polarization perpendicular to the absorbed light (I_{\perp}), independent of φ . The average of $\sin^2(\varphi)$ is given by:

$$\langle \sin^2 \varphi \rangle = \frac{\int_0^{2\pi} \sin^2 \varphi \, d\varphi}{\int_0^{2\pi} d\varphi} = \frac{1}{2} \quad \text{eq. 3.15}$$

The intensity emitted by all the fluorophores which make an angle θ with the z-axis with a polarization perpendicular to the excitation light averaged over all angles φ is then given by:

$$I_{\perp}(\theta) = \frac{1}{2} \sin^2(\theta) \quad \text{eq. 3.16}$$

We write the probability that a fluorescent molecule is excited and emits fluorescence is oriented with angle θ to the z-axis as $f(\theta)$. The amount of molecules that are oriented with an angle between θ and $\theta + d\theta$ from the z-axis is given by $\sin(\theta) d\theta$. Because only a fraction ($\cos^2\theta$) of these molecules are excited by the polarized excitation light, the factor $f(\theta) d\theta$ can be written as:

$$f(\theta)d\theta = \cos^2\theta \sin\theta \, d\theta \quad \text{eq. 3.17}$$

The measured fluorescence intensities can then be written as:

$$I_{\parallel} = \int_0^{\pi} f(\theta) \cos^2\theta \, d\theta = \frac{2}{5} \quad \text{eq. 3.18}$$

for the intensity of the parallel polarized light and:

$$I_{\perp} = \frac{1}{2} \int_0^{\pi} f(\theta) \sin^2\theta \, d\theta = \frac{2}{15} \quad \text{eq. 3.19}$$

for the intensity of the perpendicular polarized light. From eq. 3.11 the maximum anisotropy r can be calculated and equals 0.4. This maximum anisotropy value only holds for randomly orientated, non-rotating fluorophores with collinear absorption and emission transition moment. When the absorption and emission transition moments of all emitting fluorophores are oriented along the z-axis, the maximum anisotropy will be 1.

When absorption and emission transition moments in a fluorophore are not collinear, the fundamental anisotropy is given by¹:

$$r_0 = \frac{2}{5} \left(\frac{3\cos^2\beta - 1}{2} \right) \quad \text{eq. 3.20}$$

Where the angle between absorption and emission transition moments is given by β . It should be noted that a lot of factors can influence anisotropy measurements. These include fast rotation of fluorophores, the use of a high numerical aperture objective and the concentration of fluorophores. If the concentration is high enough, processes such as radiative reabsorption and resonance energy transfer have influences. The effect of resonance energy transfer will be discussed in detail, since the decrease in measured anisotropy due to resonance energy transfer plays a role in homo-FRET experiments. The Perrin equation relates the rotational motion of a fluorophore to the measured anisotropy:

$$r = \frac{r_0}{1 + \frac{\tau}{\theta}} \quad \text{eq. 3.21}$$

here r_0 is the maximum anisotropy as defined in eq. 3.20, τ is the lifetime of the fluorophore and θ is the rotational correlation time of the fluorophore, which is defined as the time it takes on average to rotate one radian.

In this chapter only steady state anisotropy is discussed. In steady state anisotropy experiments the measured anisotropy values are obtained from detecting the total parallel polarized emission intensity and the total perpendicular polarized emission intensity during the excited state lifetime of a fluorophore or several fluorophores. Time-resolved anisotropy experiments can also be performed. In time resolved anisotropy experiments, the parallel polarized emission intensity and the perpendicular polarized emission intensity are detected only in a short time interval upon pulsed excitation, where this time interval is considerably shorter than the excited state lifetime. This way, several anisotropy values can be measured for several different time points after excitation of the fluorophore. Time resolved anisotropy experiments can give information on orientation of fluorophores as a function of time.

3.1.6 Effect of resonance energy transfer on anisotropy

In the absence of resonance energy transfer between fluorophores, the molecules that are excited with polarized light will emit light with a certain fraction polarized perpendicular and a fraction parallel to the excitation light (see figure 3.6, upper part). When both fractions are detected separately, the anisotropy can be calculated from eq. 3.11 and depends on the rotational lifetime of the fluorophore and the orientation of absorption and emission transition moments. When the absorption transition moment of a fluorophore is perpendicular to the polarization of the excitation light, the fluorophore cannot be excited.

When identical fluorophores are separated by a small distance, and the dipole orientation is not perpendicular, resonance energy transfer can occur between donor and acceptor molecule. This decreases the measured anisotropy value. This is because some fluorophores, which were not excited by the polarized incoming light due to a different orientation, can be excited by resonance energy transfer from another fluorophore that was excited (see figure 3.6 lower part). These fluorophores with a different orientation then are also able to emit fluorescence with a certain polarization. Because the orientation of the dipole moments is different, the polarization of the emitted light will be different (shown with the black arrows on the right side of the image). This means that the fraction of light emitted with a polarization perpendicular to the excitation light will be higher. The anisotropy then decreases, as can be seen in eq. 3.11. Due to FRET a fluorophore with the absorption moment perpendicular to the excitation light cannot be excited directly by the excitation light, but can be in an excited state and emit fluorescence due to FRET.

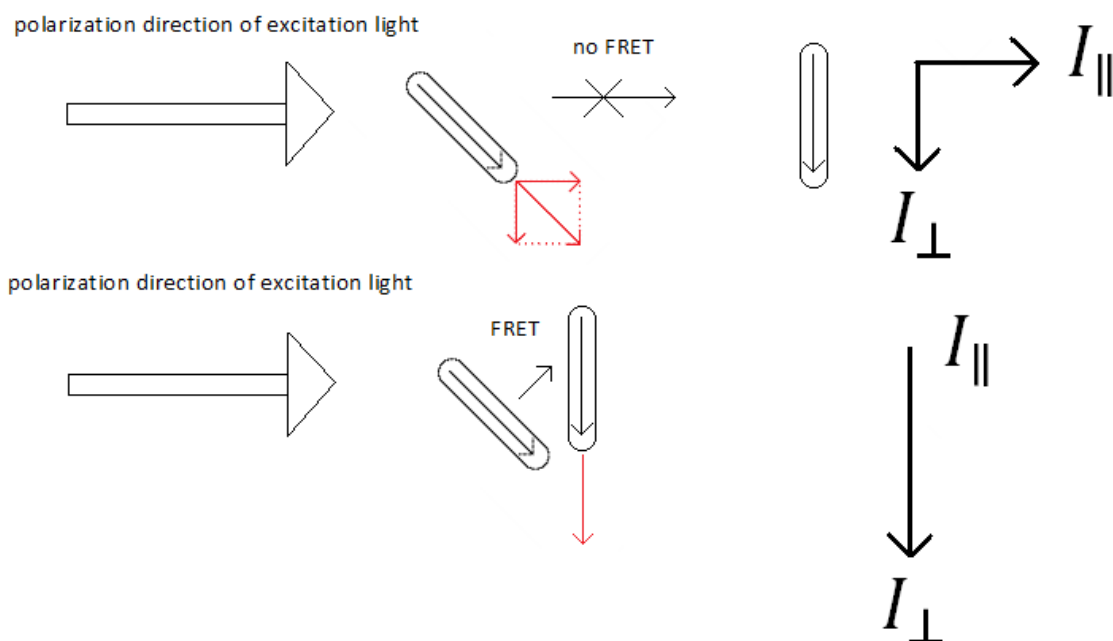


figure 3.6: Representation of fluorescence emission of fluorophores excited by polarized light in the absence and presence of FRET.

The amount of energy transfer between like fluorophores is dependent on the distance between the donor and acceptor molecule (see eq. 3.6). The larger the distance, the smaller the rate of energy transfer. Since the occurrence of this energy transfer is related to the measured decrease in anisotropy, information on fluorophore density or clustering can be withdrawn from these experiments. This is only possible when the fluorophores are close enough for FRET to occur.

3.1.7 Effect of Homo-FRET on the fluorescence lifetime of the donor

Hetero-FRET can be detected by measuring the fluorescence lifetime of the donor molecule in the presence and absence of the acceptor. In eq. 3.2 and eq. 3.10 the expressions for the fluorescence lifetime are given for the presence and absence of the acceptor respectively. From these equations it can be seen that hetero-FRET decreases the lifetime of the donor. For homo-FRET, these equations do not hold, because homo-FRET can occur multiple times between the same pair of fluorescent molecules. Therefore the effect of homo-FRET on the fluorescence lifetime is given by the following rate equations for the excited state of the donor molecule and the acceptor molecule:

$$\dot{A}_{donor} = -k_{fl}A_{donor} + k_{fret} A_{acceptor} - k_{fret} A_{donor} - k_{nr} A_{donor} \quad \text{eq. 3.22}$$

$$\dot{A}_{acceptor} = -k_{fl}A_{acceptor} + k_{fret} A_{donor} - k_{fret} A_{acceptor} - k_{nr} A_{acceptor} \quad \text{eq. 3.23}$$

Here k_{fl} , k_{fret} and k_{nr} are the fluorescence decay rate, resonance energy transfer rate and non-radiative decay rate of the donor and acceptor respectively. These rates for both molecules are assumed to be identical, because both molecules are identical. The resonance energy transfer rate may not be equal for both molecules when there is a non-zero angle between the absorption and emission transition moments. So it is also assumed that these transition moments are collinear. A_{donor} and $A_{acceptor}$ in these equations are the normalized populations of the excited state of the donor and acceptor respectively.

To solve the rate equations, the donor molecule is assumed to be in the excited state and the acceptor molecule in the ground state at $t=0$. This assumption leads to the following start conditions for the rate equations:

$$A_{donor}(0) = 1 \quad \text{eq. 3.24}$$

$$A_{acceptor}(0) = 0 \quad \text{eq. 3.25}$$

It is also assumed that no absorption of excitation light takes place during the total fluorescence decay time. This is a valid assumption at low excitation power. Solving the rate equations with the above mentioned starting conditions, led to the following expressions for A_{donor} and $A_{acceptor}$:

$$A_{donor}(t) = \frac{1}{2e^{k_{fl}t+k_{nr}t}} + \frac{1}{2e^{k_{fl}t+k_{nr}t+2k_{fret}t}} \quad \text{eq. 3.26}$$

$$A_{acceptor}(t) = \frac{1}{2e^{k_{fl}t+k_{nr}t}} - \frac{1}{2e^{k_{fl}t+k_{nr}t+2k_{fret}t}} \quad \text{eq. 3.27}$$

Because donor and acceptor are identical and the distance between them is smaller than the diffraction limit, no discrimination can be made between fluorescence light emitted by the donor and the acceptor. Therefore, the summation of $A_{donor}(t)$ and $A_{acceptor}(t)$ gives the time dependent expression for the normalized total excited state population:

$$A_{sum}(t) = e^{-(k_{fl}+k_{nr})t} \quad \text{eq. 3.28}$$

This expression is identical to the fluorescence decay of the excited state of the donor in the absence of the acceptor (see eq. 3.5 and eq. 3.6). From this it can be concluded that homo-FRET does not influence the lifetime of the total fluorescence system, and therefore cannot be detected by lifetime measurements when the dipole transition moments are collinear. When there is an angle between the absorption and emission dipole moment, the values for k_{fret} might be different between FRET from donor to acceptor and vice versa. To determine this, the following rate equations were solved:

$$\dot{A}_{donor} = -k_{fl}A_{donor} + k_{fretAD} A_{acceptor} - k_{fretDA} A_{donor} - k_{nr} A_{donor} \quad \text{eq. 3.29}$$

$$\dot{A}_{acceptor} = -k_{fl}A_{acceptor} + k_{fretDA} A_{donor} - k_{fretAD} A_{acceptor} - k_{nr} A_{acceptor} \quad \text{eq. 3.30}$$

Here k_{fretDA} is the FRET rate from donor to acceptor and k_{fretAD} is the FRET rate from acceptor to donor. Solving the equations with the same start conditions leads to the following equations for $A_{donor}(t)$, $A_{acceptor}(t)$ and $A_{sum}(t)$:

$$A_{donor}(t) = \frac{k_{fretAD}}{(k_{fretAD} + k_{fretDA})e^{k_{fl}t+k_{nr}t}} + \frac{k_{fretDA}}{(k_{fretAD} + k_{fretDA})e^{k_{fl}t+k_{nr}t+k_{fretAD}t+k_{fretDA}t}} \quad \text{eq. 3.31}$$

$$A_{acceptor}(t) = \frac{k_{fretDA}}{(k_{fretAD} + k_{fretDA})e^{k_{fl}t+k_{nr}t}} - \frac{k_{fretDA}}{(k_{fretAD} + k_{fretDA})e^{k_{fl}t+k_{nr}t+k_{fretAD}t+k_{fretDA}t}} \quad \text{eq. 3.32}$$

$$A_{sum}(t) = e^{-(k_{fl}+k_{nr})t} \quad \text{eq. 3.33}$$

The summation of $A_{donor}(t)$ and $A_{acceptor}(t)$ again leads to an expression for the excited state population identical to the fluorescence decay of the donor in the absence of the acceptor (see eq. 3.33). From this we conclude that homo-FRET does not alter the lifetime of the total fluorescence system, even when the FRET rate from donor to acceptor is not identical to the FRET rate from acceptor to donor. From this we also conclude that the decrease in lifetime of the donor in hetero-FRET experiments can be measured because the fluorescence emitted by the acceptor is not detected. We also conclude that the change in lifetime of the donor in homo-FRET experiments cannot be detected because the emission of fluorescence by the acceptor exactly compensates this decrease. The fact that homo-FRET cannot be measured by lifetime measurement is not caused by the fact that the FRET rates from donor to acceptor are identical to the FRET rates from acceptor to donor.

3.1.8 Fluorescence lifetime imaging microscopy

When detecting FRET between two different fluorophores, usually the lifetime of the donor molecule in the presence and absence of the acceptor is measured. The fluorescence lifetime can be measured in frequency domain and time domain. Here only the frequency domain method will be discussed.

In frequency domain lifetime measurements the fluorescent sample is excited with frequency modulated light where the time-dependent intensity can be written as:

$$I_{ex}(t) = I_0 + I_{m,ex} \sin(\omega t) \quad \text{eq. 3.34}$$

The fluorescence emission will then be a convolution of the fluorescence decay probability function (eq. 3.4) and the excitation function (eq. 3.34):

$$I_{em}(t) = I_0 + I_{m,em} \sin(\omega t - \vartheta) \quad \text{eq. 3.35}$$

To measure lifetimes, the detector measures the intensity at different phases with respect to the excitation light. The image intensifier is also modulated at the same frequency as the excitation light. The intensity is then imaged for different phase shifts between the excitation signal and detector signal. For every pixel, the intensity as a function of phase shift is measured. A sine is then fitted through these points, and from this sine the phase shift and the decrease in modulation depth (m) with respect to the excitation light are determined. Here m is defined as:

$$m = \frac{I_{m,em}}{I_{m,ex}} \quad \text{eq. 3.36}$$

When the phase shift, modulation depth and frequency of the excitation light are known, the fluorescence lifetime can be calculated from the modulation, called τ_m or from the phase shift, called τ_ϑ :

$$\tau_m = \frac{1}{\omega} \sqrt{\frac{1}{m^2} - 1} \quad \text{eq. 3.37}$$

$$\tau_\vartheta = \frac{1}{\omega} \tan(\vartheta) \quad \text{eq. 3.38}$$

If a single lifetime is present in a single pixel, both lifetimes are equal. If a two or higher component lifetime is expected, measurements should be done at several modulation frequencies. At a single modulation frequency, τ_m and τ_ϑ will be different.

3.2 Epidermal growth factor receptor

The epidermal growth factor receptor (EGFR, ErbB1) is an intensively studied protein. This is because it was found in a lot of malignant tumors that the EGF receptor was overexpressed.^{4,5} The EGF-receptor is a member of the ErbB family receptors and can be found on the cell membrane. The role of EGFR, controlling cell proliferation, suggests that overexpression of the EGF-receptor is related to cancer. A study showed that patients with breast tumor cells expressing EGFR have a worse prognosis than patients with EGFR-negative tumor cells.⁶ It was also found that overexpression of the EGF-receptor in lung cancer cells of lung cancer patients did not lead to an increase in tumor growth, but increased the cell motility.⁷

3.2.1 ErbB family of receptors

The ErbB family consists of the following members: ErbB1 (EGFR), ErbB2 (HER2/c-neu), ErbB3 (HER3) and ErbB4 (HER4). The ErbB-family receptors are receptor tyrosine kinases, which are the cell surface receptors that are the main regulators of cellular processes. The ErbB-members all have a similar structure and are important for cell survival and proliferation, which is the increase in cell number by division. This proliferation is regulated by activation of the receptors upon binding of a ligand on the extracellular part of the receptor. This binding then causes a structural change of the receptor, such that signaling pathways inside the cell are activated. Some ErbB-family receptors can be activated by a number of ligands, which results in homo-dimerization or hetero-dimerization between these receptors. EGFR is activated by epidermal growth factor (EGF), transforming growth factor (TGF- α), and several other ligands. ErbB3 and ErbB4 are both activated by neuregulins. ErbB3 does not have an active tyrosine kinase part. No ligand is found that binds directly to the ErbB2 receptor, but ligand binding to the other three ErbB family receptors can result in heterodimerization with the ErbB2 receptor. For additional information see Yarden et al.⁵

3.2.2 Structure of the epidermal growth factor receptor

The EGF receptor is the receptor of the ErbB-family receptors that is investigated the most. The receptor consists of an extracellular domain, a part that is in the cell membrane (transmembrane domain) and an intracellular domain. The N-terminus of the ErbB1 protein can be found in the extracellular region, whereas the C-terminus is located on the inside of the cell. The part on the outside of the cell consists of 4 domains numbered I, II, III and IV. The ligand binds to domain I and III. When a receptor is monomeric, domain I and III are too far apart for simultaneous binding of EGF to both domains. Domain II is responsible for receptor dimerization. This changes the structure of the EGF-receptor such that domain I and III are closer to each other and EGF can bind to both domains. The part of the receptor on the inside of the molecule consists of tyrosine kinase domains and is responsible for the signaling cascade upon binding of the ligand to the receptor. The intracellular part of the EGF receptor consists of a juxtamembrane domain which connects the kinase domain to the transmembrane domain. The kinase domain is connected to the tyrosin residues which are responsible for the trans-autophosphorylation of the kinase domain.

The current model of EGF-receptor activation by EGF predicts that dimerization or oligomerization upon binding of EGF leads to the activation and internalization of the EGF-receptor (see figure 3.7). Upon ligand binding, a conformational change occurs in the extracellular EGF-receptor, which allows dimerization. In this dimer the receptors are close to each other, which promotes trans-autophosphorylation of the kinase domains of the receptors. Other proteins in the signaling pathway are then able to bind to the phosphorylated kinase domains.⁸

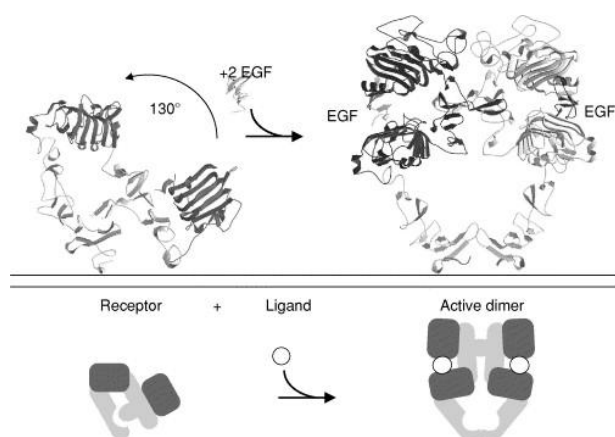


figure 3.7: schematic representation of EGF-receptor dimerization. Image taken from [9]

3.3 Oligomerization of the EGF-receptor

This part of this chapter discusses previous research on the EGF-receptor. The purpose of this part is to show that in several experiments it was found that the EGF-receptor forms clusters after stimulation with its ligand EGF and to show that this clustering can be observed with anisotropy experiments. In the literature also contradictions are found. There is no consensus yet and the observation of clustering will also depend on the used technique and experimental procedure. The main findings will be presented here.

The effect of temperature on dynamics and clustering of the EGF-receptor was investigated using image correlation spectroscopy.¹⁰ It was found that a decrease in temperature from 37° to 4° causes the EGF-receptor to form aggregates. The aggregates are formed within 15 minutes, and the process is reversible. Also the diffusion coefficients of the EGF-receptor is more than twice as low at 4° compared to 37°, which could be due to the presence of EGFR-dimers or -oligomers, or due to the lower temperature.

Previous research showed that on cells that are not stimulated with EGF, the EGF receptor might be present as monomer, dimer or even oligomer on the cell membrane.¹¹ Anisotropy experiments on A431 cells expressing EGFR-mGFP that were not stimulated with EGF show that 40% of the EGF receptors are present as dimer and 10% as oligomer.^{12,11} It was also found that after stimulation with EGF, these ratios change to 40% and 30% respectively.¹² Previous research shows that the largest change in these ratios occurs between 2 and 5 minutes after addition of EGF. After 10 minutes, a decrease in the amount of oligomers and dimers is observed.¹² Anisotropy experiments on NIH 3T3 cells expressing EGFR-FKBP-mGFP, which can be dimerized upon addition of the molecule AP20187 that has two binding sites for FKBP, show that EGFR dimers themselves did not activate the signaling pathway. However, internalization of the EGF-receptors was enhanced upon binding of EGF, compared to EGF-receptors that were not pre-dimerized.

Experiments on NIH 3T3 cells expressing 50.000 EGF receptors per cell on average show an EGF receptor cluster fraction of 0.4 using time resolved anisotropy measurements.¹³ The time resolved decay of the anisotropy showed the occurrence of homo-FRET between EGFR-GFP proteins.

Homo-FRET and time resolved homo-FRET measurements showed that predimers of the EGF receptor are formed in unstimulated cells expressing a normal amount of EGF receptors (50.000 per cell). This was shown with YFP-EGFR in live BaF/3 cells at room temperature.¹⁴

Using an Alexa488 labeled EGFR₄₅₅ antibody, it was found that in A431 cells expressing 2.000.000 EGF receptors per cell the EGF receptor is 90% monomeric and 10% oligomeric with an average cluster

size of 4 receptors before stimulation.¹⁵ This was done by measuring homo-FRET between the Alexa488 fluorescent molecules by flow cytometry. After stimulation with EGF 70% of the EGF receptors were monomeric, and the average cluster size of the oligomeric EGFR was 10 receptors per cluster.

Other research by Nagy et al. showed using the number and brightness analysis that in HeLa and CHO cells expressing 50.000 to 200.000 the EGF receptor did not form dimers or oligomers in the absence of EGF.¹⁶ In CHO cells expressing more than 500.000 EGF receptors a dimer fraction of 30 % was found in the absence of the ligand using the same technique. After stimulation with EGF the cells expressing 50.000 to 200.000 EGF receptors per cell showed an increase in the average cluster size from 1.0 to 1.5 (in molecules per cluster). CHO cells expressing 600.000 receptors per cell showed an increase from 1.3 to 1.8 in the average molecules per cluster.

Homo-FRET and image correlation spectroscopy was used to investigate the oligomerization state of the EGF-receptor.¹⁷ BaF/3 cells expressing wt-EGFR-eGFP and other BaF/3 cells expressing de2-7-EGFR-eGFP (a mutated variant of EGFR), showed an increase in anisotropy upon photobleaching in the absence of EGF (see figure 3.8). From this it was concluded that the EGF-receptor forms predimers on the cell membrane in the absence of EGF.

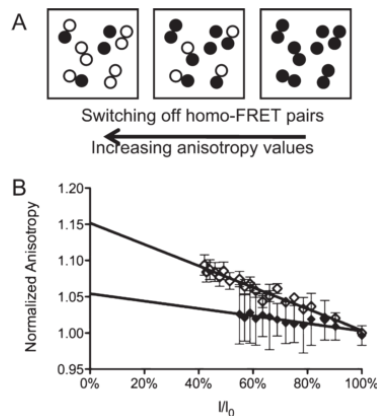


figure 3.8: The increased amount of photobleached fluorophores in dimer (white dots) decreases the amount of FRET (A). Photobleaching of BaF/3 cells expressing wt-EGFR-eGFP (empty symbols) and BaF/3 cells expressing de2-7-EGFR-eGFP (filled symbols) show an increase in normalized anisotropy. Image taken from [17]

The results and conclusions mentioned above show that the oligomerization of the EGF-receptor depends highly on the cell type, temperature, used technique and expression level. There is no consensus on the presence of EGFR dimers or oligomers before stimulation. However, all experiments performed at room temperature show consistent results. After stimulation with EGF, the fraction of dimers and oligomers increases in all above mentioned experiments. The absolute fractions here also depend on the expression level and temperature.

4 Modeling the effect of homo-FRET on the anisotropy

Although an expression exists to relate the homo-FRET efficiency between fast rotating identical fluorophores and the corresponding Förster radius to the anisotropy, the situation can be more complicated when the fluorophores do not rotate. To give more insights into the relation between homo-FRET and anisotropy in these cases, simulations are performed and discussed in this chapter. The FRET efficiency between identical fluorophores depends on several parameters. This is already discussed in chapter 2. With the use of these parameters it is simulated in this chapter how the anisotropy depends on the fluorophore density in a two-dimensional plane. It is also investigated with the simulations how the anisotropy changes when homo-FRET occurs between two fluorophores only. This is also done for several distances between the two fluorophores. The angle between the absorption and emission transition dipole in a fluorophore has an effect on the anisotropy. In this chapter it is also investigated how this angle influences the anisotropy when homo-FRET also occurs.

This chapter first focuses on the mathematical aspects of the anisotropy simulations. Then the simulation results are presented for several settings in the simulation program. Finally the results will be discussed, followed by the outlook and the limitations of this method.

4.1 Mathematical and physical background for anisotropy simulations

In these simulations, a certain amount of locations are determined in a 2-dimensional plane, by generating random x and y coordinates. Every location represents a fluorophore. The absorption transition dipole moments $\vec{\mu}_{abs}$ of these fluorophores have a random orientation in 3D. This orientation is determined by generating random numbers that define the angle θ and ϕ of the absorption dipole moment with respect to the fixed reference system described by \vec{e}_x , \vec{e}_y and \vec{e}_z (see figure 4.1). Here θ is the angle between the absorption dipole moment and the z-axis. For a random number selected from a uniform distribution between 0 and 1 the expression for θ is given by:

$$\theta = \arccos(-2 \cdot rand + 1) \quad \text{eq. 4.1}$$

This expression generates values for θ in an interval between 0 and π , with a (normalized) probability distribution function of $p(\theta)$:

$$p(\theta) = \frac{1}{2} \sin \theta \quad \text{eq. 4.2}$$

This expression corrects for the fact that more absorption moments have an angle θ of $\pi/2$ with respect to the z-axis than absorption moments with an angle θ of 0 when the orientation is completely random. Only with this expression for θ a truly random orientation in 3D of the absorption transition moment can be generated. For determination of the angle ϕ a different random number uniformly distributed between 0 and 2π is selected. This is done for all fluorophores. This angle ϕ determines the orientation of the projection of the absorption transition moment onto x,y-plane with respect to the x- and y- axes in figure 4.1.

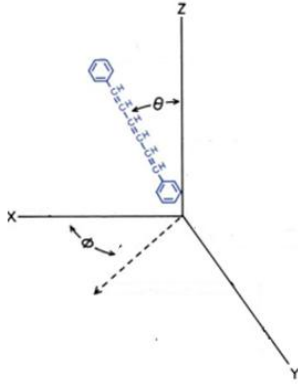


figure 4.1: Orientation of absorption dipole moment with respect to a fixed reference system as a function of angle θ and ϕ . Image adapted from [1]

Since the measured anisotropy also depends on the angle α between the absorption transition moment $\vec{\mu}_{abs}$ and emission transition moment $\vec{\mu}_{em}$, the emission transition moments of the fluorophores are generated such that an angle α can be set between the previously generated absorption transition moment orientation and the emission transition moment orientation. This is done by creating a new reference system where the absorption transition moment is collinear with the z-axis. In this new reference system the emission transition moment makes an angle α with the z-axis (and thus the absorption transition moment). The orientation of the projection of the emission transition moment onto the x, y-plane with respect to the x, y plane in this new reference system is determined by generating a random number between 0 and 2π . This is the azimuth (ϕ_{new}) of the emission transition moment in the new reference system. When we set the length of the emission transition moment to unity, the direction of the emission transition moment in the new reference system can be described as follows:

$$\vec{\mu}_{em,new} = \sin(\alpha) \cos(\phi_{new}) \vec{e}_{x,new} + \sin(\alpha) \sin(\phi_{new}) \vec{e}_{y,new} + \cos(\alpha) \vec{e}_{z,new} \quad \text{eq. 4.3}$$

For every fluorophore, the vector that represents the absorption transition moment starts in the point of origin of the reference systems. This means that each fluorophore has its own reference system. The determined locations of the fluorophores in a 2D-plane have nothing to do with the calculations shown here.

The new reference system is obtained by rotating the original reference system over the previously determined angle θ and ϕ that describe the position of the absorption transition moment in the original reference system. Since the orientation of the emission transition moment in the new reference system is known, the orientation in the old reference system can be obtained by solving the following equation:

$$\vec{\mu}_{em,new} = \begin{bmatrix} \cos(\phi) & \sin(\phi) & 0 \\ -\sin(\phi) & \cos(\phi) & 0 \\ 0 & 0 & 1 \end{bmatrix} \cdot \begin{bmatrix} \cos(\theta) & 0 & \sin(\theta) \\ 0 & 1 & 0 \\ -\sin(\theta) & 0 & \cos(\theta) \end{bmatrix} \cdot \vec{\mu}_{em} \quad \text{eq. 4.4}$$

With the use of eq. 4.3 the orientation of the emission transition moment in the original reference system is thus given by:

$$\vec{\mu}_{em} = \begin{bmatrix} \cos(\theta) & 0 & \sin(\theta) \\ 0 & 1 & 0 \\ -\sin(\theta) & 0 & \cos(\theta) \end{bmatrix}^{-1} \cdot \begin{bmatrix} \cos(\phi) & \sin(\phi) & 0 \\ -\sin(\phi) & \cos(\phi) & 0 \\ 0 & 0 & 1 \end{bmatrix}^{-1} \cdot \begin{bmatrix} \sin(\alpha) \cos(\phi_{new}) \\ \sin(\alpha) \sin(\phi_{new}) \\ \cos(\alpha) \end{bmatrix} \quad \text{eq. 4.5}$$

$\vec{\mu}_{em}$ in eq. 4.5 gives the orientation of the emission transition moment in the original reference system with length normalized to unity. The corresponding angles θ and ϕ that describe the

orientation of the emission transition moment in the original reference system in angular coordinates are given by the following equations:

$$\theta = \cos^{-1}(\vec{\mu}_{em} \cdot \vec{e}_z) \quad \text{eq. 4.6}$$

for θ , and

$$\phi = \cos^{-1} \left(\frac{\vec{\mu}_{em} \cdot \vec{e}_x}{\sqrt{(\vec{\mu}_{em} \cdot \vec{e}_x)^2 + (\vec{\mu}_{em} \cdot \vec{e}_y)^2}} \right) \quad \text{eq. 4.7}$$

when $\vec{\mu}_{em} \cdot \vec{e}_y$ is positive and:

$$\phi = 2\pi - \cos^{-1} \left(\frac{\vec{\mu}_{em} \cdot \vec{e}_x}{\sqrt{(\vec{\mu}_{em} \cdot \vec{e}_x)^2 + (\vec{\mu}_{em} \cdot \vec{e}_y)^2}} \right) \quad \text{eq. 4.8}$$

when $\vec{\mu}_{em} \cdot \vec{e}_y$ is negative for ϕ .

Now each fluorophore has a position in a 2D-plane and a 3D-orientation of the absorption and emission dipole transition moment. These parameters are needed to calculate the FRET efficiency from a single donor to a single acceptor as will be shown later. The steps that are taken to obtain results from the simulations are described at first.

First of all a subset of the fluorophores in this 2D-plane is excited with polarized light. The polarization direction here is in the x,y-plane. The probability that a fluorophore is excited is given by:

$$P_{abs} = 0.2 \cos^2(\theta_{pol,abs}) \quad \text{eq. 4.9}$$

Here $\theta_{pol,abs}$ is the angle between the direction of the polarized light and the direction of the absorption transition moment. The factor 0.2 is introduced such that only 20% of the fluorophores with the absorption transition moment perfectly aligned with the polarization of the excitation light is excited. This is done because now only a low percentage of the fluorophores will be excited, such that the probability that FRET occurs between an excited fluorophore and a non-excited fluorophore is higher.

Now for every excited fluorophore it is determined whether the fluorophore decays to the ground state under emission of fluorescence or via non-radiative decay, or whether it transfers energy to another fluorophore. The probability of a specific process happening is given by the rate of this specific process divided by the sum of the rates of all processes. For example, the probability that the excited molecule decays under the emission of fluorescence is given by:

$$P_{fl} = \frac{K_f}{K_f + K_{nr} + \sum_{i=1}^N K_{i,ET}} \quad \text{eq. 4.10}$$

with

$$K_f = \frac{Q}{\tau} \quad \text{eq. 4.11}$$

and

$$K_{nr} = \frac{1 - Q}{\tau} \quad \text{eq. 4.12}$$

Here K_f and K_{nr} are the fluorescence and non-radiative decay rates respectively. N is the amount of fluorophores in the model that are not excited. $K_{i,ET}$ is the rate of energy transfer between the excited fluorophore and a non-excited fluorophore i and is given by eq. 3.6 and eq. 3.7. This value is calculated from the positions and orientations of the fluorophores and the values shown in table 4.1. Selection of a fluorophore in the excited state and determination of the process (fluorescence, FRET or non-radiative decay) that will happen is done by random number generation. The properties, such as lifetime, quantum yield and overlap integral, of the fluorescent protein mCherry are used for calculation of the Förster radius R_0 in this model (see table 4.1). For an orientation factor of $2/3$, R_0 equals 4.37 nm. The overlap integral was calculated from the absorption and emission spectra using eq. 3.8.

Quantity	Value
Fluorescence lifetime	1.46 ns
Quantum yield	0.22
Overlap integral	$2.07 \cdot 10^{15} M^{-1} cm^{-1} nm^4$

table 4.1: Photophysical properties of mCherry

When the simulation determines that the excited fluorophore decays to the ground state under the emission of fluorescence light, the light emitted is detected in the program. A part of the light is detected by the detector that only detects light with a polarization parallel to the excitation light and a part of it is detected by the detector that only detects light with a polarization perpendicular to the excitation light. For example, when the direction of the emission dipole orientation of the fluorophore has an angle $\theta_{em,pol}$ with respect to the polarization of the excitation light, the total detected intensity from a single fluorophore with emission light polarization parallel to the excitation light (I_{\parallel}) is calculated as:

$$I_{\parallel} = \cos^2(\theta_{em,pol}) \quad \text{eq. 4.13}$$

The total detected intensity from a single fluorophore with emission light polarization perpendicular to the excitation light (I_{\perp}) is calculated as:

$$I_{\perp} = \sin^2(\theta_{em,pol}) \sin^2(\varphi_{em,pol}) \quad \text{eq. 4.14}$$

Here the total intensity emitted by the fluorophore is set to unity. $\varphi_{em,pol}$ in this equation is the azimuth that describes the orientation of emission transition moment with respect to the plane perpendicular to the polarization direction.

Due to fluorescence emission or non-radiative decay, the amount of excited fluorophores decreases. The program that executes all calculations shown above runs until all 900 fluorophores are in the ground state. For example when that the program runs until fluorophores that were excited The described procedure is repeated 200,000 times, to average over enough iterations. All the values for I_{\parallel} are summed and all the values for I_{\perp} are also summed. The anisotropy (r) is then calculated as follows:

$$r = \frac{I_{\parallel} - I_{\perp}}{I_{\parallel} + 2I_{\perp}} \quad \text{eq. 4.15}$$

4.2 Effect of homo-FRET on anisotropy for different fluorophore densities

The anisotropy is now calculated for several fluorophore densities, where the amount of fluorophores was equal for all fluorophore densities. The angle between the absorption and emission transition moment was 0 in this case. The results from these calculations are shown in figure 4.2. This figure shows the relation between fluorophore density (in amount/nm²) and the calculated anisotropy values. It can be seen that for a very low fluorophore density, the anisotropy equals 0.4, which is indeed the average anisotropy of a sample in which no FRET or rotation occurs, as calculated in chapter 2. When the fluorophore density is increased, the average anisotropy decreases until it is close to the value 0. The value 0 represents complete depolarization of the emission light and the anisotropy cannot reach a value lower than this when averaged over enough iterations.

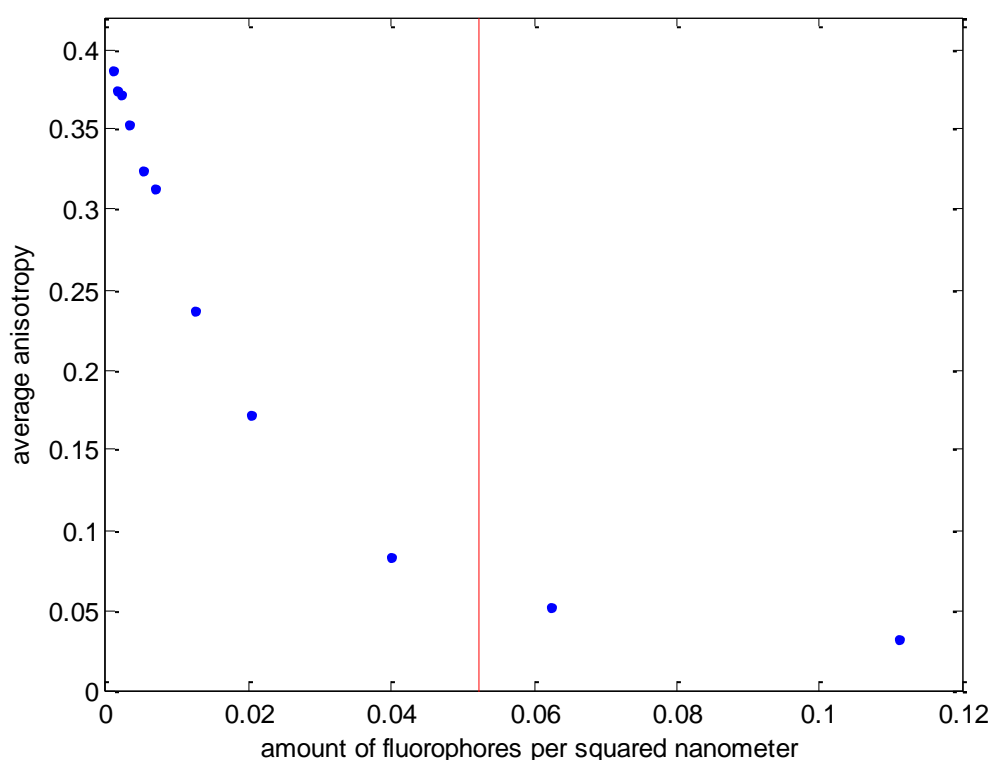


figure 4.2: average anisotropy calculated using the program discussed in this chapter as a function of fluorophore density in a 2D-plane. The red line indicates the value $1/R_0^2$ for κ^2 equals $2/3$.

Previously shown results were calculated for several fluorophores in a plane. However, it was shown by Koushik et al.^[18] that when FRET occurs from a donor to multiple acceptors, the expression shown in eq. 4.10 is not valid anymore. The FRET efficiency is much higher in practice than would be expected from this equation. This means that the anisotropy would decrease faster as a function of fluorophore density than it does in figure 4.2. The results shown in figure 4.2 thus only give an idea on how the anisotropy decreases as a function of fluorophore density, but an exact expression for the FRET efficiency for multiple acceptors is not available yet. It should also be noted that this relation depends on the excitation power. For different excitation powers the expression in eq. 4.9 is also different. For higher excitation power for example there is a higher probability that two fluorophores that are close together are excited simultaneously, such that no FRET occurs between these two fluorophores until one of them decays to the ground electronic state.

4.3 Effect of homo-FRET between two fluorophores on anisotropy

The effect of homo-FRET between two fluorophores is also investigated. This is done for several given distances between the donor and acceptor and for several different angles between the absorption and emission transition moment in a single fluorophore. For this, the same model is used, but here only two molecules are placed in a 2D plane with fixed distance between them. The completely random orientation of the absorption transition moments in the program is done as shown earlier. The emission transition moment was taken to have a certain angle α with the absorption transition moment. Earlier in this chapter it is also discussed how the orientations of the emission transition moments are determined for a given angle α . For this orientation also a random ϕ_{new} is determined, as shown earlier. The same settings and photophysical properties of the fluorescent protein mCherry as used before are used here. The calculations are done for angles from 0 to 0.5π between the absorption and emission transition moment in a single fluorophore and for distances between the fluorophores from 0.4 to 16 nm. The probability that two fluorophores in this program are excited simultaneously is set to 0 in these simulations. This is defined by only exciting one of the two fluorophores, which is done according to eq. 4.9. The polarization direction of the excitation light is in the direction of the x-axis. The vector connecting the two fluorophores is in the direction of the y-axis.

As also mentioned in chapter 3, eq. 4.16 gives the expression for the maximum average anisotropy that can be measured as a function of α :

$$r_0 = \frac{2(3\cos^2(\alpha) - 1)}{5} \quad \text{eq. 4.16}$$

This maximum measurable average anisotropy only holds in the case no FRET occurs and the fluorophores do not rotate during the excited state lifetime.

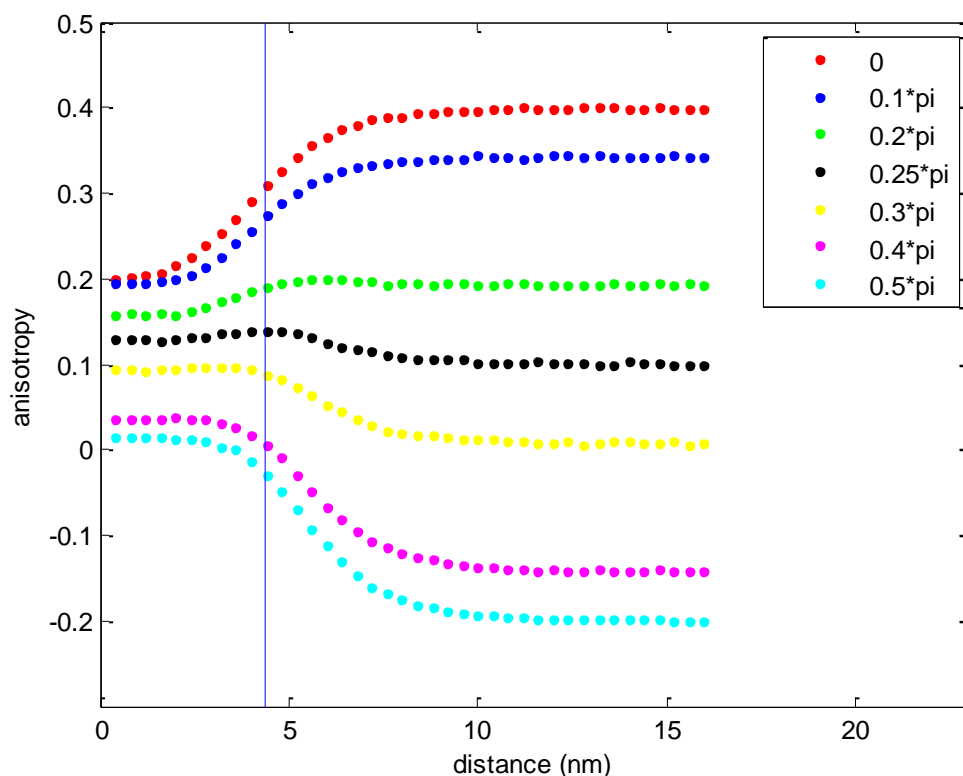


figure 4.3: Calculated anisotropy as a function of distance between two fluorophores. The anisotropy is calculated for several angles between the absorption and emission dipole moment. The blue line shows the value of R_0 for k^2 of $2/3$ for mCherry.

The graphs in figure 4.3 shows the calculated anisotropy as a function of distance between the fluorophores and as a function of angle between the absorption and emission transition moment in each fluorophore. The anisotropy for a large distance between the fluorophores and an angle of 0 is 0.4, which is as expected. This anisotropy gradually decreases when the distance between the fluorophores becomes smaller. For a very small distance the anisotropy equals 0.2 (see red graph in figure 4.3). This can be explained by the fact that for a small distance the FRET efficiency from donor to acceptor and from acceptor to donor is equal and high (close to 1) for any orientation factor. This means that when the donor is excited, FRET occurs with a high probability. Then there is again an identical high probability that FRET occurs from acceptor to donor (identical because of an angle of 0 between the absorption and emission transition moment in a fluorophore). FRET will occur several times, which means that the probability for the donor or the acceptor emitting a fluorescence photon will be equal. This then leads to an average anisotropy for small distances of 0.2 (0.4 on average for the photons emitted by the donor and 0 on average for the photons emitted by the acceptor). When there is an angle between the transition moment in the molecule the FRET rates from donor to acceptor and vice versa are not always equal, which means that the anisotropy in figure 4.3 for small distances is not the mean value of 0 and the corresponding anisotropy value in the absence of FRET.

The anisotropy calculations show that when an angle is introduced between the absorption transition moment and emission transition moment in a single fluorophore, the anisotropy values at a high distance between the fluorophores become lower for an increasing angle. These anisotropy values should be identical to the values calculated from eq. 4.16, because this value is not influenced by FRET or rotation of the fluorophore. In figure 4.4 it can be seen that this is indeed the case. Here the red line is the average anisotropy value as a function of angle calculated using eq. 4.16. The blue dots are the average anisotropy values determined with the simulation for a distance of 16 nm between the fluorophores obtained from figure 4.3.

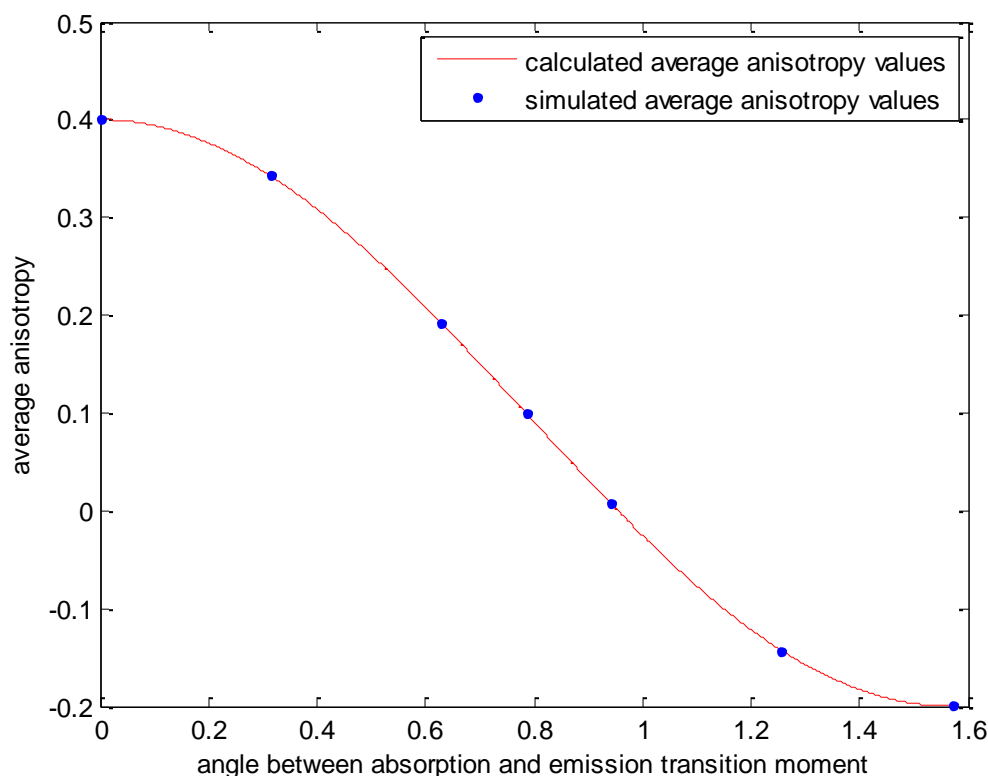


figure 4.4: Average anisotropy in the absence of FRET and rotation, as a function of angle between the absorption and emission transition moment calculated using eq. 4.16 (red) and simulated (blue)

For an angle of 0.1π between the absorption and emission dipole moments, the anisotropy also decreases when the distance between the donor and acceptor decreases (see the dark blue graph in figure 4.3). However, this decrease is lower compared to an angle of 0 between the absorption and emission dipole orientation. When the angle is increased from 0 to 0.25π , the maximum change in anisotropy due to homo-FRET becomes even smaller. From this we can conclude that for homo-FRET experiments one should use fluorophores with a small or no angle between the absorption and emission transition moment, since these will give the largest change in anisotropy when homo-FRET occurs.

For an angle of exactly 0.25π the anisotropy is 0.1 when no FRET occurs. When the distance between the fluorophores is decreased, the anisotropy increases slightly and then decreases to a value above 0.1. This is caused by the fact that for large distances between donor and acceptor FRET only occurs between the fluorophores that have a parallel orientation between the emission dipole of the donor and the acceptor dipole of the acceptor. When the distance decreases further, more fluorophores can transfer energy, also those with lower orientation factors. For this particular angle the anisotropy value for a very large distance equals the anisotropy value for a very small distance between donor and acceptor.

For angles higher than 0.25π the anisotropy increases when the distance between the fluorophores decreases, as can be seen for the bottom three graphs in the figure. The large angle between the absorption and emission transition moment causes that the acceptor that emits fluorescence light will have an emission transition moment with a larger component parallel to the polarization of the excitation light. This results in a higher anisotropy value.

From the simulations it follows that the largest decrease in anisotropy due to homo-FRET for randomly orientated non-rotating fluorescent molecules that can be observed equals 0.2. This is only valid for homo-FRET between two fluorescent molecules. This maximum difference cannot be increased by selecting fluorophores with a higher overlap integral or a higher Förster radius. An increase of these values will only result in a steeper slope or a shift to the right of the anisotropy – distance curves in figure 4.3.

4.4 Outlook

Homo-FRET experiments are able to give information about distances between the (identical) fluorescent probes. Homo-FRET is detected by anisotropy measurements. The relation between measured anisotropy and distance between the identical fluorophores depends on several parameters. When in an experiment a certain change in anisotropy is measured and it is expected that this change is caused by a change in distance between the fluorescent probes, the distance between the probes can be estimated from the anisotropy simulations presented in this chapter. For these simulations the following properties of the fluorescent probes should all be known for a correct determination of the distance between the fluorescent probes in homo-FRET experiments:

1. Photophysical properties of the fluorophore:
 - Overlap integral
 - Fluorescence lifetime (all components for multi-component fluorescence lifetimes)
 - Quantum yield of the fluorophore in the absence of homo-FRET
2. Properties of the measurement system:
 - Rotational and translational dynamics of fluorophore in measurement system
 - Orientation distribution function of the absorption transition moment of the fluorophore in the measurement system
 - Angle between absorption transition moment and emission transition moment in the fluorophore
 - Anisotropy of the fluorophore in the absence of homo-FRET in the measurement system (if this is known, only three of the following four properties should be known: lifetime, dynamics, orientation distribution and angle between absorption and emission transition moment).

It should be noted that the simulations in this chapter only hold for excitation powers for which the probability that two fluorophores that are close enough together for FRET are excited simultaneously is sufficiently low. In general experiments this assumption is valid. It should also be noted that for homo-FRET with multiple acceptors for one donor the simulations do not predict the measured anisotropy correctly, since the FRET efficiency for multiple acceptors is higher than one would expect according to eq. 4.17.^[18]

$$E = \frac{\sum_{i=1}^{i=N} K_{i,ET}}{K_f + K_{nr} + \sum_{i=1}^{i=N} K_{i,ET}} \quad \text{eq. 4.17}$$

4.5 Limitations

The simulation methods presented in this chapter to investigate the effect of homo-FRET on the measured anisotropy decrease can be useful for predictions for anisotropy experiments. However,

this method has its limitations. One limitation is that rotation and motion of the fluorophore is not implemented. This also influences the measured anisotropy values and should thus be considered. To do this, the simulation routine described in this chapter should be extended to a time dependent simulation where the position and orientation changes over time. The probability that a fluorophore emits fluorescence or transfers energy to an acceptor should then be modeled by a time dependent exponential decay law (with the use of eq. 3.4). This also increases the calculation time.

Also the size of the fluorophores in the calculations in this chapter is not taken into account. The size of the fluorophore gives additional restrictions on the positions of the fluorophores; they cannot be separated by less than the size of the fluorophore, which is 3-5 nm for fluorescent proteins.

5 Experimental setup

In this chapter the implementation of a fluorescence polarization microscope in an existing fluorescence microscope will be discussed. In this chapter the experimental setup that contains the fluorescence polarization microscope will be discussed. In chapter 3 the theoretical background on fluorescence anisotropy experiments was already given. With the polarization microscope presented in this chapter, fluorescence anisotropy images can be recorded.

The fluorescence microscope used to do fluorescence anisotropy experiments is first explained in this chapter. Also the necessary procedures to calibrate the fluorescence anisotropy setup are explained. Verification experiments are shown, such as an anisotropy measurement of a sample with a known anisotropy value.

5.1 Experimental setup

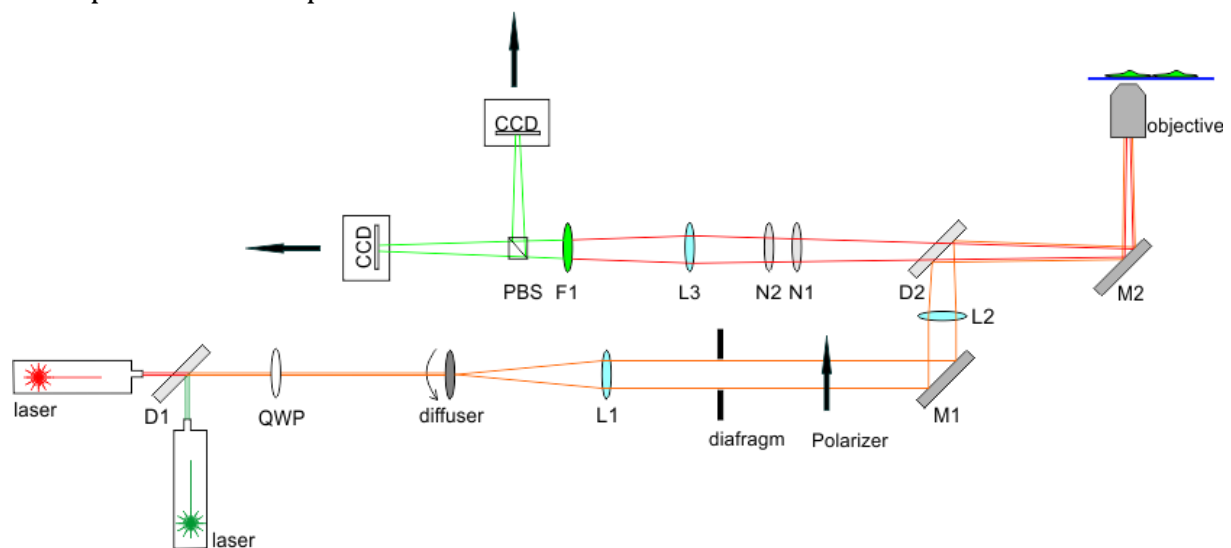


figure 5.1: Schematic representation of the fluorescence polarization microscope

A schematic representation of the setup that is used for fluorescence anisotropy measurements is shown in figure 5.1. The setup contains three lasers, although the figure only shows two. One laser operates at 473 nm wavelength, another one at 532 nm and one at 640 nm. Dichroic mirrors are used to guide laser light from all lasers into the path that is indicated with orange in figure 5.1. All lasers pass a quarter-wave plate to turn the polarized laser light into circularly polarized light (QWP in the figure). For this the polarization of the laser should make an angle of 45 degrees with the polarization of the light that is phase shifted by the quarter wave plate. After it passes the quarter wave plate, the light passes a rotating engineered diffuser to average out all phase information, such that the samples on the microscope table are excited with quasi non-coherent light. The diffuser also turns the Gaussian intensity distribution in a circularly shaped homogeneous intensity distribution. The full-width-half-maximum divergence angle of this diffuser is 1 degree. A lens ($f=200$ mm, L1) is positioned 200 mm behind this diffuser with the diffuser in focus such that a parallel beam is formed by this lens. This parallel beam passes a linear polarizer (Thorlabs, lpvise 100-A), to polarize the laser light. The polarizer is placed in a rotation mount, such that the direction in which the light is polarized can be adjusted (see figure 5.2 right). The laser light is then focused by another lens ($f=400$ mm, L2) into the objective. Behind this lens a dichroic mirror (Semrock, FF 494/540/650, D2) is placed, to reflect the light from the three lasers to the microscope. Light of other wavelengths is transmitted through this mirror, to detect the fluorescence emitted light. For example light emitted by the Rhodamine 6G and fluorescein dyes is transmitted through the dichroic mirror.

The microscope (axiovert 135 TV) consists of a microscope stage and objectives that can both be heated to 37 degrees Celsius. A part of the fluorescence light that is emitted from the samples on the microscope table returns to the dichroic mirror via the objective and is transmitted towards the detection part of the setup. Behind this mirror notch filters (488, 532 and 633 nm wavelength, N1 and N2 in the figure) can be placed, to block the remaining laser light that still passes the dichroic mirror. The notch filters are followed by a tube lens ($f=300$ mm, L3). This lens is positioned such that an image of the sample on the microscope table is created on both cameras.



figure 5.2: Photograph of the polarizing beam splitter (left) and the polarizer, placed in the rotation mount (right)

The light is then separated into two directions by a polarizing beam splitter cube (Thorlabs, PBS251, PBS in figure 5.1). A photograph of the polarizing beam splitter can be seen in figure 5.2 (left). When the polarizer is aligned properly, the transmitted light has a polarization parallel to the excitation light and the reflected light has a polarization perpendicular to the excitation light. This can of course be interchanged by rotating the polarizer over 90 degrees. For detecting the fluorescence intensity images, two EMCCD cameras (Andor, iXon^{EM+}, DV897) are used; one for the light transmitted by the polarizing beam splitter cube and one for the reflected light. The polarization of the detected light by the cameras with respect to the polarization of the excitation light is indicated with the arrows in figure 5.1.

The image recorded with the camera that detects the light reflected from the polarizing beam splitter is inverted with respect to the images recorded with the other camera. This should be corrected in the camera software, or manually after the measurements. In front of the beam splitter a band pass filter (F1 in the figure) can be placed, to only look at the emission light of the fluorescent probe. The transmission of the band pass filter should match the emission spectrum of the used fluorescent probe.

5.2 Implementation of polarization microscope

The fluorescence polarization microscope is implemented in the existing fluorescence microscope. This is partly done by positioning a polarizer in the path to the microscope that is followed by the laser light. An important parameter that needs to be considered before selecting the polarizer is the

wavelength range that can be polarized. Since excitation lasers with wavelengths of 473, 532 and 640 nm are present, a polarizer should be used that can polarize light with these wavelengths. The size of the polarizer is also important, since it should match the radius of the laser beam in the setup. The linear polarizer LPVISE100-A supplied by Thorlabs has the mentioned properties. The extinction ratio of this polarizer equals approximately 10^4 , which is high enough for this application.

A polarizing beam splitter is also added to the fluorescence microscope. Light with wavelengths that can be split by the polarizing beam splitter should match the emission wavelength range of the fluorophores that can be excited by the excitation lasers. This wavelength range is from 480 nm to approximately 720 nm. The polarizing beam splitter PBS251 supplied by Thorlabs is suitable for this application. In the mentioned wavelength range the reflectance and transmission of s-polarized light by the PBS251 polarizing beam splitter are close to 100% and 0% respectively. The reflectance and transmission of p-polarized light are close to 5% and 95% respectively.

Initially, before the implementation of the polarization microscope, the emission filters were placed right in front of the two cameras. Since only one filter of each type is present, the emission filters are positioned in front of the polarizing beam splitter instead of in front of the two cameras. This is possible, since no dual color microscopy is performed with the polarization microscope.

5.3 Calibration procedures and setup verification

This section discusses the calibration procedures that are necessary to calculate anisotropy images with the polarization setup described earlier. All measurements in this chapter are done using a 100x water immersion objective with an NA of 1.20. The routines that are used to apply the calibration processes to the recorded images are shown in appendix A.

5.3.1 Image alignment of the two cameras

In fluorescence anisotropy imaging experiments the light emitted by the sample is separated by the polarizing beam splitter into two components. Light with a certain polarization is reflected by the polarizing beam splitter and detected by one camera. Light with a polarization that is perpendicular to the reflected light polarization will be transmitted by the polarizing beam splitter and detected by the other camera. Thus two images are recorded from the same sample with the two cameras at the same time. Because the intensity per pixel for both cameras is required to calculate an anisotropy value, an overlay of both images is needed with sub-pixel precision. This is done with a sample of fluorescent beads excited by the 532 nm laser. The polarizing beam splitter is positioned such that the same beads are approximately on the same pixels on both cameras. Since the incoming laser beam is circularly polarized, both cameras approximately detect an equal amount of photons. In front of the beam splitter cube a 580/60 band pass filter is placed.

In figure 5.3 A an image of the beads recorded with one of the cameras is shown and figure 5.3 B shows an image of the same beads recorded with the other camera. In figure 5.3 C the sum of both images is shown. From this image it can be seen that the images do not overlay exactly (see figure 5.3 D). With functions *fmmatch*, *find_affine_trans* and *affine_trans* from the *dip_image* toolbox¹⁹ a transformation of one image can be calculated and performed, such that the overlay is perfect. This can be seen in figure 5.3 E and F. These figures show the sum of the corrected images from both cameras. The function *fmmatch* roughly calculates a zoom, translation and rotation for one of both images. The function *find_affine_trans* then needs the roughly calculated zoom, translation and rotation as input and calculates a zoom, translation and rotation more accurately. The function *affine_trans* then performs a transformation on one figure such that both figures correctly overlay.

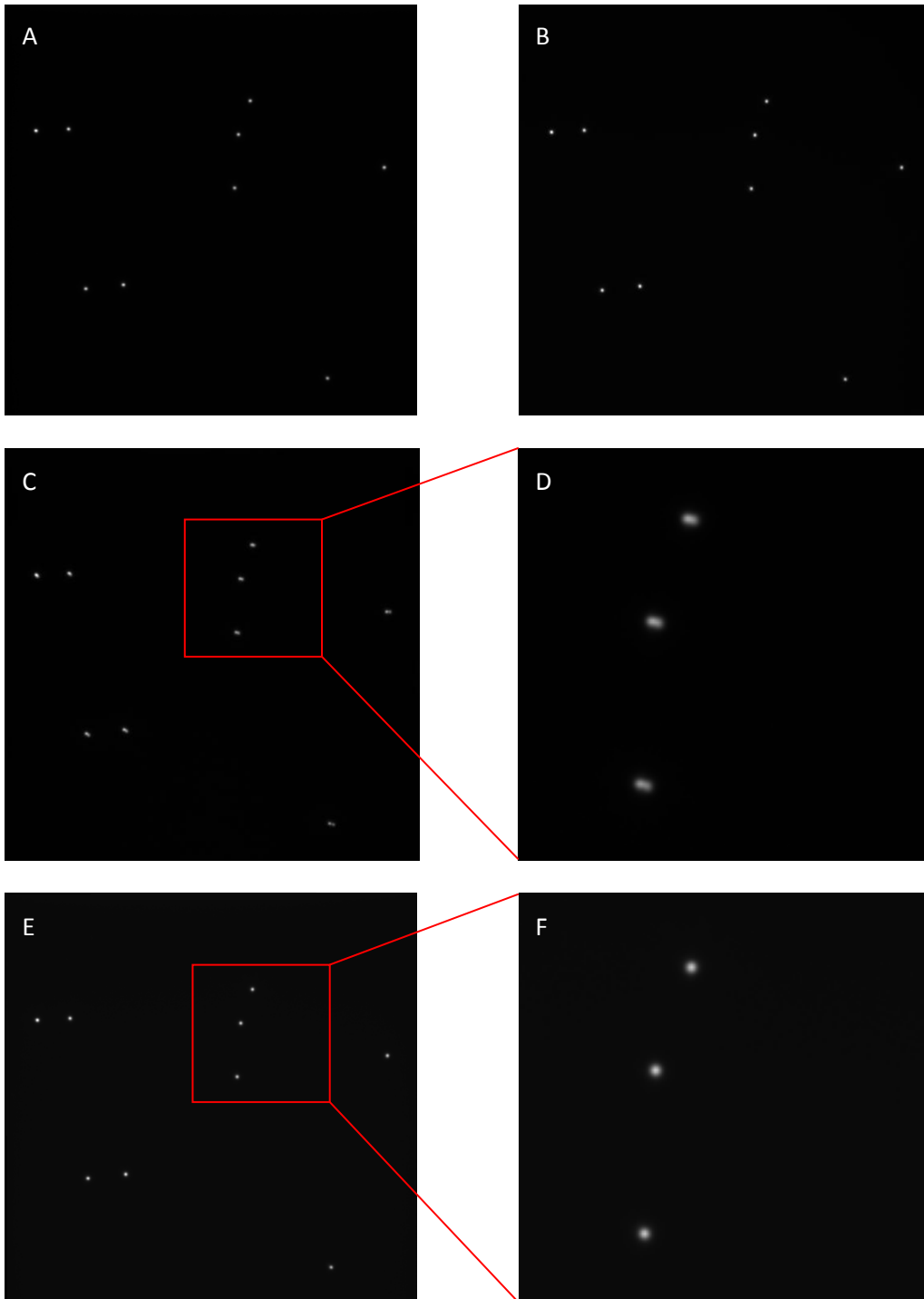


figure 5.3: Fluorescent beads detected by camera in transmitting direction of beam splitter (A), in reflecting direction (B), both images in one figure (C), magnified part of this figure (D), both images in one figure after translation of one image (E) and a magnified part (F).

In this case of the figures shown the correction factors are: 1.0048 , 1.0025 (horizontal and vertical zoom), -3.0355 , -1.1007 (horizontal and vertical shift) and -0.0036 (rotation). This procedure must be repeated each time one of the cameras or the polarizing beam splitter is moved. Now after every anisotropy measurement, one of the images must be transformed with the function *affine_trans* using the correction factors determined from the bead alignment to overlay both images.

5.3.2 Background correction

When anisotropy images are recorded of a sample of interest, a correction for the background intensity and baseline is performed. The sample of interest is usually present in a solvent. The background correction is done by recording the parallel and perpendicular emitted intensities of the solvent only upon excitation by polarized light. The background corrected parallel intensity ($I_{\parallel,back_cor}^i$) measured from the sample of interest is given by:

$$I_{\parallel,corrected}^i = I_{\parallel}^i - \langle I_{\parallel,back}^i \rangle \quad \text{eq. 5.1}$$

Here I_{\parallel}^i is the parallel intensity measured from the sample of interest. $\langle I_{\parallel,back}^i \rangle$ is the average parallel intensity measured from the solvent only. For the measured perpendicular intensity this procedure is also followed.

5.3.3 Calibration with a reference dye

In fluorescence anisotropy measurements the perpendicular intensity and parallel intensity need to be determined, as described in chapter 2. Because both values are measured with a different camera, a calibration factor (G) is determined to correct for a difference in sensitivity of the cameras for different light polarizations. This factor also corrects for differences in sensitivity of the setup components to different light polarizations. This factor can be determined by measuring the perpendicular and parallel background corrected intensities of a fluorophore in solution with known anisotropy value. G is then given by:

$$G^i = \frac{I_{\parallel}^i(1 - r_{ref})}{I_{\perp}^i(1 + 2r_{ref})} \quad \text{eq. 5.2}$$

Here r_{ref} is the known anisotropy of the fluorophore used for the calibration measurement, and I_{\parallel} and I_{\perp} are the background corrected parallel and perpendicular intensities respectively. The superscript i indicates that the calculation is done for each pixel. This G -image is then smoothed with a Gaussian filter with a box size of 8 by 8 pixels and a standard deviation of 3 pixels to eliminate statistical noise in individual pixels. The average parallel intensity measured in the absence of the fluorophore is then subtracted from the average parallel intensity measured in the presence of the fluorophore. This is also done for the perpendicular intensities.

After this calibration the anisotropy per pixel can be calculated from experiments using the following equation:

$$r^i = \frac{I_{\parallel}^i - G^i I_{\perp}^i}{I_{\parallel}^i + 2G^i I_{\perp}^i} \quad \text{eq. 5.3}$$

Here I_{\perp} and I_{\parallel} are the background corrected intensities. The factor G is calculated from a measurement of a solution of fluorescein in phosphate buffered saline (PBS). For this a 514/30 band pass filter is used. This fluorophore should have an anisotropy value close to 0 because fluorescein is a small fast rotating dye and has a long lifetime (4.1 ns). Also at concentrations of 10 μM or lower, no FRET occurs between the fluorescent molecules. In figure 5.6 the average uncorrected ($G=1$) value of the anisotropy for different concentrations of fluorescein are shown and figure 5.7 also shows the average uncorrected anisotropy values of Oregon green for different concentrations (lifetime: 4.1 ns). The average values are calculated from a part in the centre of the background corrected anisotropy images. Since the lifetime and size of both fluorophores are similar, the anisotropy of

both fluorophores in solution should be identical. It can be seen in the figures that this is indeed the case for concentrations of 6 and 10 μM . For 1 μM concentrations a small deviation is seen. This can be caused by the short integration time that is used. When a longer acquisition time is used, the average value for this concentration might also be equal to the measured anisotropy values for higher concentrations.

From the uncorrected anisotropy images a G-factor can be calculated per pixel with eq. 5.2. It is important to note that the G-factor should be determined with a fluorescent dye with a known anisotropy value, and with the same experimental components such as filter and objective, as the sample is measured. Therefore, when a sample is measured with a fluorescent probe that has a different emission spectrum than Oregon green or fluorescein, also a different calibration dye should be used. For example rhodamine 6G (lifetime of 4.08 ns) can be used when excitation is done with the 532 nm laser. The reference anisotropy value for Oregon green was measured by Squire et al.²⁰ on a spectrofluorometer and found to be 0.012 ± 0.002 . The reference anisotropy of Rhodamine 6G was also measured previously and found to be 0.012 as well by Ganguly et al.²¹ In figure 5.4 and figure 5.5 the absorption and emission spectra of fluorescein, Oregon green and Rhodamine 6G are shown.

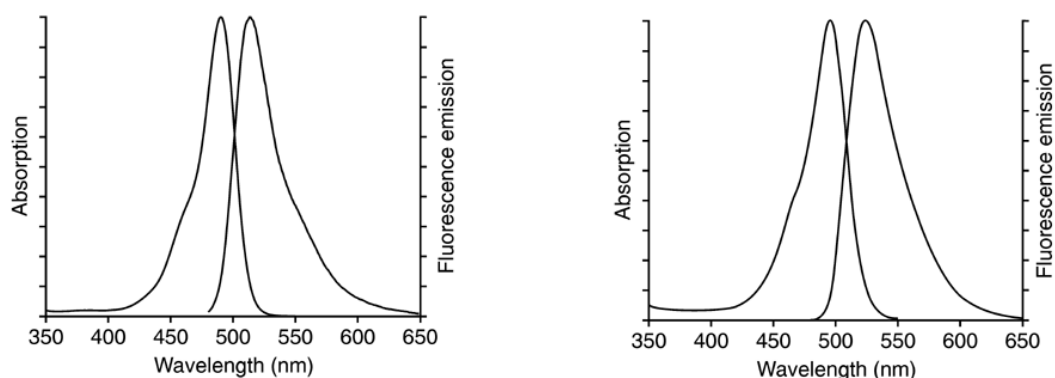


figure 5.4: Absorption and emission spectrum of fluorescein (left) and Oregon green (right). Images taken from [22]

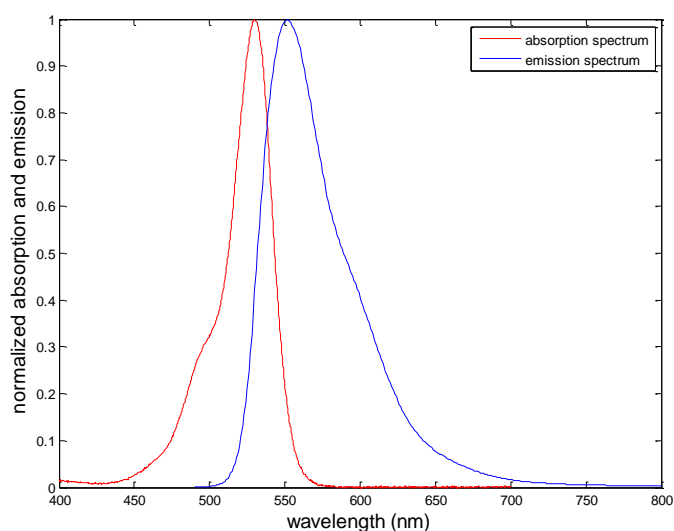


figure 5.5: Normalized absorption and emission spectrum of Rhodamine 6G

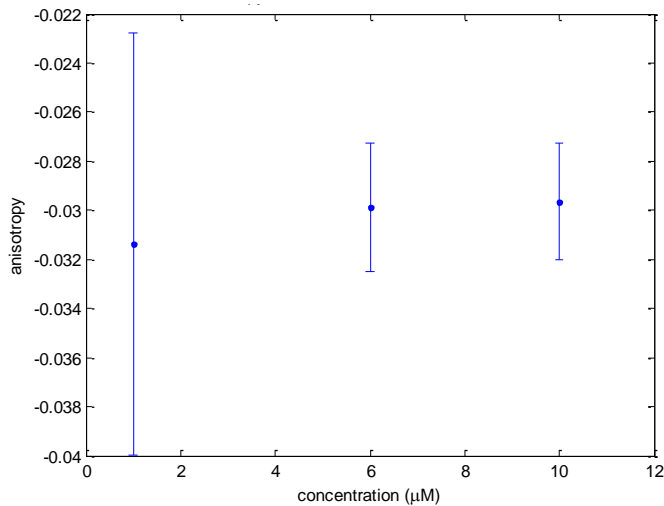


figure 5.6: Measured uncorrected anisotropy of several concentrations of fluorescein in PBS

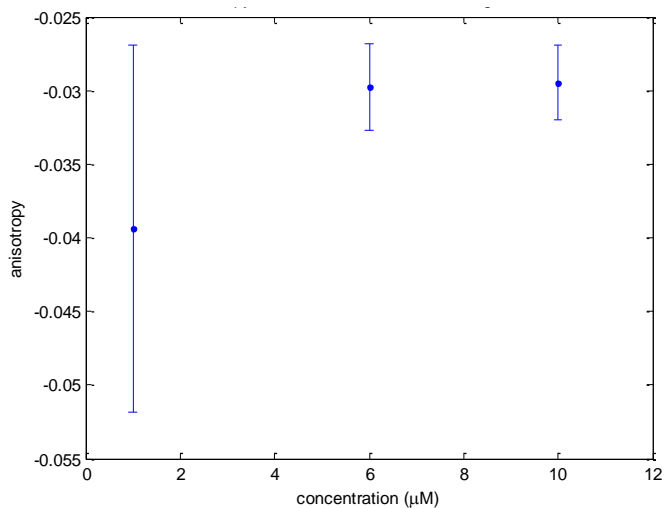


figure 5.7: Measured uncorrected anisotropy of several concentrations of Oregon green dissolved in PBS

5.3.4 Gain calibration

Anisotropy measurements in live cells are done with EM gain values. Because two different cameras are used, there may be a difference in gain between both cameras, even when both selected gain values are the same. This difference can be quantified by measuring the uncorrected anisotropy values of a solution of 10 μM fluorescein at different gain values. The graph in figure 5.8 show the average uncorrected anisotropy for different gain values, including the standard deviation obtained from several pixels in the image. It can be seen that there is a difference in gain between both cameras, because the measured uncorrected anisotropy increases with gain. If the real gain values were identical for both cameras, the measured anisotropy should not vary with gain value.

To circumvent a gain problem, a G-factor calibration is done at the same gain as used during the actual measurement. This way the G-factor also corrects for differences in gain between both cameras. This will be shown now.

When the measured I_{\parallel}^i and I_{\perp}^i are not the actual emitted parallel and perpendicular intensities because there is an influence of a difference in gain between both cameras, the factor $gain^i$ in eq.

5.4 corrects for this difference. In eq. 5.5 the perpendicular intensity is corrected with the factor $gain^i$ such that the anisotropy values are calculated correctly.

$$gain^i = \frac{I_{\parallel}^i}{I_{\perp}^i} \quad \text{eq. 5.4}$$

$$r^i = \frac{I_{\parallel}^i - G^i gain^i I_{\perp}^i}{I_{\parallel}^i + 2G^i gain^i I_{\perp}^i} \quad \text{eq. 5.5}$$

In this equation G^i is the correction factor that only corrects for differences in responses of the setup for light with different polarizations. Now a new G-factor is defined:

$$G_{new}^i = G^i gain^i \quad \text{eq. 5.6}$$

This G_{new}^i is exactly the G-factor that is determined with eq. 5.2, when the calibration measurement is done at the exact same gain values on the cameras as used during the actual measurement.

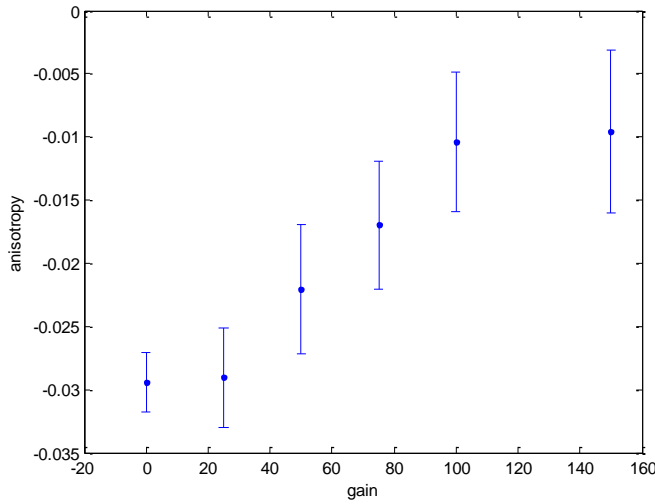


figure 5.8: Measured uncorrected average anisotropy of a solution of 10 µM fluorescein for different gain values. Standard deviations are also shown.

5.3.5 Polarizer alignment

In anisotropy measurements it is necessary that the polarization of the excitation light is parallel to the polarization of the light that is totally reflected or totally transmitted by the polarizing beam splitter. The alignment of the polarizer is done by measuring a sample of the fluorescent protein mStrawberry dissolved in 25 % glycerol and 75 % tris buffer. Anisotropy measurements are done for different angles of the polarizer. The different angles are shown on the scale bar of the rotation mount that contains the polarizer (see figure 5.2). Measurements on this sample should result in an anisotropy that is maximal when the polarizer is perfectly aligned with respect to the polarizing beam splitter. This is the case when the total intensity emitted by the fluorophores with identical polarization as the excitation light will be detected by one camera and the total emitted intensity with polarization perpendicular to the excitation light will be detected by the other camera. The anisotropy decreases when the angle between the polarizer and the polarizing beam splitter cube increases. When this angle is exactly 45 degrees, the measured anisotropy should be 0.

In this experiment the anisotropy values are always calculated as follows:

$$r = \frac{I_{cam1} - I_{cam2}}{I_{cam1} + 2I_{cam2}} \quad \text{eq. 5.7}$$

Here I_{cam1} and I_{cam2} are the measured corrected intensities on camera 1 and camera 2 respectively. The intensities measured on both cameras depend on the orientation of the polarizer and can be given by the following equations:

$$I_{cam1} = (\cos(\theta - \theta_{max}))^2 I_{\parallel} + (\sin(\theta - \theta_{max}))^2 I_{\perp} \quad \text{eq. 5.8}$$

$$I_{cam2} = (\sin(\theta - \theta_{max}))^2 I_{\parallel} + (\cos(\theta - \theta_{max}))^2 I_{\perp} \quad \text{eq. 5.9}$$

Thus eq. 5.7 can be written as follows:

$$r = \frac{(2(\cos(\theta - \theta_{max}))^2 - 1)I_{\parallel} + (2(\sin(\theta - \theta_{max}))^2 - 1)I_{\perp}}{(1 + (\sin(\theta - \theta_{max}))^2)I_{\parallel} + (1 + (\cos(\theta - \theta_{max}))^2)I_{\perp}} \quad \text{eq. 5.10}$$

The set position of the polarizer is defined by θ . The unknown position for which the polarizer is perfectly aligned with the polarizing beam splitter is defined as θ_{max} in this equation. At this angle the measured anisotropy as defined in eq. 5.7 is maximal. Here I_{\parallel} and I_{\perp} are the parallel and perpendicular polarized intensities emitted by the fluorophores with respect to the excitation light. These quantities are unknown in this equation. A parallel polarization here means a polarization in the same direction as the polarization of the excitation light. In figure 5.9 the measured anisotropy as a function of polarizer position is shown. This figure also shows a fit to eq. 5.10. From this fit θ_{max} was found to be 178.1 ± 0.4 degrees. Here 0.4 indicates the 95 % confidence interval of the fit. From the fit the ratio between I_{\parallel} and I_{\perp} is also determined. From this ratio the anisotropy of the fluorescent protein mStrawberry was found to be 0.314 ± 0.007 . When anisotropy experiments are performed, the polarizer should always be at the determined angle of 178.1 degrees to give the best results.

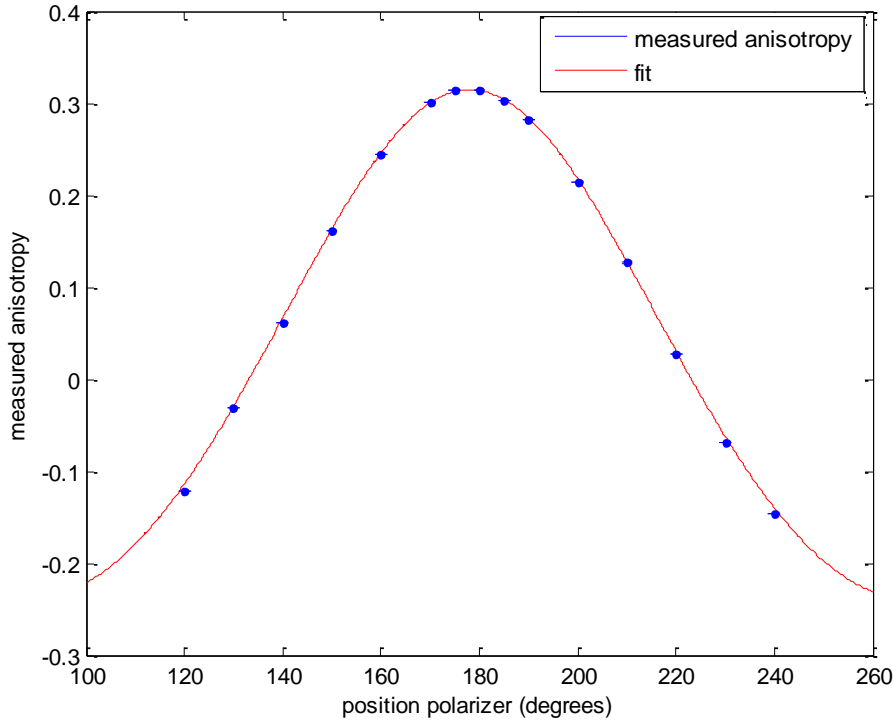


figure 5.9: Measured anisotropy as a function of polarizer angle of the fluorescent protein mStrawberry dissolved in 75%/25% buffer/glycerol.

5.3.6 Effect of numerical aperture on measured anisotropy

As mentioned by Bader et al.¹³, the use of a high numerical aperture (NA) objective results into an underestimation of anisotropy values. This is caused by the fact that a fluorophore that has a low probability of being excited by low NA excitation light, can be excited with a higher probability by a high NA excitation light. This fluorophore then might emit fluorescent light that follows the path to the objective in a low NA direction. This way the detected emission has a higher component with a polarization perpendicular to the excitation light, such that the measured anisotropy decreases. It is advised in the literature²³ that a low numerical aperture should be used, to prevent underestimation of the average anisotropy. This however also reduces the amount of detected emission intensity.

To verify this effect, a sample of 50 μM EGFP is dissolved in approximately 55%/45% glycerol/buffer is prepared and the average anisotropy of this sample is measured for two values of the numerical aperture. This is shown in figure 5.10. From this figure it can be seen that we do not observe that the average anisotropy changes much as a function of numerical aperture. However, since literature shows that numerical aperture certainly has an influence, this will be considered in the experiments.

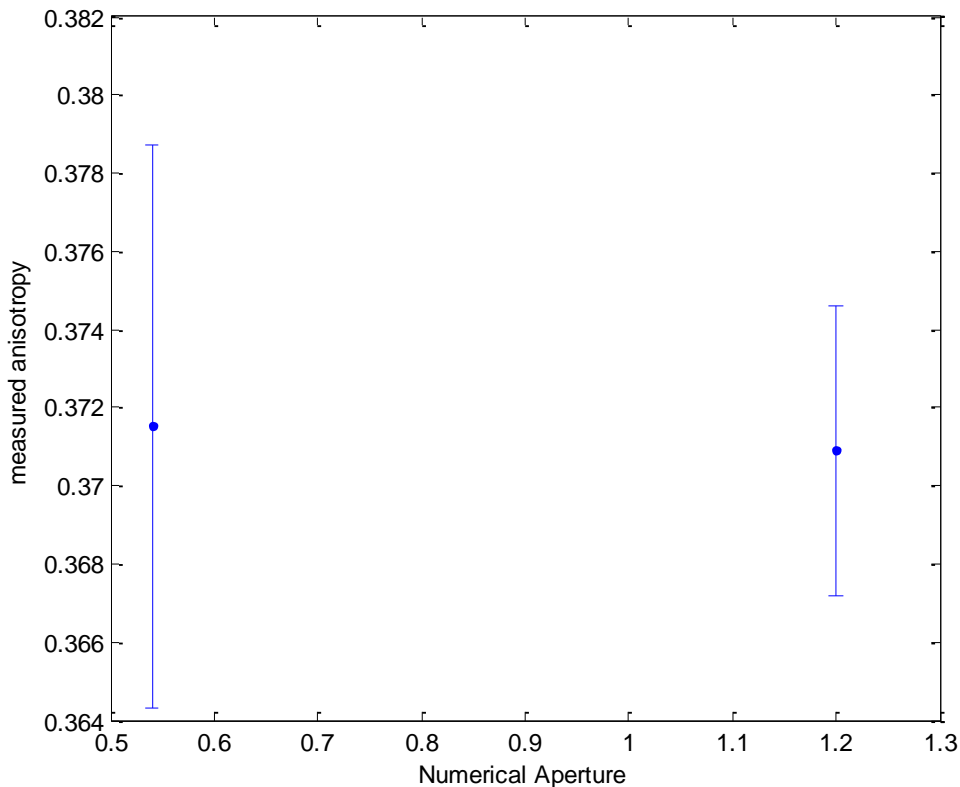


figure 5.10: Measured average anisotropy of 50 μM EGFP as a function of numerical aperture.

5.3.7 Anisotropy of EGFP in glycerol

To verify the anisotropy microscopy setup and the calibration methods, anisotropy measurements are done on a solution of EGFP in two different concentrations of glycerol and buffer. In table 5.1 the measured average anisotropies including standard deviations are shown for two different concentrations of glycerol. These average values and standard deviations are calculated from the sum of several pixels in the measured perpendicular and parallel intensity images. Since glycerol is viscous, rotation of EGFP is minimized when dissolved in glycerol. Thus for increasing concentrations of glycerol the measured average anisotropy should increase. The measured anisotropy values are

close to the values measured by Bader et al.¹³ which is 0.382 for GFP in 50%/50% glycerol/ buffer. Small deviations may be caused by the use of a higher numerical aperture objective or temperature effects.

	50 % glycerol	65 % glycerol
Measured anisotropy	0.366 ± 0.009	0.391 ± 0.010

table 5.1: measured anisotropy of 50 μ M EGFP dissolved in different concentrations of glycerol

6 HeLa cells expressing mCitrine and mCitrine-mCitrine Proteins

In this chapter fluorescence lifetime and anisotropy experiments are performed on HeLa cells expressing the fluorescent protein mCitrine. The same experiment is also done on HeLa cells expressing a fusion protein that consists of two mCitrine fluorescent proteins connected by an aminoacid linker (mCitrine-mCitrine). Between the fluorescent protein domains in the last sample homo-FRET can occur, because in the fusion protein the two fluorescent parts (both mCitrine) are always close together. In figure 6.1 the absorption and emission spectrum of mCitrine are shown.

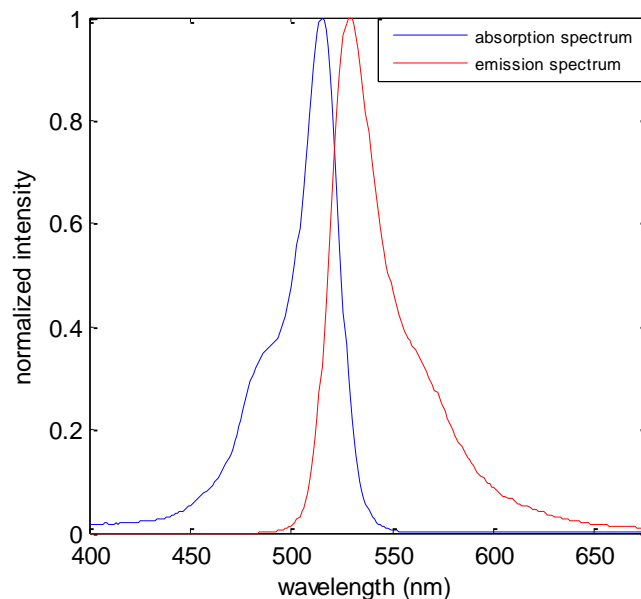


figure 6.1: Absorption and emission spectrum of the fluorescent protein mCitrine

It is expected, according to the calculation presented in chapter 2, that the fluorescence lifetime of the double mCitrine proteins is not different from the lifetime of the single mCitrine fluorescent proteins. It is also expected that the measured anisotropy of the double mCitrine proteins should be lower than the anisotropy of the single mCitrine fluorescent protein, because homo-FRET decreases the measured anisotropy. When the double mCitrine proteins are photobleached, the anisotropy should increase, because in some double mCitrine proteins one of the mCitrine parts will be photobleached. This means FRET cannot occur between the mCitrine parts in this particular protein.

The anisotropy experiments in this chapter are mainly done to verify that homo-FRET between mCitrine fluorescent proteins can be detected with the polarization microscope and that mCitrine can be used as a probe for homo-FRET.

6.1 Photobleaching of fluorescent protein dimers

In the anisotropy experiments in this chapter HeLa cells expressing the double mCitrine proteins are photobleached. When the sample is photobleached, and FRET occurred between the mCitrine parts in the HeLa cells, the anisotropy of the sample should increase. The anisotropy that is measured after photobleaching is a linear combination of the anisotropy corresponding to the fraction of double mCitrine proteins that have one mCitrine photobleached and the anisotropy corresponding to the fraction of double mCitrine proteins that have no mCitrine photobleached. These fractions depend on the photobleached fraction (f_{bleach}) in the sample, which defined here as the amount of photobleached mCitrine parts divided by the total amount of mCitrine parts.

The measured average anisotropy of a sample that contains two different anisotropy values can be written as follows:

$$r_{sum} = \frac{I_{mono}}{I_{mono} + I_{di}} r_{mono} + \frac{I_{di}}{I_{mono} + I_{di}} r_{di} \quad \text{eq. 6.1}$$

Here I_{mono} is the total intensity emitted by the double mCitrine proteins of which exactly one mCitrine is photobleached (called monomer from now on). I_{di} is the total intensity emitted by the double mCitrine proteins of which both mCitrine parts are not photobleached (called dimer further on). The ratio in the equation is such that the sum of all contributions equals 1. In this equation r_{mono} is the average anisotropy value that would be measured if every mCitrine dimer that is present has exactly one mCitrine photobleached. r_{di} is the anisotropy that would be measured if no photobleaching occurred yet.

In the equation above I_{mono} and I_{di} can be written as follows:

$$I_{mono} = \frac{P_{mono}}{2P_{di} + P_{mono}} \quad \text{eq. 6.2}$$

$$I_{di} = \frac{2P_{di}}{2P_{di} + P_{mono}} \quad \text{eq. 6.3}$$

Here P_{mono} is the fraction of monomer molecules that have one photobleached mCitrine. P_{di} is the fraction of dimer molecules that have no photobleached mCitrine. The factor 2 accounts for the fact that the mCitrine dimer emits twice the intensity emitted by a monomer. The expression for P_{mono} and P_{di} can be given by:

$$P_{mono} = (1 - f)f + f(1 - f) \quad \text{eq. 6.4}$$

$$P_{di} = f^2 \quad \text{eq. 6.5}$$

where f is the labeled (unbleached) fraction and is defined as $1 - f_{bleach}$. f can also be described as the non-photobleached fraction.

In eq. 6.5 P_{di} represents the probability that an mCitrine-dimer has both mCitrine parts not photobleached, as a function of bleached fraction. There is also a probability that an mCitrine dimer has both mCitrine part photobleached (P_{zero}), however, this quantity is not relevant since no fluorescence is emitted by these dimers.

Now the labeled fraction f is calculated by dividing the total intensity in a partially photobleached image by the intensity in the non-photobleached image. It should be noted that the total intensity in an image is calculated as:

$$I_{tot} = I_{\parallel} + 2I_{\perp} \quad \text{eq. 6.6}$$

This accounts for the fact that only light with one of the two perpendicular polarization directions is detected in anisotropy experiments. If the total intensity is calculated by simply adding the parallel and perpendicular intensities, the bleached fraction is not calculated correctly.

In the equations above it is assumed that the photobleaching rates of mCitrine is equal, independent of the fact that it is present in a dimer or a monomer. After combining eq. 6.2 - eq. 6.5 and substituting in eq. 6.1, the result is:

$$r_{sum} = (1 - f)r_{mono} + fr_{di} \quad \text{eq. 6.7}$$

6.2 Experimental procedure

In this section the experimental procedures followed to do the mentioned lifetime and anisotropy experiments are explained. The procedures consist of sample preparation methods, fluorescence lifetime imaging and fluorescence anisotropy imaging.

6.2.1 Sample preparation

HeLa cells were plated on 2 cm² cover chambered glass dishes and transfected at a confluency of 50% using the effectene transfection reagent kit supplied by Qiagen. 200 ng of plasmid DNA was used per well, with 1.6 μ L enhancer and 5 μ L effectene reagent. The procedure was carried out according to the standard protocol supplied by the manufacturer. The HeLa cells were transfected in penicillin/streptomycin free Dulbecco's modified eagle medium supplemented with 10% fetal bovine serum. After 12 hours the medium containing the plasmid DNA was removed and replaced with DMEM containing 10% FBS and 1% PS. Before fluorescence imaging is performed, the medium is replaced with PBS with calcium and magnesium to reduce the background fluorescence that would be present if DMEM is used.

6.2.2 Fluorescence lifetime imaging

The fluorescence lifetime images are recorded with a Lamberts' instruments LIFA microscope attachment using a 40x objective (Nikon plan Fluor 40x/0.75). The fluorescence lifetime measurements are done in the frequency domain. A 468 nm LED is used as excitation source. A 470/40 band pass filter is used as excitation filter and a 520 LP filter is used as emission filter. A 505 LP dichroic mirror is used. The system response is calibrated by using a 10 μ M solution of rhodamine 6G in water. Rhodamine 6G has a known lifetime of 4.011 ns. All lifetime images are recorded with the lightsource modulated at 20 MHz.

6.2.3 Fluorescence anisotropy imaging

The fluorescence anisotropy images are recorded with the setup described in chapter 3. The excitation source is a LED (LedEngin, LZ100G100). A 490/40 excitation filter, a 515 long pass dichroic mirror and a 550/40 emission filter are used. The same objective as used for the lifetime imaging experiments is also used here. The exposure time of the cameras is 1 s and the used gain is 30 for both cameras. Calibration is performed by the standard calibration procedure described earlier. For this procedure Rhodamine 6G is used as a reference dye. An estimation of the background intensity was done by selecting a region in the image where no fluorescent cells were visible.

6.3 Results and discussion

This part of this chapter shows the results from the fluorescence lifetime experiments and fluorescence anisotropy experiments on HeLa cells expressing mCitrine and mCitrine-mCitrine.

6.3.1 Effect of homo-FRET on the measured fluorescence lifetime

In order to compare the fluorescence lifetimes of single mCitrine and double mCitrine proteins, fluorescence lifetime images are measured of HeLa cells expressing mCitrine and HeLa cells expressing double mCitrine proteins. Both plasmids encoding for the mCitrine proteins are expressed in the cytosol of the cells. The results from the lifetime experiments are shown and discussed here. From these results we are able to conclude whether there is a difference in fluorescence lifetime between both proteins.

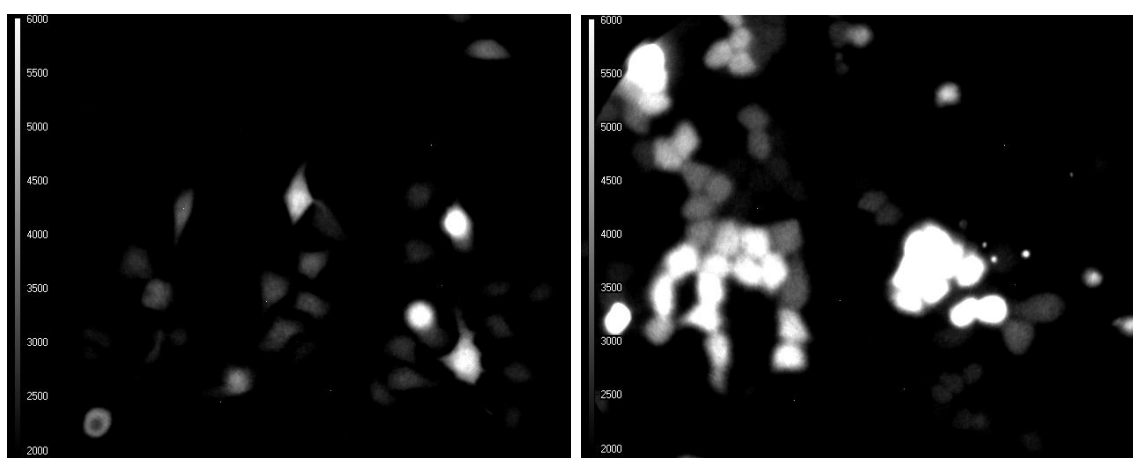


figure 6.2: Fluorescence intensity image of HeLa cells expressing the fluorescent protein mCitrine (left). These figures show the selected region of interest as well. Fluorescence intensity image of HeLa cells expressing the double mCitrine proteins.

In figure 6.2 shows the fluorescence intensity images of HeLa cells expressing mCitrine (left) and double mCitrine (right) are shown. The corresponding phase lifetime images are shown in figure 6.3. These figures are made by applying an intensity threshold on the intensity image to discard the pixels in the phase lifetime image that form the background. The intensity thresholds are selected such that the phase and modulation lifetime histograms do not look skewed. Also a region of interest is selected in the lifetime image. Only the pixels located in this region will be used for the calculation of the average phase and modulation lifetime of the sample.

From the modulation lifetime histograms of the HeLa cells expressing mCitrine and mCitrine-mCitrine shown in figure 6.3, it can be seen that the histogram for the mCitrine is broader than the lifetime histogram of mCitrine-mCitrine. This is caused by the fact that the images of the HeLa cells expressing mCitrine show lower fluorescence intensity than the images of HeLa cells expressing double mCitrine (see figure 6.2). The lifetime in each pixel will be closer to the mean fluorescence lifetime of the entire sample when more fluorescent molecules contribute to the fluorescence emission detected in each pixel. From the histograms the average phase lifetimes were calculated for both samples and presented in table 6.1. The average value for the modulation lifetime is also shown in table 6.1.

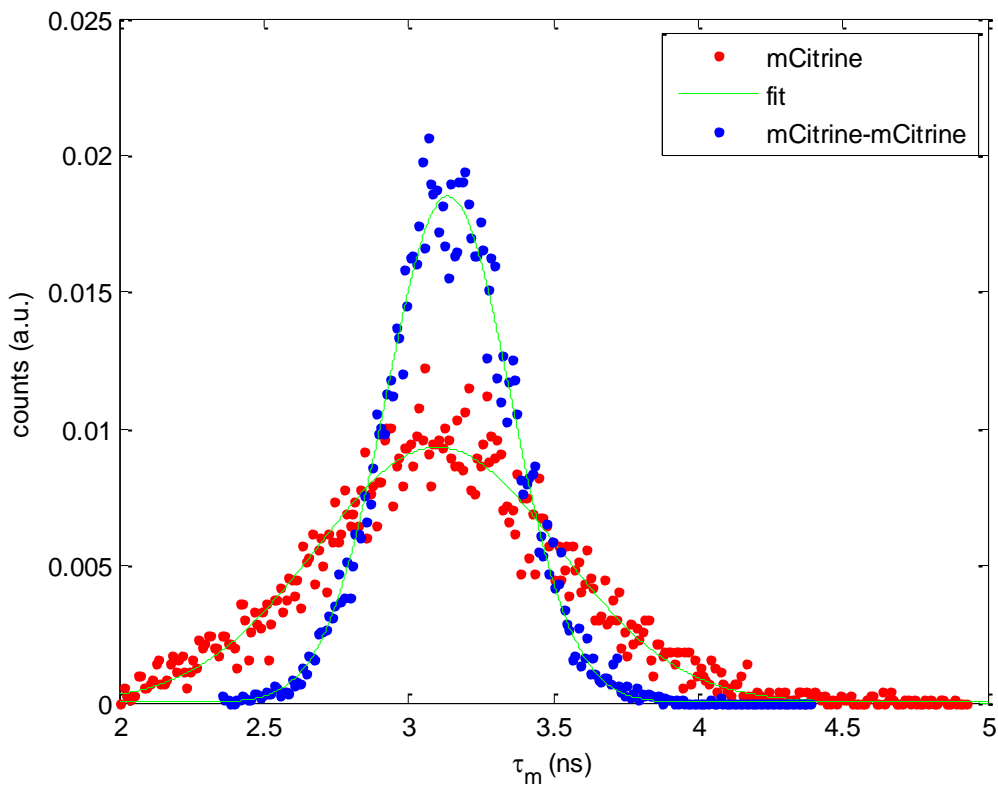
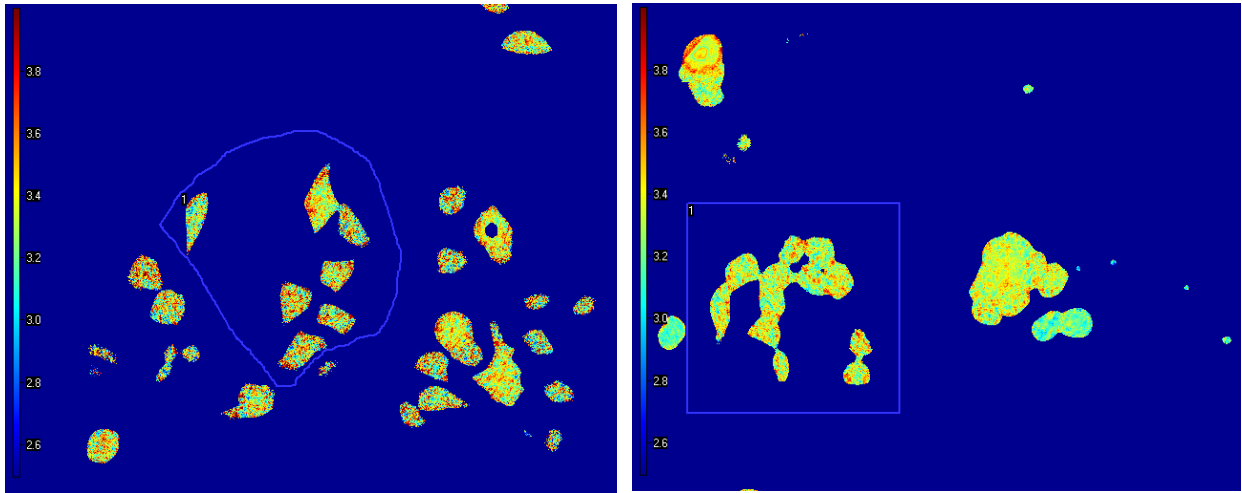


figure 6.3: Phase lifetime image of HeLa cells expressing the fluorescent protein mCitrine (upper left). Phase lifetime image of HeLa cells expressing the double mCitrine protein (upper right). An intensity threshold is applied to discard the pixels in the region with low fluorescence intensity. Histogram of the modulation lifetime (τ_m) of the HeLa cells expressing mCitrine and the HeLa cells expressing mCitrine-mCitrine (lower figure). The histograms are calculated from the modulation lifetime of the selected pixels shown in the upper figures. The histograms are fit to the normal distribution function.

	τ_ϕ (ns) (\pm s.e.)	τ_m (ns) (\pm s.e.)
mCitrine	3.370 ± 0.006	3.102 ± 0.010
mCitrine-mCitrine	3.341 ± 0.002	3.137 ± 0.004

table 6.1: measured average phase and modulation lifetimes from HeLa cells expressing mCitrine and mCitrine-mCitrine.

The average phase and modulation lifetimes calculated from the histogram are almost identical in both samples. There is a small difference between the lifetimes measured from the different samples. However, this can also be caused by the fact that no correction is done for differences in

intensities per pixel. Each pixel in figure 6.3 has an equal contribution, independent of the intensity in that pixel. When this correction is done, small changes in lifetime values may occur. Also, the fluorescence intensity of the HeLa cells expressing mCitrine is lower compared to the intensity of HeLa cells expressing double mCitrine as can be seen in figure 6.2. This means that the contribution of background intensity and autofluorescence of the cells is higher in the mCitrine fluorescence images than in the double mCitrine fluorescence images. This could also cause small changes in the mean phase and modulation lifetime.

Since homo-FRET can occur in the double mCitrine proteins (as will be shown with anisotropy experiments presented in this chapter as well) we can conclude that homo-FRET cannot be detected by changes in the fluorescence lifetime of the donor. This confirms the calculations on the relation between lifetime and homo-FRET presented in chapter 3.

Since the phase and modulation lifetimes are not equal, it can be concluded that the fluorescence emission of mCitrine does not show a single exponential decay behavior. To determine the lifetimes for the multi-exponential decay, fluorescence lifetime images should be recorded for different modulation frequencies. However, we are not interested in the exact values of the lifetime components, but only in the differences in lifetime between both samples.

6.3.2 Effect of homo-FRET on the measured fluorescence anisotropy

To verify that homo-FRET indeed occurs between the mCitrine-mCitrine proteins and can be observed with the polarization microscope, anisotropy images of the HeLa cells expressing mCitrine and the HeLa cells expressing double mCitrine are recorded.

In figure 6.4 a fluorescence intensity image of HeLa cells expressing the double mCitrine proteins are shown. The intensity values in this image per pixel are the sum of the intensities per pixel of the parallel and perpendicular images. In figure 6.5 the anisotropy images for several label fractions are shown.

Label fraction is defined as the sum of the intensity of the 200 highest pixel values in the selected region divided by the sum of the intensity of the 200 highest pixel values in the selected region in the first image. This was done to obtain a fair estimate of the decrease in intensity per image and to circumvent the selection of an intensity threshold per image, as the intensity decreases due to photobleaching.

In the first image the photobleached fraction is assumed to be 0. In these images only the region of interest is shown. A color scale shows the corresponding anisotropy values per pixel in the image. The green measurement points in figure 6.8 show the average anisotropy value as a function of label fraction. Here it is assumed that the label fraction in the first image is 1. These measured average anisotropy values are calculated by selecting a region of the cells where the anisotropy values are homogeneously distributed. In figure 6.5 it can be seen that each image contains a region with no or a small gradient in the anisotropy values.

In figure 6.8 it can be seen that the average anisotropy before photobleaching is low, around 0.11. This low value can be caused by depolarization of the emission light due to homo-FRET, or by the fact that there is a large angle between the absorption and emission transition moment. Fast rotation of the fluorescent protein is not a cause for this low anisotropy value, because the rotational correlation time for fluorescent proteins is usually much longer than the fluorescence lifetime (~ 20 ns for the rotational correlation time²⁴). The average anisotropy value increases when the label fraction decreases after photobleaching. This effect shows that the low anisotropy values measured

before photobleaching are caused by homo-FRET between the mCitrine fluorescent proteins. The increase in anisotropy values after photobleaching is caused by the fact that in a dimer of mCitrine fluorescent proteins, one can be photobleached. As no FRET can occur in this molecule, the average anisotropy value of this specific molecule will be close to the value of single mCitrine fluorescent proteins.

The expression for the anisotropy as a function of label fraction in eq. 6.7 is fitted to the measured average anisotropy values in figure 6.8. This fit is shown in figure 6.8. From this fit the average anisotropy of mCitrine dimer was determined and equals 0.103 ± 0.008 and for monomers this equals 0.302 ± 0.008 . This is a change in anisotropy of approximately 0.20. In chapter 4 it was determined that the maximum decrease in anisotropy that can occur equals 0.20. This is only the case when an experiment satisfies the following conditions (or when monomers have an anisotropy of 0.40):

- Completely random orientation of fluorescent molecules
- No rotation of the fluorophores during the excited state lifetime
- No angle between the absorption and emission dipole orientation in the fluorophore

Since the anisotropy in the absence of homo-FRET equals 0.302 ± 0.008 , in this case, a change of 0.2 is more than expected. For a random orientation of the mCitrine parts with respect to the other mCitrine parts in the same protein, the lowest expected anisotropy for dimers equals 0.151 ± 0.004 when the anisotropy for monomers equals 0.302 ± 0.008 . The fact that a larger change of 0.20 is nonetheless observed in this case cannot be explained by the following causes:

- Rotation of the double mCitrine protein: Rotation will decrease the anisotropy values, but since homo-FRET does not change the lifetime of the entire sample, rotation has an equal effect on the measured anisotropy of the mCitrine proteins with two non-photobleached mCitrine parts and on the measured anisotropy of the mCitrine proteins with one photobleached mCitrine part. So for a completely random orientation, the minimum anisotropy that could be measured would still be 0.151 ± 0.004 .
- High excitation powers, such that two mCitrine parts in a double mCitrine fluorescent protein are excited simultaneously. This is not the case, since this would only increase the average anisotropy because no or less FRET occurs in this case.
- The fact that there is an angle between the absorption transition moment and the emission transition moment in mCitrine. It was shown using the simulations that an angle between the absorption and emission transition moment only results in a decrease lower than 0.2 when FRET occurs. For higher angles even an increase in the anisotropy values is expected.
- A wrong determination of the G-factor. If the G-factor is not determined correctly, the measured anisotropy values are different from the real values. However, if for example the value 0.302 ± 0.008 would be higher, then also the value 0.103 ± 0.008 would be higher. The difference in anisotropy values would then even be larger than 0.2. If the G-value should be lower, a smaller change is found. However, the anisotropy value of 0.302 ± 0.008 for monomers would also be much lower in this case, which would result in unreasonable low anisotropy values for monomeric fluorescent proteins.

Since for a completely random distribution of the fluorescent proteins in the sample it is highly unlikely that the average anisotropy of the double mCitrine protein can be lower than 0.151 ± 0.004 , we can conclude that the mCitrine parts in the protein have a nonrandom orientation with respect to the other mCitrine part in the same protein. The measured anisotropy (r_{meas}) of 0.103 ± 0.008 is a

combination of the anisotropy (r_{abs}) measured from the fluorescence emitted by the mCitrine part that absorbed the polarized excitation light (donor) and the anisotropy ($r_{non-abs}$) measured from the fluorescence emitted by the mCitrine part that was not excited, but received energy from the fluorophore that absorbed excitation light (acceptor):

$$r_{meas} = \frac{I_{abs}}{I_{abs} + I_{non-abs}} r_{abs} + \frac{I_{non-abs}}{I_{abs} + I_{non-abs}} r_{non-abs} \quad \text{eq. 6.8}$$

In this equation I_{abs} and $I_{non-abs}$ are the intensities emitted by the absorbing part and the non-absorbing part in the double mCitrine protein respectively, with $I_{abs} + I_{non-abs}$ normalized to 1. Since the FRET rates from the absorbing mCitrine part to the non-absorbing part is equal to the FRET rate for energy transfer vice versa under the assumption that the angles between the absorption and emission transition moment in mCitrine are close to 0, the factor $I_{non-abs}$ cannot be higher than I_{abs} . Using this we can calculate an upper boundary for the anisotropy that would be measured if we only detect emission by the non-absorbing mCitrine parts (acceptors), which is given by the following equation:

$$0.103 = \frac{1}{2} \cdot 0.302 + \frac{1}{2} \cdot r_{non-abs} \quad \text{eq. 6.9}$$

so $r_{non-abs}$ equals -0.096. This means that the emission by the fluorescent protein parts that did not absorb excitation light (the acceptors), has a stronger component with polarization perpendicular to the excitation light than parallel to the excitation light.

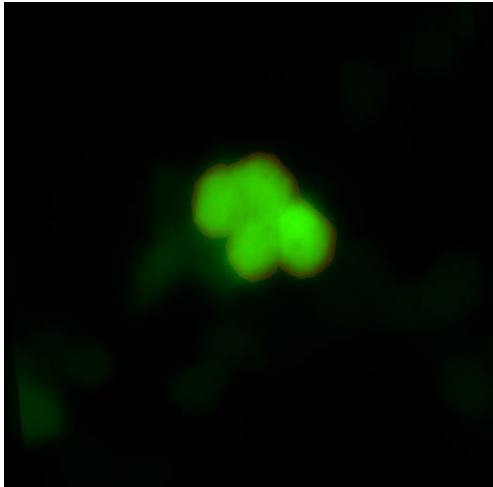


figure 6.4: Fluorescence intensity image of HeLa cells expressing the double mCitrine protein (green) and the region of interest used to make anisotropy images (red).

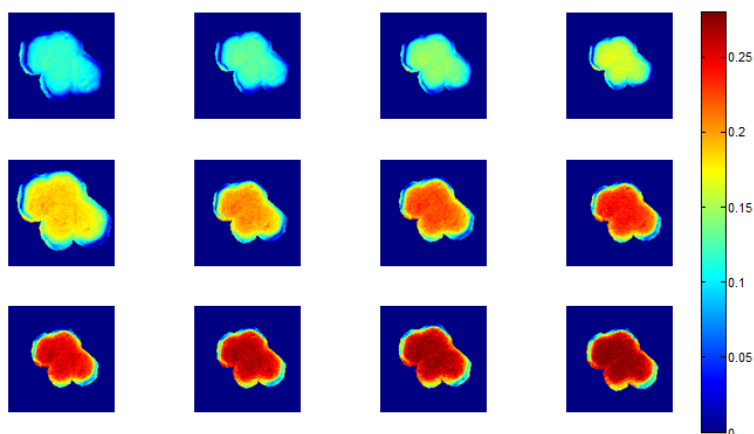


figure 6.5: Fluorescence anisotropy images of HeLa cells expressing the double mCitrine protein. From left to right the fluorescence intensity decreases due to photobleaching. The color bar indicates the anisotropy values according to the color shown in the image. The corresponding label fractions from left to right from top to bottom are the following: 1, 0.89, 0.80, 0.68, 0.55, 0.47, 0.39, 0.32, 0.27, 0.22, 0.19 and 0.16.

As a control, a similar experiment is performed on HeLa cells expressing single mCitrine fluorescent proteins. In this experiment it is expected that the average anisotropy is close to 0.302 ± 0.008 , it is also expected that this anisotropy value does not change after photobleaching.

In figure 6.6 the fluorescence intensity image of a HeLa cell expressing mCitrine is shown. In this figure also the region of interest is shown. This region of interest is used to make the anisotropy images shown in figure 6.7. The anisotropy images in figure 6.7 are recorded for several label fractions, by photobleaching the sample for a certain amount of time after each measurement. From these images it can be seen that the anisotropy values before photobleaching are higher compared to the anisotropy values measured on HeLa cells expressing mCitrine-mCitrine. This can be explained by the fact that no or less FRET occurs between the single mCitrine fluorescent proteins. Also after photobleaching, the average anisotropy value does not increase, so no FRET was occurring.

In figure 6.8 the average anisotropy values as a function of label fraction are shown for the single mCitrine experiment (green points in the figure). These values are calculated from a region in figure 6.7 where the anisotropy values look homogeneous. In the figures it can be seen that the average anisotropy does not increase after photobleaching. When we compare this anisotropy value with the low anisotropy value measured on HeLa cells expressing the double mCitrine protein, we can conclude homo-FRET between the two mCitrine parts in a double mCitrine protein definitely occurs.

The measured anisotropy of the single mCitrine fluorescent proteins equals 0.288 ± 0.003 . This value was obtained by fitting the measured anisotropy value as a function of bleached fraction to a constant function, because no change in anisotropy is expected after photobleaching. This value is close to the average anisotropy value for the double mCitrine proteins of which one mCitrine part is photobleached, which is 0.302 ± 0.008 .

A reason for this small difference can be that the double mCitrine protein is more rigid and therefore rotates less than the single mCitrine fluorescent protein. This would then yield a higher anisotropy value according to the Perrin equation (eq. 3.21), since the fluorescence lifetime of mCitrine in both proteins (single and double mCitrine) is equal.

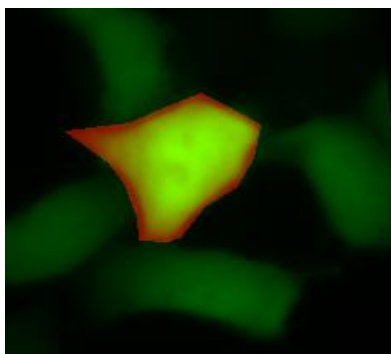


figure 6.6: Fluorescence intensity image of HeLa cells expressing mCitrine (green) and the region of interest used to make anisotropy images (red).

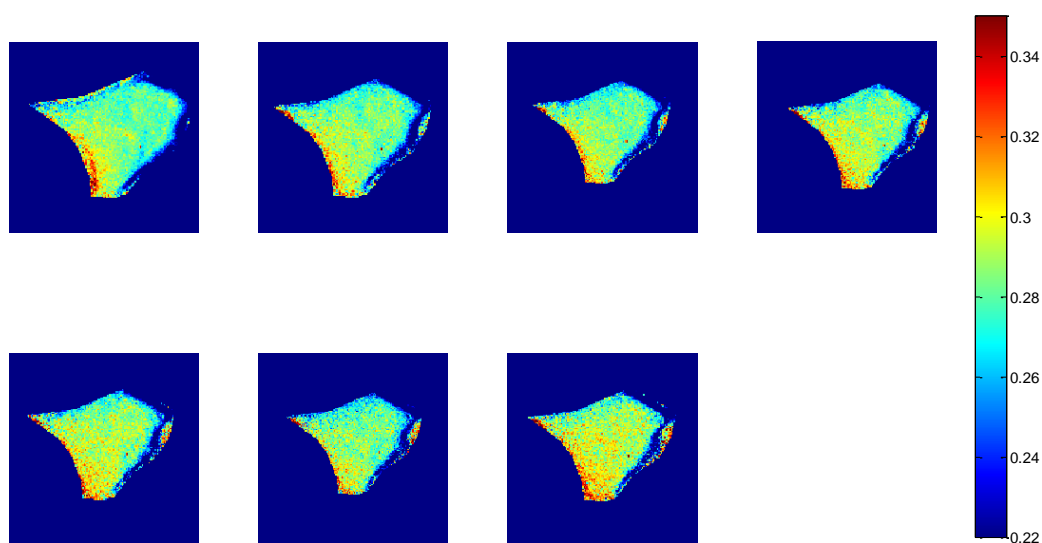


figure 6.7: Fluorescence anisotropy images of HeLa cells expressing the double mCitrine protein. From left to right the fluorescence intensity decreases due to photobleaching. The color bar indicates the anisotropy values according to the color shown in the image. The label fractions from left to right from top to bottom are the following: 1, 0.76, 0.71, 0.58, 0.51, 0.44 and 0.39.

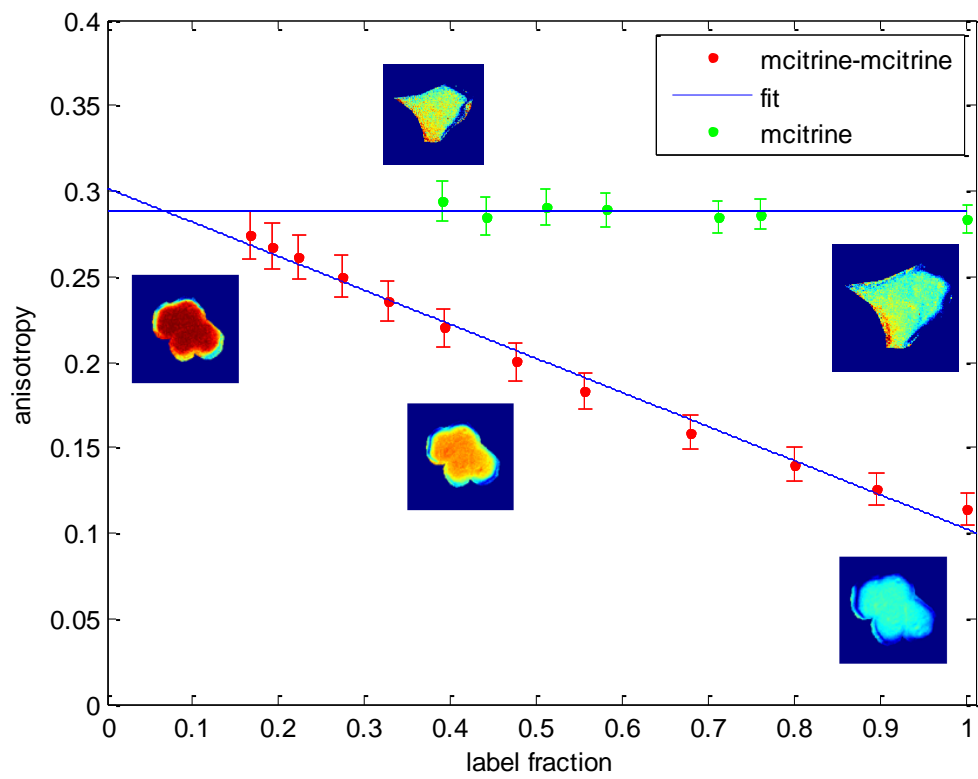


figure 6.8: Average anisotropy of HeLa cells expressing mCitrine and HeLa cells expressing mCitrine-mCitrine as a function of label fraction.

7 MCF-7 cells expressing EGFR-mCherry fusion proteins

In chapter 3 it was mentioned that previous research shows that the EGF receptor forms oligomers upon binding to its ligand EGF. The extent to which this happens can be monitored by visualizing homo-FRET inside live cells as shown in chapter 3. When fluorescent labels are attached to the EGF-receptors, and these receptors form clusters, homo-FRET between these labels can occur and can be visualized by observing a decrease in the fluorescence anisotropy. In this experiment is investigated with anisotropy microscopy if clustering of the EGF-receptor on the cell membrane can be observed and when, after addition of EGF, this clustering occurs. In order to do this, MCF-7 cells expressing EGFR-mCherry are used. Earlier experiments show that the EGF receptor clustering is highest 5 minutes after addition of EGF.

The outline of this chapter is as follows: At first the photophysical background on the fluorescent protein mCherry is discussed. Then we explain why MCF-7 cells are used. After this the sample preparation and imaging procedure is explained. Finally the results are presented and discussed.

7.1 The fluorescent protein mCherry

In this experiment the fluorescent protein mCherry is used, because it is a monomeric fluorescent protein and can be excited with the 532 nm wavelength laser in the anisotropy microscopy setup. The normalized absorption and emission spectrum of this fluorescent protein are shown in figure 7.1.

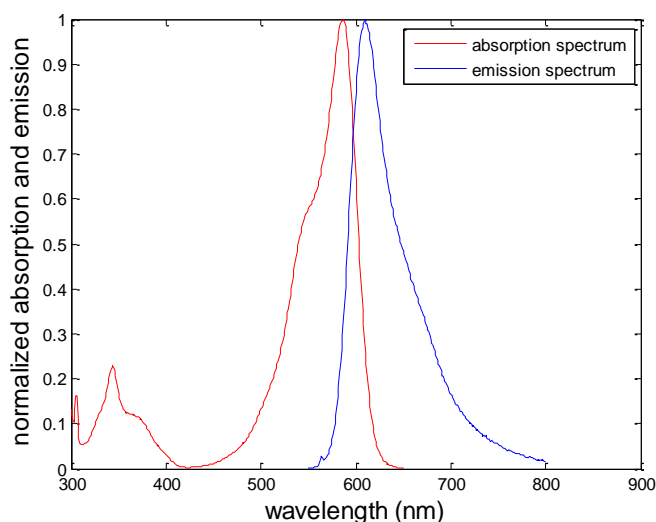


figure 7.1: Normalized absorption and emission spectrum of the fluorescent protein mCherry

7.2 Selection of cell type

For the experiments in this chapter MCF-7 cells are used, because this cell type expresses only a small amount of endogenous EGF-receptors.²⁵ This is important, because when a cell type is used that expresses a high amount of endogenous EGF-receptors, clusters might be formed that partly consist of EGF-receptors that do not have a fluorescent protein attached to it. In that case no or less homo-FRET can occur in these clusters.

7.3 Experimental procedure

This part covers the experimental procedures followed to perform the experiments, of which the results are shown and discussed in this chapter.

7.3.1 Sample preparation

MCF-7 cells were grown in Dulbecco's modified eagle medium (DMEM) with L-glutamine, phenol red, 10% fetal bovine serum (FBS) and 1% penicillin/streptomycin (PS) at a temperature of 37 °C in 5% CO₂. Before transfection, cells are grown on a cover chambered glass dishes to 50% confluency at the time of transfection. Transfection was done with 250 ng EGFR-mCherry plasmid, 0.85 μL LipofectamineTM LTX and 0.25 μL PLUSTM Reagent in 100 μL Opti-MEM I Reduced Serum Medium per 2 cm² well according to standard protocol. Transfection was done in 500 μL PS-free culture medium per well. 18 hours after transfection cells were placed on normal growth medium. 6 hours later the MCF-7 cells were starved for 12 hours using FBS-free medium. Before the measurements the starvation medium is replaced with PBS containing calcium and magnesium.

7.3.2 Fluorescence anisotropy imaging

The cells transfected plasmid DNA encoding for EGFR-mcherry proteins are imaged on the fluorescence polarization microscope setup and excited with the 532 nm wavelength laser. The 532 nm notch filter was used to get rid of reflected laser light from the microscope glass that passed the dichroic mirror. The 100x objective described in chapter 3 was used to image the MCF-7 cells and for the necessary calibration procedures. The 617/40 nm single band pass filter was placed in front of the polarizing beam splitter. The calibration procedure is performed as described in chapter 3. Rhodamine 6G was used as a calibration dye.

Fluorescence anisotropy images are recorded from MCF-7 cells that express EGFR-mCherry proteins before the addition of EGF. This means that an image is recorded by the camera that only detects the fluorescence emission with a polarization perpendicular to the excitation light and that an image is recorded by the camera that only detects the fluorescence emission with a polarization parallel to the excitation light. After this EGF is added to the medium in which the measured cell is located at a final concentration of 200 ng/mL. Every one minute after the addition of EGF anisotropy images are recorded until 10 minutes after addition of EGF. All measurements were done with a gain of 200 on both cameras and an acquisition time of 50 ms. For every measurement a background measurement is done using a cover chambered glass dishes with PBS only. The average values of the background intensities for the parallel and perpendicular images are subtracted from the measured parallel and perpendicular images.

7.4 Results and discussion

To obtain the anisotropy values from the parallel and perpendicular intensity images, only a certain region in the intensity image is selected. A fluorescence intensity image of a single cell expressing EGFR-mCherry is shown in figure 7.2. This image is created by summing the measured background corrected perpendicular and parallel fluorescence intensity images. To select the region of interest that is used to calculate an average anisotropy value, a mask is created based on the fluorescence intensity to select mainly the pixels that form the cell membrane. The red pixels in figure 7.3 form a mask that is created by applying a combination of an intensity threshold and a threshold in the second derivative of the intensity image in figure 7.2. With this mask only the pixels that are red in

figure 7.3 are used to calculate an average anisotropy value. The anisotropy values are calculated with this procedure for all images recorded before and after addition of EGF.

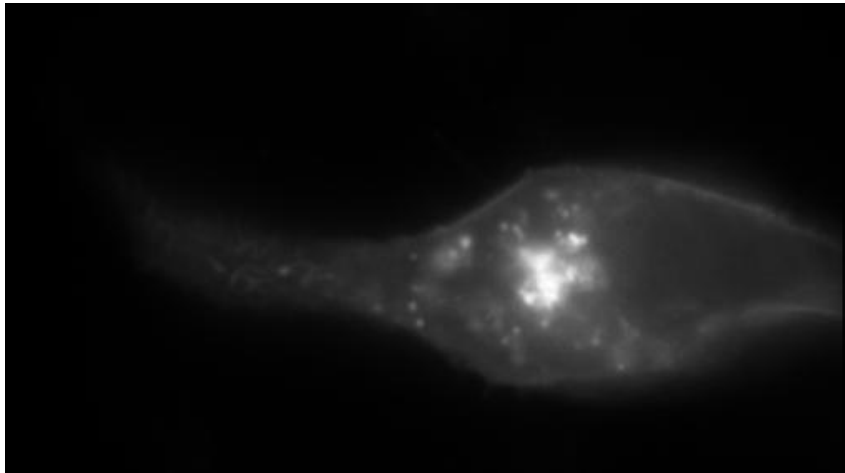


figure 7.2: Fluorescence intensity image of an MCF-7 cell expressing EGFR-mCherry

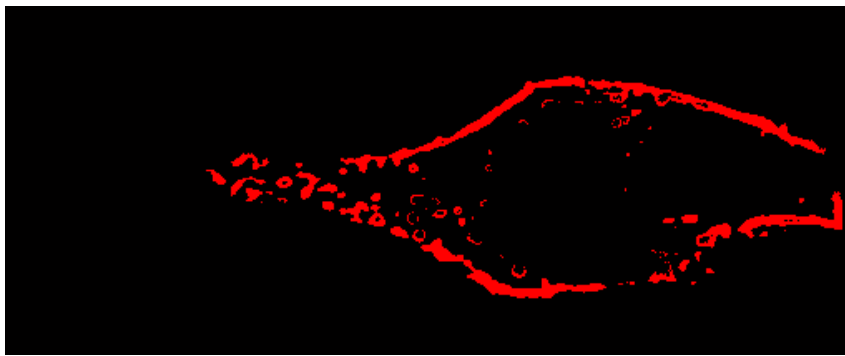


figure 7.3: Mask that is created, such that only the pixels on the cell edge are selected.

In figure 7.4 the average anisotropy as a function of time after addition of EGF is shown. In this figure 0 minutes after addition of EGF means before addition of EGF. In this figure it can be seen that no change occurs in anisotropy after addition of EGF. It is expected that the anisotropy decreases, but all values are close to 0.28. Small differences in the anisotropy values are observed. This can be caused by the fact that a slightly different region is selected with the mask in figure 7.3. This is because this mask had to be determined separately for every intensity image, because of movement of the cell.

A repeat of the experiment on MCF-7 cell expressing EGFR-mCherry is done. The recorded intensity images are processed in a similar way. The average anisotropy values as a function of time after addition of EGF are shown in figure 7.5. Also here it can be seen that no large change in anisotropy occurs after addition of EGF. In this figure it can be seen that the average anisotropy values are approximately equal to the anisotropy values in figure 7.4.

A possible explanation for the fact that no change is observed in anisotropy can be that the expression level of EGFR-mCherry by the MCF-7 cells is too low. This means that the EGF-receptors do not dimerize within 10 minutes after addition of EGF, because the probability of two receptors being close together is too low.

In the literature it is also stated that the fluorescent protein mCherry tends to form clusters when expressed in certain protein fusions.²⁶ However, it is expected that the average anisotropy in this case would be lower than 0.28. This is expected because of the measurements on the double mCitrine proteins presented in chapter 6. The double mCitrine protein here shows an average

anisotropy that is far lower than 0.28. This is not entirely comparable, since mCitrine is a different fluorescent protein.

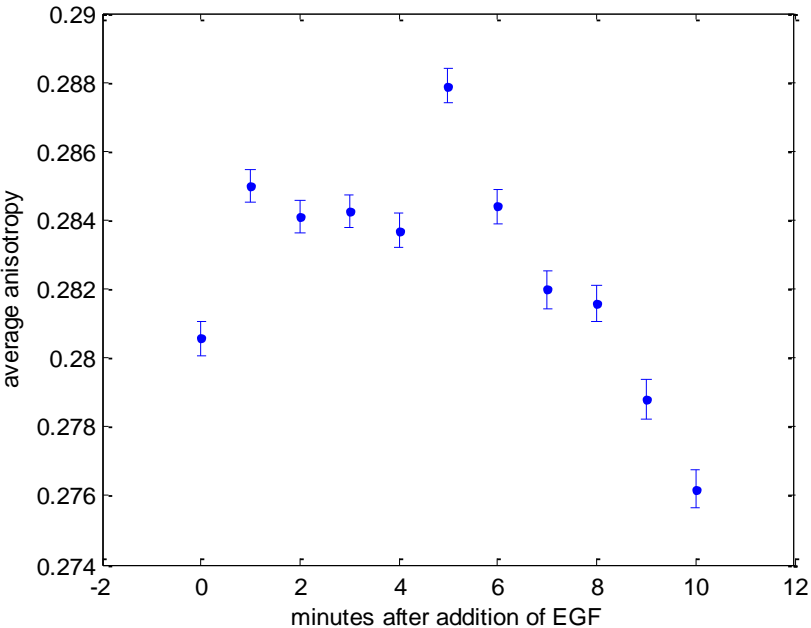


figure 7.4: Average anisotropy calculated from the pixels in the parallel and perpendicular intensity images that are selected by the mask in figure 7.3 as a function of minutes after addition of EGF.

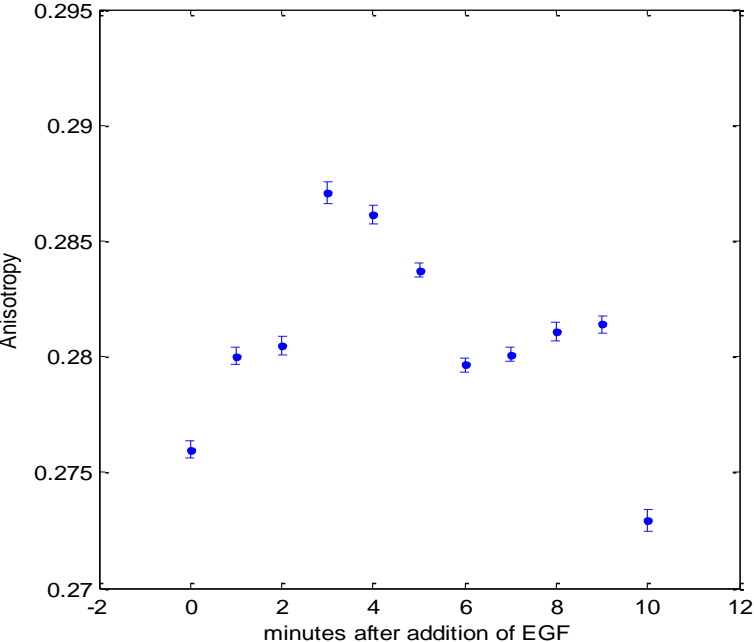


figure 7.5: Average anisotropy calculated from the pixels in the parallel and perpendicular intensity images that are selected by the mask in figure 7.3 as a function of minutes after addition of EGF for a different cell.

8 Visualizing EGFR clustering using SNAP-EGFR Fusion Proteins

In this chapter an approach different from labeling the EGF-receptor with fluorescent proteins is discussed. This approach uses a SNAP-tag, which is attached to the EGF-receptor on the extracellular part. The advantage of this is that any organic dye can be used for labeling, as long as it can be synthesized such that the organic dye can label the SNAP-tag. This new approach might improve the system in the sense that a larger decrease in anisotropy can be observed when the right fluorescent probe is selected. This is because dyes that have a short lifetime or a large Förster radius compared to fluorescent proteins can now be used for labeling the EGF-receptor. A larger Förster radius means that homo-FRET will occur when the fluorophores are further away from each other compared to fluorescent probes with a smaller Förster radius, or that the FRET efficiency will be higher for identical distances between the probes compared to fluorescent probes with a smaller Förster radius. Using a fluorescent dye with a shorter lifetime can have the advantage that the fluorescent probe does not rotate much during the excited state lifetime. The observed decrease in anisotropy due to homo-FRET will thus be larger. The FRET efficiency is not influenced by the decrease in fluorescence lifetime.

In this chapter also measurements on HeLa cells expressing SNAP-TMD-Fv are discussed. SNAP-TMD-Fv is a protein that is transported to the cell membrane and can be artificially dimerized upon addition of a specific molecule. Dimerizing this protein might tell whether FRET between fluorescent dyes attached to the SNAP-tag is observable in our setup.

This chapter first discusses the used protein fusions and fluorescent labels, followed by an outline of the experimental procedures for cell transfection and labeling of the SNAP-tag with fluorescent dyes. Then an outline of the successful and unsuccessful experimental procedures is given. Finally the results of the experiments on cells that were successfully labeled will be presented and discussed.

8.1 The SNAP-tag

The SNAP-tag is a protein domain that can be used to form a fusion protein with a protein of interest. In an expressed fusion protein, the SNAP-tag is then connected to this protein via an amino acid linker. The SNAP-tag can be labeled with a fluorescent dye, under the condition that this fluorescent dye has a benzylguanine group attached to it. The SNAP-tag reacts fast with the benzylguanine group. This reaction results in a covalent bond between the SNAP-tag and the benzylgroup (see figure 8.1). The advantage of this method is that the protein of interest with a SNAP-tag attached to it can be labeled with any dye that can be synthesized to have a benzylguanine group attached to it.

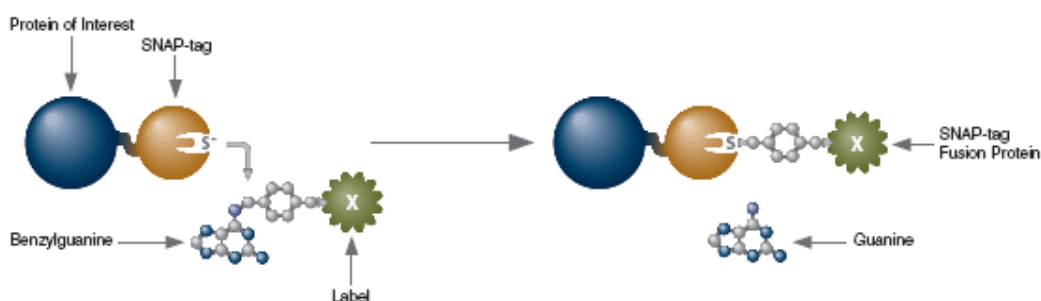


figure 8.1: Schematic representation of protein labeling with the use of a SNAP-tag. Image taken from [27]

8.2 Artificially induced dimerization

To verify that a decrease in anisotropy can be observed when using the SNAP-tag, cells transfected with a plasmid that encodes for a protein consisting of a SNAP-tag, a transmembrane domain, and a linker with an Fv domain are used. These proteins are transported to the cell membrane and are on the cell membrane such that the SNAP-tag is on the outside and the Fv-domain is on the inside of the cell membrane. The proteins can then be dimerized upon addition of a molecule named AP21087. One AP21087 molecule has two binding sites for the Fv molecule and can thus dimerize the Fv-domains. This also brings the SNAP-tags that are part of the molecules close together. When both SNAP-tags are labeled with a fluorescent dye, FRET may occur between these dyes such that a decrease in the anisotropy is observable.

8.3 Selection of fluorescent dyes

Selection of fluorescent dyes depends on the Förster radius and the lifetime of the fluorophore. The Förster radius was calculated for several fluorophores using eq. 3.7. From the fluorophores that specifically bind to the SNAP-tag Atto-532 and Alexa-647 were chosen in this experiment. Atto-532 has a Förster radius of 5.7 nm and Alexa-647 a Förster radius of 7.0 nm, for a refractive index of 1.4. The lifetime of the fluorescent dye is also important for anisotropy experiments. The fluorescence lifetimes of Atto-532 and Alexa-647 when bound to the SNAP-tag were measured by Stöhr²⁸ and are 3.82 ns and 1.0 ns respectively. Also the dye dyomics-630 was selected based on the short lifetime. In [28] the fluorescence lifetime of dyomics-630 could not be measured, since the exponential decay function of the fluorophores could not be separated from the instrument response function. Therefore the lifetime of dyomics-630 is lower than 0.3 ns.

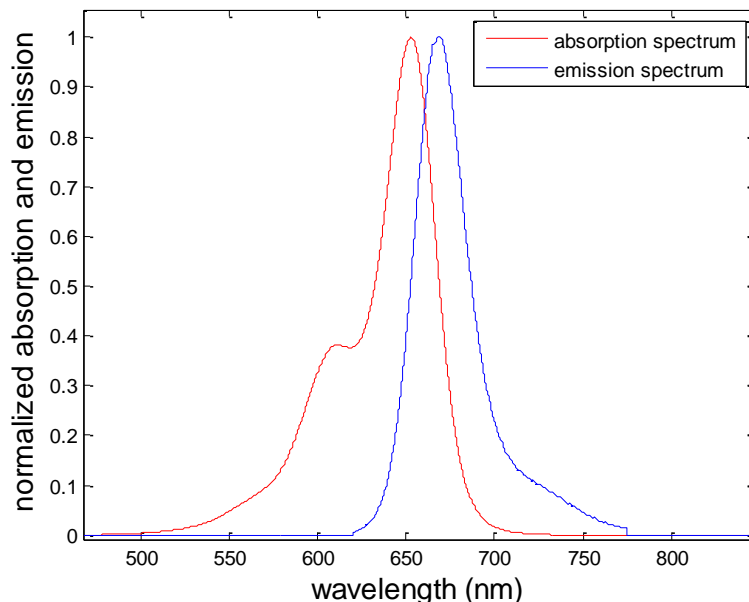


figure 8.2: Normalized absorption and emission spectrum of Alexa-647

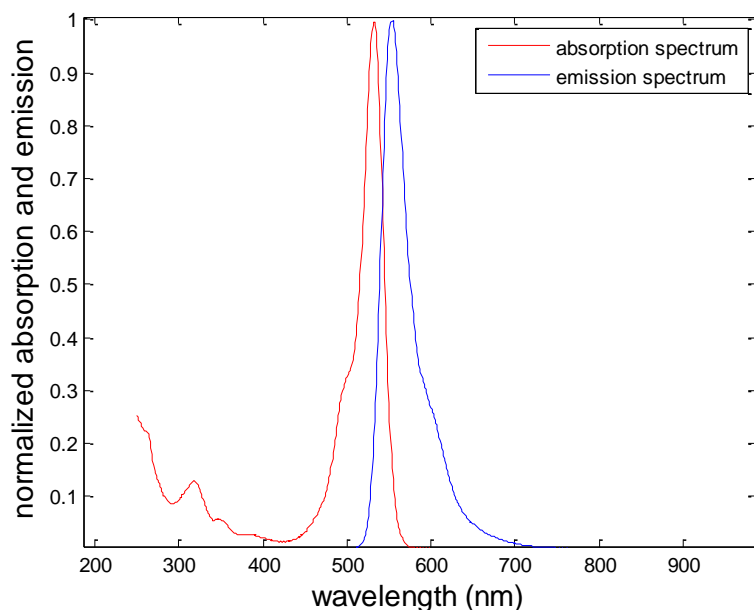


figure 8.3: Normalized absorption and emission spectrum of Atto-532

8.4 Experimental procedure

The experimental procedures that are followed to perform experiments on cells expressing SNAP-EGFR are discussed next. These procedures consist of cell culturing, dye labeling and fluorescence anisotropy imaging.

8.4.1 Sample preparation

In the experiments on EGFR discussed in this chapter MCF-7 cells and NIH-3T3 cells were used. The cells were cultured according to the earlier mentioned protocol in chapter 6. Before transfection, cells were plated on 2 cm² cover chambered glass dishes. The cells were transfected using different amounts of plasmid DNA and different amounts of reagents and different transfection reagent brands, as will be discussed in section 8.4.4. Before the experiments on the cells expressing the SNAP-EGFR proteins the cells were starved for approximately 12 hours. After this the SNAP-EGFR proteins were labeled with a fluorescent dye. This procedure will be discussed later. Fluorescence anisotropy images are recorded before and after the addition of EGF to the cells expressing SNAP-EGFR. EGF was added to the medium at a final concentration of 200 ng/mL.

For the experiments on HeLa cells expressing the SNAP-TMD-Fv fusion protein, the molecule AP20187 is added at a final concentration of 100 nM.

8.4.2 SNAP-tag labeling with fluorescent dyes

The procedure for labeling the SNAP-tag that is attached to the protein of interest (for example EGFR) with the fluorescent dyes will be described here. Per 2 cm² well with cells 1 μ L of 500 nM BG-dye is dissolved in 250 μ L DMEM (without FBS) containing 0.5 % Bovine Serum Albumine. This is mixed by pipetting up and down 10 times. The medium on the cells is replaced by this labeling medium for 15 minutes. Then the medium containing the fluorescent labels is removed from the cells and the cells are washed with PBS containing calcium and magnesium three times. The cells are imaged in imaging medium without FBS and phenol red.

8.4.3 Fluorescence anisotropy imaging

For the anisotropy experiments on fusion proteins labeled with Alexa-647 excitation is done with the 640 nm wavelength laser, and a 670/50 emission band pass filter is used. For excitation of samples labeled with Atto-532 the 532 nm laser is used, with a 580/60 emission band pass filter.

The integration times and gain values of the cameras depend on the measured sample, for the experimental results obtained from measurements on NIH-3T3 cells expressing SNAP-EGFR labeled with Alexa-647 an integration time of 3 ms and a gain of 100 are used for both cameras. For the experiments on HeLa cells expressing SNAP-TMD-Fv labeled with Alexa-647 an integration time of 10 ms and a gain of 50 are used. On the microscope the 100x water immersion objective is used as presented in chapter 5 for all experiments.

8.4.4 Outline of experimental settings

Not all prepared samples allowed fluorescence imaging. Here we discuss the preparation methods and whether it was possible to perform fluorescence imaging with the sample. In table 8.1 an overview of the used experimental settings and their outcome is shown. This table shows the used plasmid DNA, the used type and amount of transfection reagent, the used labeling dye and a short description of the experimental results. A difference is made in the table between MCF-7 cells cultured in the absence and presence of phenol red. Although phenol red is only used as pH indicator, there is an effect of this indicator dye on the cell division speed and cell survival. The presence of phenol red increases cell survival and cell division speed.²⁹

Cell type	plasmid	Plasmid DNA per well in ng (hours before removal)	LTX microliter (μL)	Plus-reagent (μL)	Observation	Experiment done	Result
MCF7 cells without phenol red in culture medium	SNAP-EGFR	500 (6 hours)	1.5	0.5	lot of cells died	No	-
	SNAP-EGFR	750 (6 hours)	2.5	0.75	Lot of cells died	No	Phenol red should be present in medium
MCF7 with phenol red in culture medium	SNAP-EGFR	500 (6 hours)	1.5	0.5	some cells died, remaining cells showed no fluorescence when labeled with Atto-532 and Alexa-647	No	-
	SNAP-EGFR	750 (6 hours)	2.5	0.75	some cells died, labeling with Atto-532 and Alexa-647, no fluorescence	No	-

					after labeling		
	SNAP-TMD-FV	500 (6 hours)	0.75	0.25	No fluorescence after labeling	No	-
	SNAP-TMD-FV	500 (6 hours)	0.75	0.25	No fluorescence after labeling	No	-
NIH 3T3	SNAP-EGFR	500 (6 hours)	1.5	0.5	Low amount cells showed fluorescence, some cells died	Yes, labeling with Alexa-647	No change in anisotropy upon stimulation with EGF
	SNAP-TMD-FV	750 (6 hours)	2.5	0.75	No fluorescence after labeling	No	-
	SNAP-TMD-FV	500 (6 hours)	1.5	0.5	No fluorescence after labeling	No	-
	EGFR-mturquoise	500 (24 hours)	Effectene reagent kit: 4 μ L Effectene 12 μ L Enhancer		Low fluorescence intensity	-	-
	SNAP-EGFR	500 (24 hours)	Effectene reagent kit: 4 μ L Effectene 12 μ L Enhancer		A lot of cells died/ washed away, remaining cells showed no fluorescence after labeling	No	-
Hela cells	SNAP-TMD-FV	500 (7 hours)	1.5	0.5	Low, 1-3 cells per well showed fluorescence	Yes, labeling with Alexa-647	No change in anisotropy after addition of AP20187

table 8.1: Outline of experimental settings used for the experiments in this chapter

MCF-7 cells were first selected to investigate clustering of the EGF-receptor with the use of a labeled SNAP-tag. However transfection with the plasmid DNA encoding for SNAP-EGFR, a lot of cells died. This was probably due to the absence of phenol red in the culture medium. This procedure was repeated, but with phenol red in the cell culture medium. Approximately 50% of the cells died, and the remaining cells showed no fluorescence after labeling with Atto-532 or alexa-647.

MCF-7 cells were also transfected with plasmid DNA encoding for SNAP-TMD-Fv. After labeling with the two dyes indicated in the table, these cells also showed no fluorescence.

Since MCF-7 cells did not show fluorescence after transfection and labeling, a different cell type, NIH-3T3 cells, with low expression level of endogenous EGF-receptors³⁰ is used. The NIH-3T3 cells are also transfected with SNAP-EGFR. These cells were labeled with Atto-532 and Alexa-647. Only some cells labeled with Alexa-647 showed fluorescence (approximately 3-4 per well). An experiment was performed on these cells. In the wells where Atto-532 was used as a label, no fluorescence was visible.

The NIH-3T3 cells were also transfected with plasmid DNA encoding for SNAP-TMD-Fv. These cells showed no fluorescence after labeling.

As a control, NIH-3T3 cells were transfected with plasmid DNA encoding for EGFR-mTurquoise at the same time as transfection was done with SNAP-TMD-Fv and NIH-3T3. These cells showed low fluorescence. Approximately 30% of the cells showed fluorescence, which indicates problems with transfecting MCF-7 cells and NIH-3T3 cells with SNAP-EGFR and SNAP-TMD-Fv.

It is not important to consider the cell type that is used for transfection with plasmid DNA encoding for SNAP-TMD-Fv, because no cell types express endogenous TMD-Fv proteins. Thus, when cells express labeled SNAP-TMD-Fv, dimerization will always occur between two fluorescently labeled snap-TMD-Fv proteins. Transfection with this plasmid encoding for SNAP-TMD-Fv is therefore also tried on HeLa cells. Approximately four HeLa cells per well after transfection with plasmid DNA encoding for SNAP-TMD-Fv showed fluorescence after labeling with Alexa-647. Atto-532 was also used as a dye for labeling; however no cells showed fluorescence after labeling with Atto-532.

MCF-7 cells transfected with plasmid DNA encoding for SNAP-EGFR are also labeled with dyomics-630. In this experiments all cells showed fluorescence, which is probably caused by aspecific binding of dyomics-630 to the membrane of MCF-7 cells. This dye is thus not suitable for labeling membrane proteins with the use of a SNAP-tag.

8.5 Results and discussion

In this section the results from experiments on NIH-3T3 cells expressing snap-EGFR and HeLa cells expressing SNAP-TMD-Fv are presented and discussed.

8.5.1 NIH-3T3 cells expressing SNAP-EGFR labeled with Alexa-647

First the results from anisotropy experiments on NIH-3T3 cells expressing SNAP-EGFR labeled with Alexa-647 will be discussed. In figure 8.4 (left) on page 71 a fluorescence intensity image is shown of an NIH-3T3 cell expressing SNAP-EGFR. A region of interest is also shown in this figure. Also a threshold is set based on the intensity, such that only the anisotropy values in the pixels in the region of interest with intensity higher than the threshold intensity are selected. The average anisotropy is calculated from these pixels. This is done for the images recorded from 3 minutes before addition of EGF, until 6 minutes after addition of EGF. The average anisotropy values obtained from the images are shown in figure 8.4 in the right figure. -3 minutes after addition of EGF in this figure means 3 minutes before addition of EGF.

In this figure it can be seen that the anisotropy value before addition of EGF changes from 0.305 to 0.302 approximately. No changes are expected here, since nothing changes in the environment of the cell during the first three images. Therefore it is expected that this change is caused by intrinsic fluctuations that could result in a small change in the average anisotropy value. The average anisotropy value after addition of EGF in this figure is lower than before addition of EGF, which is as expected. However, the change in anisotropy per minute here is approximately equal to the change per minute in the measurement points before addition of EGF, and cannot be regarded as a change due to clustering of the EGF-receptor. Therefore no change in anisotropy is observed due to homo-FRET. This means that the conclusion can be drawn that no (additional) homo-FRET occurs between the fluorescent dyes that label the SNAP-tag on the EGF-receptor after addition of EGF.

Explanations for the fact that no change in anisotropy is observed can be found in the fact that when a dimer is formed, the fluorescent dyes are still not close enough for FRET to occur. In a dimer the amino acid chain connecting the SNAP-tag to the EGF-receptor could have a completely different orientation with respect to the EGF dimer than the other SNAP-tag in the dimer, such that the distance between the fluorophores in a dimer is for example twice the distance between the fluorophore and the EGF-receptor it is attached to. This means that the fluorophores attached to the SNAP-tag are still too far away for FRET to occur, although the EGF-receptors are close together.

Another explanation could be that not all SNAP-tags on the EGF-receptors are labeled with a fluorescent dye. However, 10 times the dye concentration tested for complete labeling was used per well and the labeling procedure was executed according to the protocol, so it is unlikely that this is the cause.

To see the effect of the applied intensity threshold, figure 8.4 shows the anisotropy as a function of minutes after addition of EGF for the same region of interest in figure 8.4 for a higher intensity threshold. This means that fewer pixels are selected for the calculation. Although slightly higher anisotropy values are measured for a higher threshold, the intensity threshold has no influence on the change in anisotropy after addition of EGF (see figure 8.4).

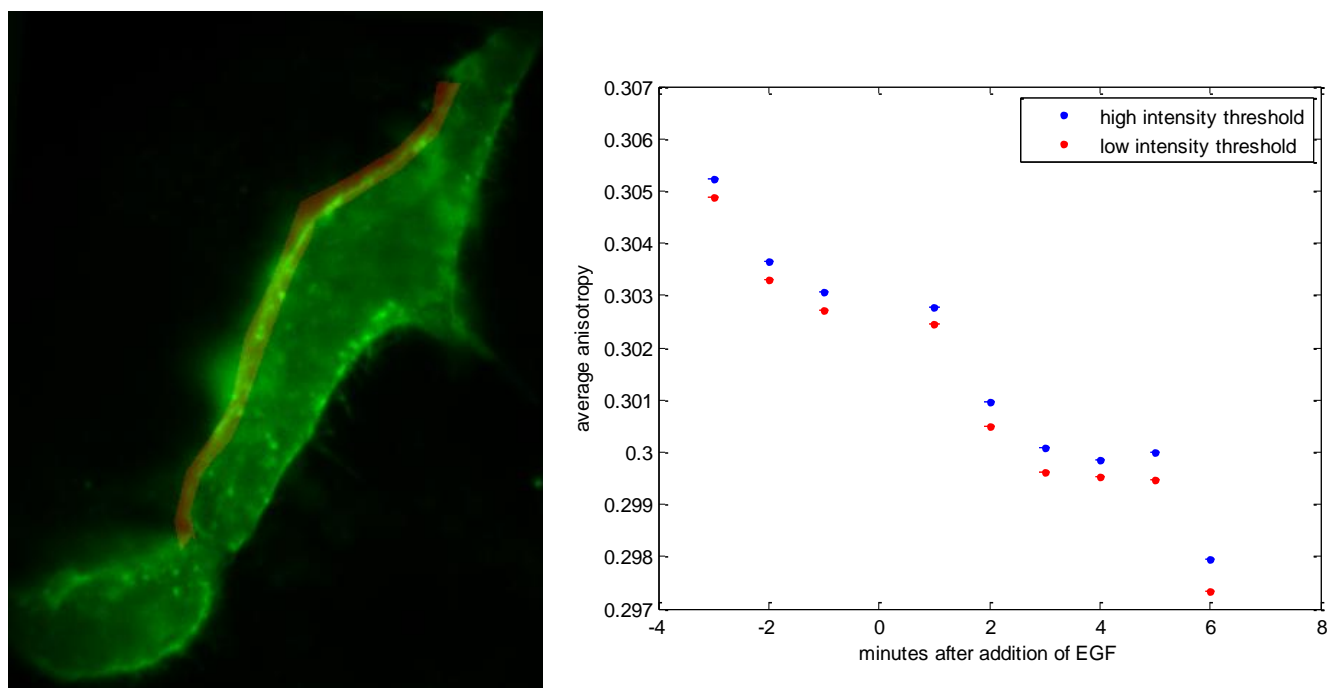


figure 8.4: Left: Fluorescence intensity image of an NIH-3T3 cell expressing SNAP-EGFR (green) including the region of interest (red). Right: Average anisotropy as a function of minutes after addition of EGF for two different intensity thresholds.

8.5.2 NIH-3T3 cells expressing SNAP-TMD-Fv labeled with alexa-647

To test the possibility to observe a change in anisotropy due to homo-FRET between fluorophores bound to the SNAP-tag in a SNAP-tag fusion protein, anisotropy experiments are performed on HeLa-cells expressing the SNAP-TMD-Fv proteins. The SNAP-TMD-Fv proteins are therefore also labeled with the dye Alexa-647. A fluorescence intensity image of a HeLa cell expressing these labeled proteins is shown in figure 8.5 (left). In this image it can be seen that most fluorescent molecules are present on the cell membrane, as expected. Also some labeling on the inside of the cell is shown. Apparently the BG-Alexa-647 dyes are able to penetrate the cell membrane and bind to SNAP-tags inside the cell, or a part of the labeled SNAP-TMD-Fv fusion protein is internalized after labeling.

From the pixels in the region of interest in this figure the average anisotropy value is calculated and shown in the right figure in figure 8.5. Also an intensity threshold is applied here, such that the amount of pixels that is used for the calculation of the average anisotropy value is equal in each image, independent on the shape of the region of interest. If only an intensity threshold would have been applied, also the fluorescence emitted by the dyes inside the cell would be selected for the calculation of the average anisotropy value. To see the effect of the addition of the dimerizer

molecule AP20187, the average anisotropy values are calculated from the images recorded several different minutes after addition of AP20187. 0 minutes before in this figure means that the image is recorded right before AP20187 was added. It is expected that the average anisotropy decreases after addition of AP20187, since this molecules dimerizes two SNAP-TMD-Fv proteins and thus may bring the fluorophores bound to the SNAP-tag close together.

The anisotropy decreases in the figure after the addition of AP20187. However, this decrease is so small, approximately 0.005 after 5 minutes, and can thus not be attributed to homo-FRET between Alexa-647 dyes that are attached to the SNAP-tag. Also here it could be that this small change is for example caused by fluctuations in the cell or by small differences in the selection of the region of interest or the intensity threshold.

In figure 8.6 the results from different cells measured in a different well are shown, analyzed in an identical way as the results in figure 8.5. In the right figure in figure 8.6 it can be seen that the anisotropy values are similar to the values in the right figure in figure 8.5. Also here a negligible decrease in anisotropy is observed after the addition of AP20187. This decrease is approximately 0.0012 in 5 minutes.

From both experiments on HeLa cells expressing SNAP-TMD-Fv we cannot conclude that it is possible to measure homo-FRET between the Alexa-647 fluorescent molecules that are attached to the SNAP-tag upon addition of AP20187. A possible explanation for the fact that no homo-FRET occurs between the dyes is that there is too much AP20187 is added. This means that every AP20187 molecule is bound to a SNAP-TMD-Fv fusion protein, and therefore no dimers can be formed on a short timescale. The timescale on which dimers can be formed then depends on the rate at which the AP20187 molecules dissociate from the Fv domains, and could be longer than 5 minutes. However, by Song et al.³¹ it was found that dimers are formed 1 min after addition of AP20187, also at a concentration of 100 nM, but this finding cannot be directly extrapolated to these results, since the expression level of SNAP-TMD-Fv might be different.

Another explanation is that the SNAP-tags are also too far away in this case. This is a possibility since the dimer is formed with the intracellular part (Fv) of the SNAP-TMD-Fv protein. The fluorescent label is bound to the extracellular part (SNAP-tag) of this protein.

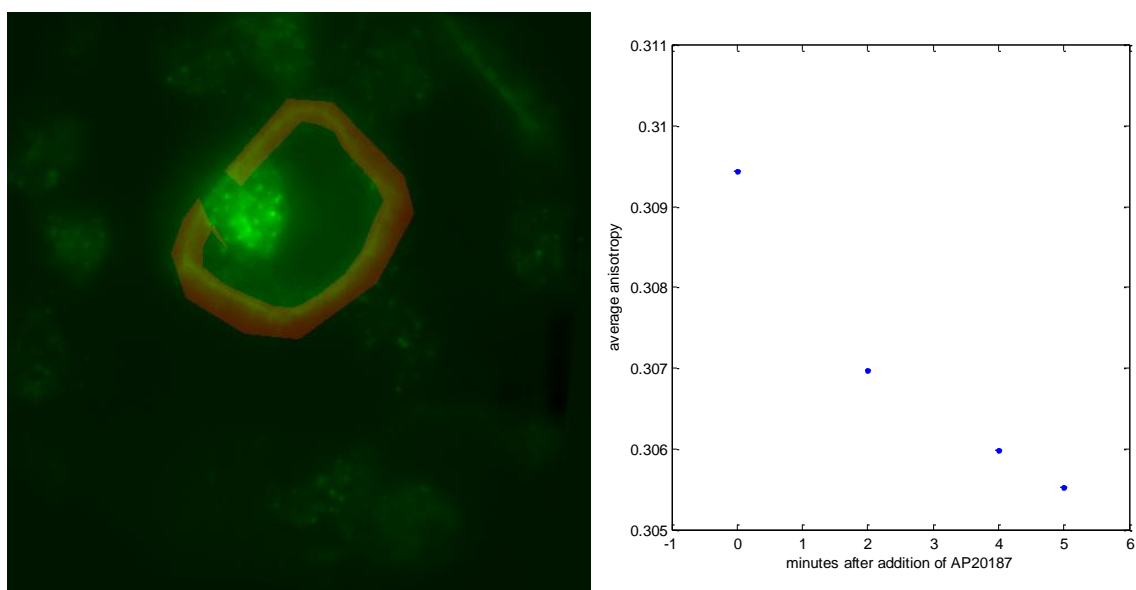


figure 8.5: Left: Fluorescence intensity image of a HeLa cell expressing SNAP-TMD-Fv labeled with Alexa 647 (green). The region of interest is also shown in this figure (red). Right: Average anisotropy as a function of minutes after addition of AP20185 determined from the region of interest that is shown left.

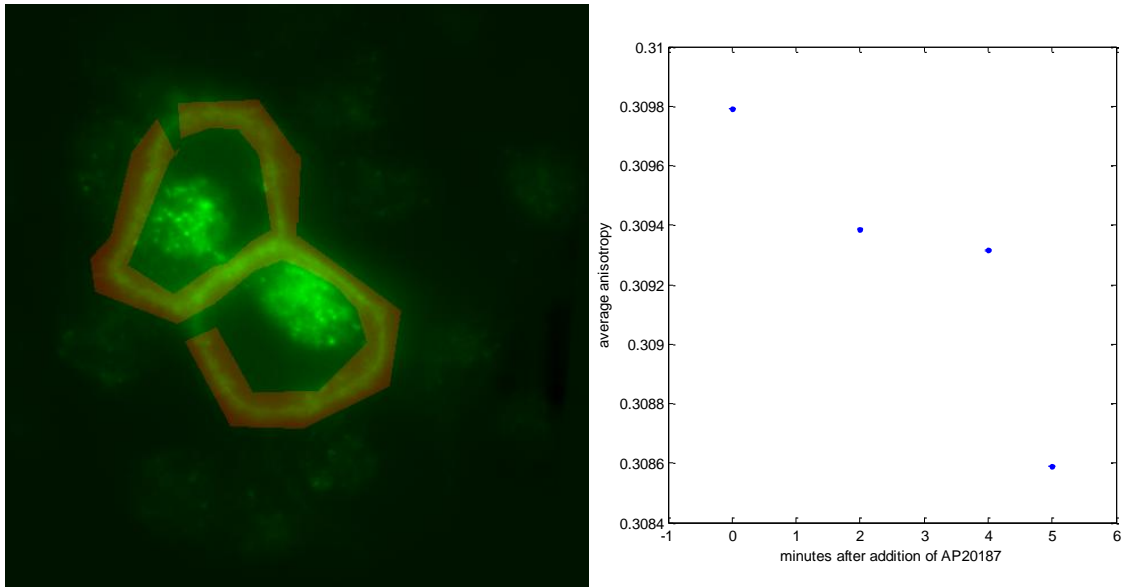


figure 8.6: Left: Fluorescence intensity image of two HeLa cells expressing SNAP-TMD-Fv labeled with Alexa 647 (green) and the region of interest (red). Right: Average anisotropy as a function of minutes after addition of AP20187 determined from the region of interest that is shown left.

9 EGF-receptor clustering after addition of antibodies against EGFR

We know from chapter 6 that homo-FRET between mCitrine fluorescent proteins is observable with the polarization microscope. Therefore we use the protein EGFR-mCitrine in this chapter. The effect of addition of EGF and the effect of addition of Cetuximab³², an antibody against the EGF-receptor, on the measured anisotropy is investigated, using MCF-7 cells. Cetuximab has two binding sites to the EGF-receptor, and can thus bind to two EGF-receptors.³²

The results from experiments with the anti-EGFR-antibodies are discussed first. This is followed by results from MCF-7 cells expressing EGFR-mCitrine.

9.1 Experimental procedure

Cell culturing and preparation for anisotropy imaging and the anisotropy imaging procedure will be discussed here shortly.

9.1.1 Sample preparation

MCF-7 cells are cultured according to the earlier mentioned protocol and plated on 2 cm² glass well plates. At a confluency of approximately 50% the cells were transfected using 0.5 µg of EGFR-mCitrine plasmid DNA per well and 3.4 µL Enhancer and 6 µL Effectene reagent supplied by the manufacturer mentioned earlier. Transfections were done in Penicillin/streptomycin (PS) free Dulbecco's modified eagle medium (DMEM) with 10 % fetal bovine serum (FBS). After 14 hours the transfection medium is replaced with normal growth medium containing PS and FBS. The cells are starved with FBS-free DMEM for 12 hours before fluorescence imaging. Right before the cells are imaged, the medium is replaced with PBS. The Cetuximab antibodies are added to the cells at a final concentration of 600 nM. Also experiments on stimulation with EGF are done. EGF is added to the cells at a final concentration of 300 ng/mL.

9.1.2 Fluorescence anisotropy imaging

The fluorescence anisotropy images are recorded using the same equipment as described in chapter 5. The used exposure time of the camera is 2 seconds for all results in this chapter. The used gain value for measurements on MCF-7 cells expressing EGFR-mCitrine stimulated with EGF is 30, while the gain value used for the experiments where Cetuximab is added to the medium is 10. All fluorescence anisotropy images are recorded with the focus on the bottom part of the cell in this chapter. Image alignment between the two cameras is done by selecting a region in the images from both cameras that contains the cell of interest. The image alignment parameters are then determined from these images using the algorithms explained in chapter 3.

9.2 Results and discussion

In this section the results from experiments performed on MCF-7 cells expressing EGFR-mCitrine will be discussed. At first we present results that show the effect of Cetuximab on the measured anisotropy. This is followed by an anisotropy experiment in which EGF is added.

9.2.1 MCF-7 cells expressing EGFR-mCitrine and addition of Cetuximab

Anisotropy images are recorded before and after the addition of Cetuximab until 27 minutes after, to allow enough time for the antibodies to bind to the EGF-receptors³². The time between each image is 1 minute.

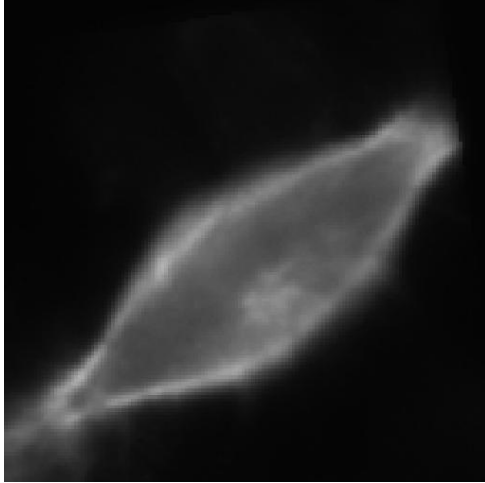


figure 9.1: Fluorescence intensity image of an MCF-7 cell expressing EGFR-mCitrine

A fluorescence intensity image of an MCF-7 cell expressing EGFR-mCitrine is shown in figure 9.1. This image was obtained by calculating the intensity in each pixel as follows:

$$I^i = I_{\parallel}^i + 2I_{\perp}^i \quad \text{eq. 9.1}$$

The anisotropy images are shown in figure 9.2 for different time values before and after addition of Cetuximab (see caption).

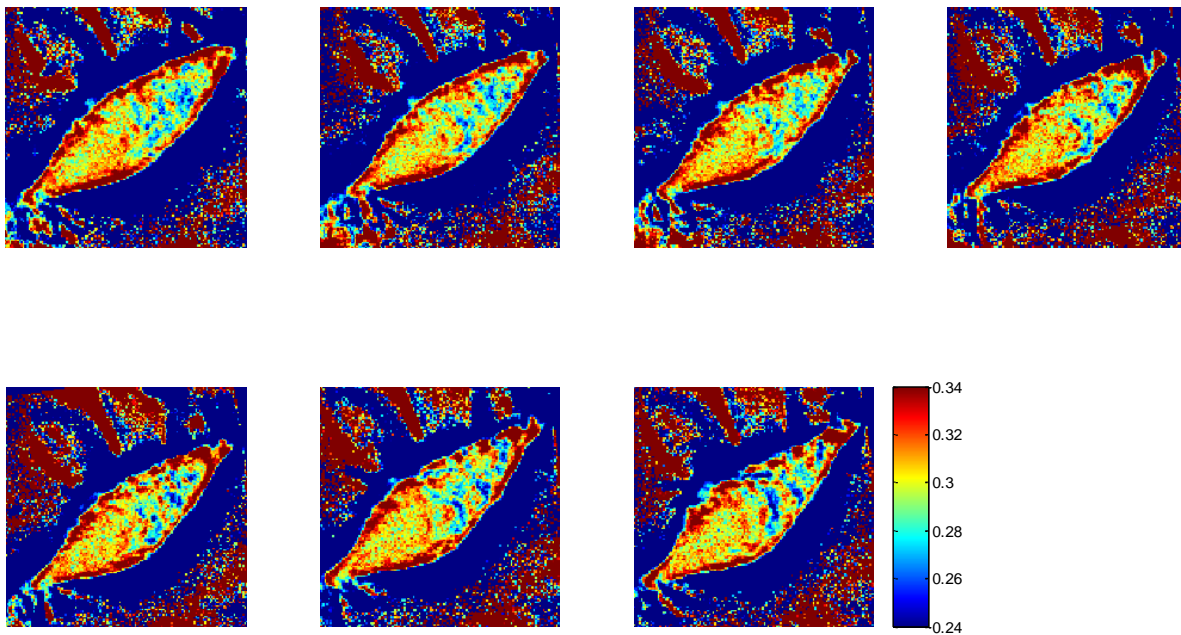


figure 9.2: Color scaled anisotropy images of a single cell expressing EGFR-mCitrine. The first image is recorded 3 minutes before addition of Cetuximab. The images from left to right and from top to bottom correspond to the images recorded 2, 7, 12, 17, 22 and 27 minutes after addition of Cetuximab

From these figures, no change in anisotropy can be observed, not even 27 minutes after addition of Cetuximab. To see whether there is a small change in anisotropy that cannot be observed in the anisotropy images and to see if the anisotropy values depend on the intensity in the pixels, the average anisotropy per intensity bin is calculated for each image. This is done as follows: first a single maximum intensity value (I_{max}) of all 30 anisotropy images is determined. Then 25 bins are determined based on intensity values, such that the first bin contains all pixels in a single image with intensity values between 0 and $0.04 \cdot I_{max}$, the second bin contains all pixels with intensity values between $0.04 \cdot I_{max}$ and $0.08 \cdot I_{max}$, until all bins are filled. For each bin, the average anisotropy value is calculated from the pixels in the anisotropy images corresponding to each bin. This is done separately for all anisotropy images. This results in an average anisotropy value for each intensity bin. These bins are generated because it is expected that pixels with a higher intensity values contain more EGFR-mCitrine proteins and are therefore more likely to be brought together by an antibody. This means that a lower anisotropy is expected for higher intensity bins.

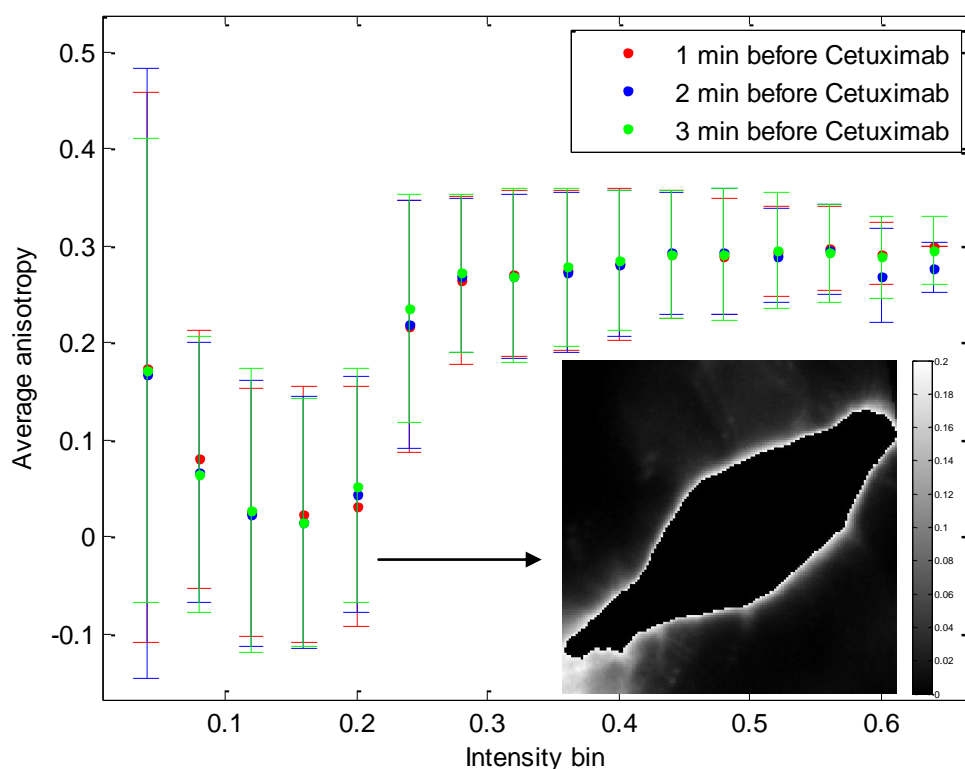


figure 9.3: Average anisotropy as a function of intensity bins for three anisotropy images recorded before addition of Cetuximab. The errorbars show the standard deviation in the anisotropy values of the pixels corresponding to the specific intensity bin. The intensity image that only shows pixels with intensity lower than $0.20 \cdot I_{max}$ is also shown.

In figure 9.3 the average anisotropy values as a function of intensity bin are shown for the anisotropy images recorded 3, 2 and 1 minutes before addition of Cetuximab. It can be seen that for these three images there is no difference in the average anisotropy per intensity bin. Also, for lower intensity bins, the average anisotropy is lower. These lower intensity pixels ($<0.20 \cdot I_{max}$) are also shown inside figure 9.3 and from this image it can be seen that these pixels are located on the outer edge of the cell. It could be that this lower anisotropy on the cell edge is caused by an artifact, and not by the fact that FRET occurs in the pixels with lower fluorescence intensity. Therefore in the next figures, the intensity bins lower than $0.20 \cdot I_{max}$ are not shown. Intensity bins higher than $0.64 \cdot I_{max}$ are not shown, since no pixels exist in the first three images with a higher intensity that this value.

To observe the effect the addition of Cetuximab on the measured anisotropy values, the average anisotropy value as a function of intensity bin is shown for the anisotropy images recorded several minutes after the addition of Cetuximab in figure 9.4. In this figure also one of the results from the images recorded before addition of Cetuximab is shown to compare the anisotropy values before and after addition of Cetuximab. It is expected here that the anisotropy decreases when Cetuximab is added. However, it can be seen in figure 9.4 that the average anisotropy for all intensity bins remains equal, around 0.28 for all intensity bins higher than 0.2. From this we can conclude that a decrease in anisotropy due to homo-FRET cannot be observed after addition of Cetuximab. We can also conclude that locations in the cell with a higher EGF-receptor density do not show higher FRET efficiencies compared to regions with lower EGF-receptor densities, which is not as expected.

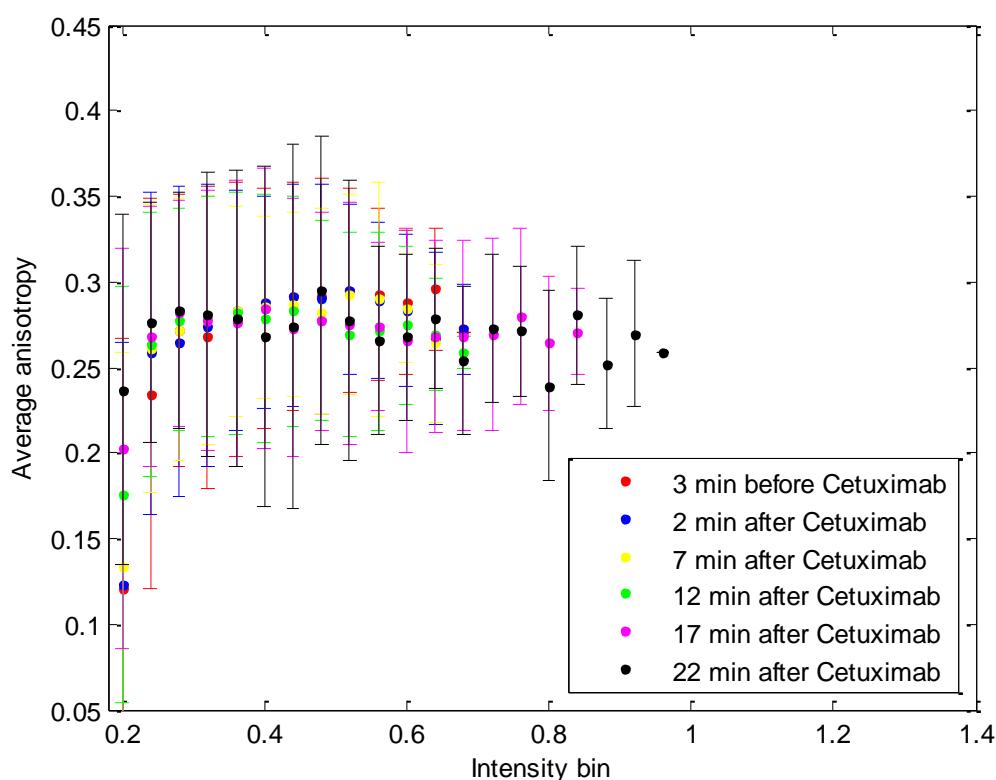


figure 9.4: Average anisotropy as a function of intensity bins calculated from anisotropy images recorded several minutes after addition of Cetuximab.

A possible explanation for the fact that no change in anisotropy is observed could be that, even though the EGF-receptors are dimerized as a cause of the addition of Cetuximab, the mCitrine fluorophores linked to the EGF-receptors are too far away from each other to allow FRET. Since the antibodies bind to domain 3 of the extracellular part of the EGF-receptor and the fluorescent protein is attached to the intracellular part of the EGF-receptor, it could be that the mCitrine fluorescent proteins are not close enough together.

Another explanation could be that, even though not expected, the EGF-receptors are already present as dimers on the cell membrane before addition of antibodies. In this case FRET may occur between the mCitrine fluorescent proteins before and after addition of Cetuximab, and thus no change in anisotropy could be observed. However, the average anisotropy values are close to 0.28, which is the anisotropy value that was also found for single mCitrine fluorescent proteins expressed in HeLa cells as shown in chapter 6. When FRET occurs between the mCitrine fluorescent proteins, a lower anisotropy value is expected.

9.2.2 MCF-7 cells expressing EGFR-mCitrine stimulated with EGF

Now experiments performed on MCF-7 cells also expressing EGFR-mCitrine will be discussed. In these experiments EGF is added to the cells instead of Cetuximab.

To see the effect of addition of EGF, in figure 9.5 several anisotropy images are shown. The first three anisotropy images are recorded before addition of EGF, the last five 1 to 5 minutes after addition of EGF. From these images the average anisotropy values are again calculated per intensity bin. The graph in figure 9.6 shows the average anisotropy as a function of intensity bin for the three measurements before addition of EGF. The lower intensity bins are not shown here, since these correspond to the anisotropy values on the background. The average anisotropy values per bin for the measurements after the addition of EGF are shown in figure 9.7. For all bins and for images after addition of EGF the average anisotropy values are equal to the average anisotropy values before addition of EGF.

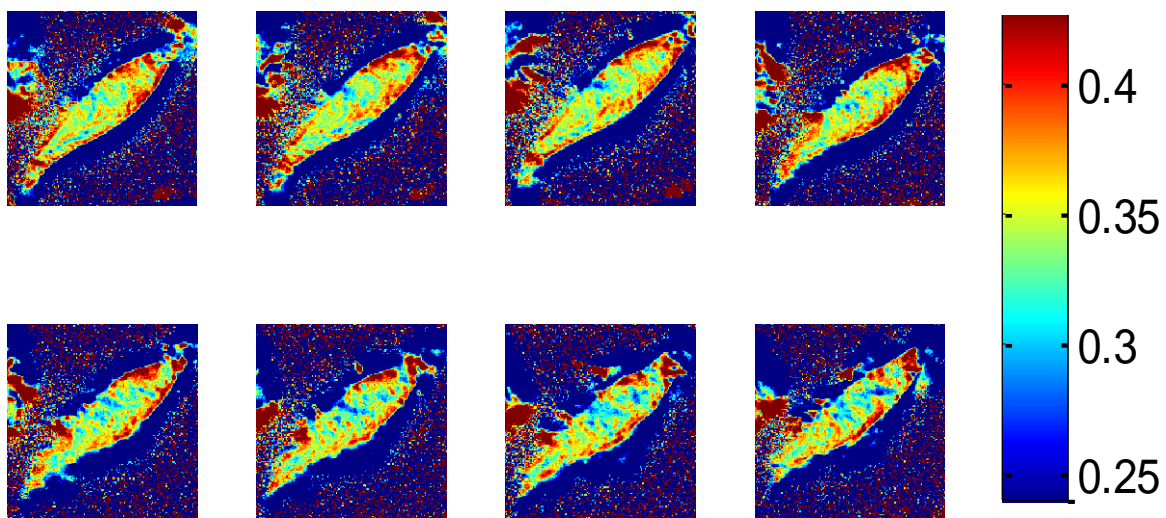


figure 9.5: Color scaled anisotropy images of a single cell expressing EGFR-mCitrine. The first three images from left to right are recorded 3, 2 and 1 minutes before addition of EGF. The other images are recorded from 1 to 5 minutes after addition of EGF.

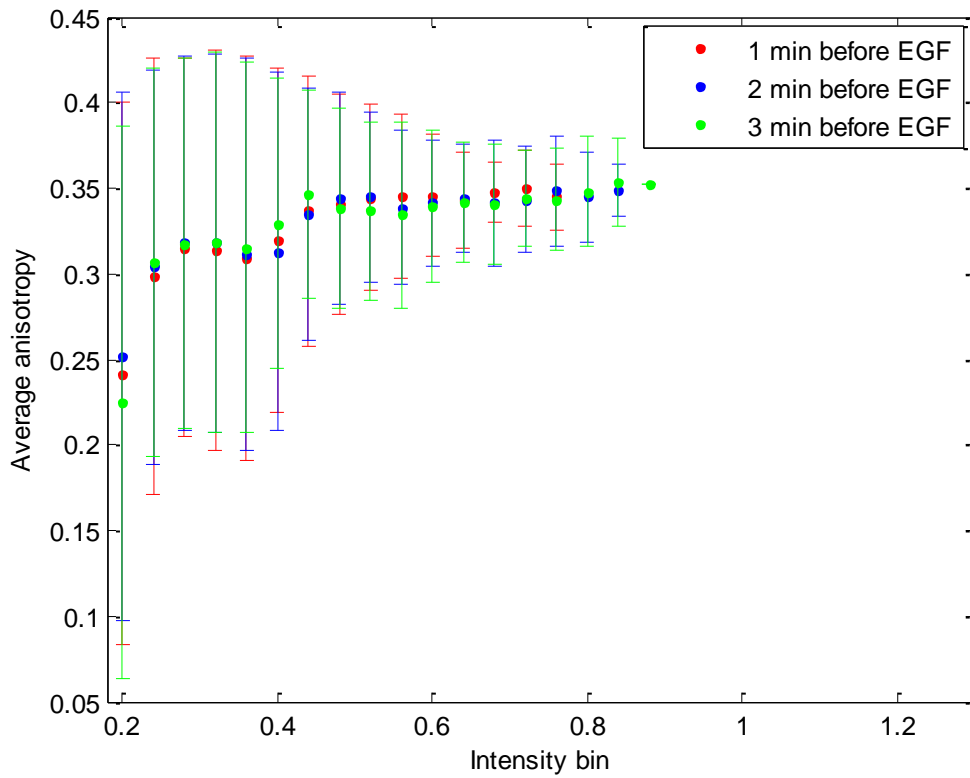


figure 9.6: Average anisotropy as a function of intensity bins calculated from anisotropy images recorded several minutes before addition of EGF.

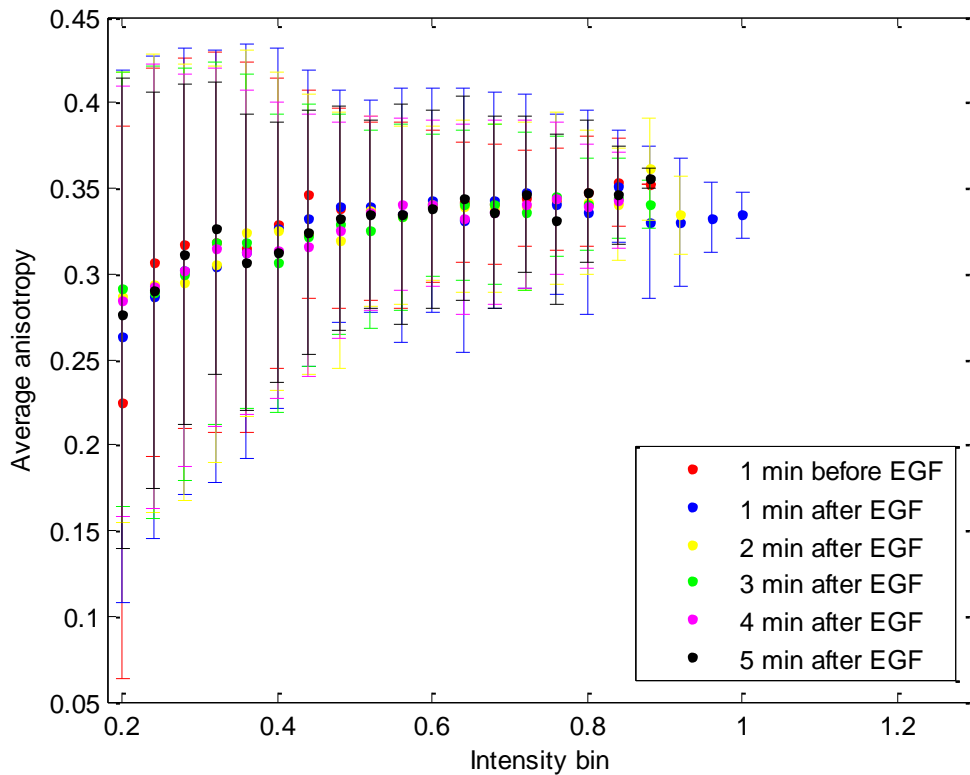


figure 9.7: Average anisotropy as a function of intensity bins calculated from anisotropy images recorded several minutes after addition of EGF.

The experiment was repeated, but again no difference in anisotropy was observed upon addition of EGF, not even 22 minutes after addition of EGF.

10 Conclusions and Recommendations

In this section the conclusions are presented for the different experiments presented in this report. Also recommendations based on these conclusions will be discussed.

10.1 Fluorescence polarization microscopy setup

The fluorescence polarization microscope was successfully implemented in the existing fluorescence microscopy setup. To measure correct anisotropy values with this setup, the calibration procedure consists of the following steps: The first step is to properly align the two cameras with a sample of fluorescent beads. This is followed by determining the optimal orientation of the polarizer with a sample that has a non-zero anisotropy value. Finally a G-factor should be determined, which corrects for differences in sensitivity of the setup to different light polarizations. This should be done with a sample that has a known anisotropy value. It is recommended to do this G-factor calibration for identical gain values on the cameras and with identical optical components such as band pass filters, excitation light source and dichroic mirror as used for the actual anisotropy measurement. With the polarization microscope the anisotropy of enhanced green fluorescent protein dissolved in 50%/50% glycerol/buffer was found to be 0.366 ± 0.009 , which is close to the value 0.38 reported in the literature.

10.2 Anisotropy simulations

Using simulations, the effect of homo-FRET on the measured anisotropy can be quantified and related to the distance between the fluorophores and the photophysical properties of these fluorophores.

From anisotropy simulations that predict the anisotropy decrease due to homo-FRET as a function of fluorophore density in a 2D plane, we conclude that the anisotropy decreases as a function of fluorophore density, as expected. It is not recommended to use this method to quantify the relation between anisotropy and fluorophore density, because the FRET-rate from a single donor to multiple acceptors is higher than the sum of all individual FRET-rates from the donor to each acceptor. The simulations can thus only be used to find a lower boundary of the decrease in anisotropy due to homo-FRET.

The decrease in anisotropy due to homo-FRET between a single donor and a single acceptor can be predicted using simulations. From the simulations it can be concluded that the maximum decrease in anisotropy for randomly orientated, non-rotating fluorophores that can be observed is 0.20. When there is an angle between the absorption and emission transition moments in a fluorophore, the decrease in anisotropy becomes smaller. When the angle is higher than 0.25π , the anisotropy increases when the FRET efficiency increases.

It can be concluded that the anisotropy change due to homo-FRET can be predicted with anisotropy simulations, but only if FRET occurs from a single donor to a single acceptor and for non-rotating fluorophores. In order to exactly predict this, all experimental parameters should be known, including the dynamic behavior of the fluorophores in the sample of interest, which is experimentally impossible.

The simulations can be used to predict which fluorophore is best for a certain experiment in which homo-FRET is expected to occur. It is advantageous to use fluorophores with a short lifetime when

the fluorophores in the sample of interest are expected to rotate and the fluorophores are close enough together (3-4 nm). When the sample does not rotate, the distance and orientation of the fluorophores with respect to other fluorophores are the most important parameters. A fluorophore with a high Förster radius is advantageous in this case. If the fluorophores rotate during the excited state lifetime and a large distance (between 5-10 nm) between the fluorophores is expected, the fluorescence lifetime and Förster radius are both important. In this case, simulations can determine which fluorophore will give the largest change in anisotropy when homo-FRET occurs. However, in most cases predicting the rotational motion of the fluorophores is impossible. When using fluorescent proteins in a homo-FRET experiment, a monomeric fluorescent protein should be used.

10.3 Homo-FRET anisotropy and lifetime

We conclude that homo-FRET cannot be detected by a change in the fluorescence lifetime of the donor. This finding is in agreement with the predicted effect determined by solving the rate equations that describe the fluorescence decay of fluorophores during the occurrence of homo-FRET.

Furthermore, it is confirmed using anisotropy measurements that homo-FRET occurs between two closely spaced mCitrine fluorescent proteins and that this can be observed with the implemented fluorescence microscope. From photobleaching of the double mCitrine protein it is found that the anisotropy decrease due to homo-FRET between the mCitrine parts is 0.20. This is not expected when the mCitrine fluorescent proteins are randomly orientated. From this we conclude that an mCitrine part in a double mCitrine protein has a nonrandom orientation with respect to the other mCitrine part in the same protein.

It is recommended that homo-FRET is detected with fluorescence anisotropy measurements and not with fluorescence lifetime measurements.

10.4 Cells expressing protein-SNAP-tag fusions

From the experiments on NIH-3T3 cells expressing SNAP-EGFR labeled with Alexa-647 it was concluded that dimerization of SNAP-EGFR cannot be observed with anisotropy experiments within 5 minutes after addition of EGF. Also from experiments on HeLa cells expressing SNAP-TMD-Fv, dimerization of the SNAP-TMD-Fv proteins upon addition of AP20187 was also not observed within 5 minutes. Based on these findings we conclude that the SNAP-tags are too far away in both the SNAP-EGFR and SNAP-TMD-Fv for FRET to occur, because it was found in literature that dimers were formed in both experiments.

To test whether it is possible to observe a decrease in anisotropy in a model system, cells expressing TMD-Fv-FP, where FP stands for a fluorescent protein, should be used. In this protein, the fluorescent part is directly followed by the domain (Fv) that forms the dimer upon addition of AP20187. This means that the fluorescent parts are closer together than when SNAP-TMD-Fv is used.

Dimer formation between TMD-Fv fusion proteins might take longer than 5 minutes, so prolonged imaging might tell whether dimerization is much slower than expected.

10.5 Cells expressing EGFR-fluorescent protein fusions

From experiments on MCF-7 cells expressing EGFR-mCherry it can be concluded that no change in anisotropy is observed after addition of EGF. Also from experiments on MCF-7 cells expressing EGFR-

mCitrine no change in anisotropy is observed after the addition of Cetuximab or EGF. The average anisotropy does not depend on the intensity per pixel. From these results the conclusion can be drawn that it is not possible to observe homo-FRET between the used fluorescent proteins, since the fluorescent proteins are too far away for FRET to occur. Using an EGFR-mCitrine fusion protein or a SNAP-EGFR fusion protein which has a smaller amino acid chain between the EGF-receptor and the fluorescent part might solve this problem. This will decrease the distance between the fluorescent parts of the EGFR fusion protein when an EGFR-dimer is formed, such that the FRET efficiency between the fluorescent parts is higher.

As mentioned earlier, a decrease of the temperature at which the cells expressing EGFR are measured, results in clustering of the EGF-receptor. To verify that the distances between the fluorophores that label the EGF-receptors are too far away, anisotropy images should be recorded of cells expressing fluorescently labeled EGFR at environmental temperatures lower than 37°C. If lower anisotropy values are observed when the environmental temperature decreases, clustering of EGF-receptors can be visualized by a decrease in anisotropy due to homo-FRET. This would then yield that the distance between the fluorophores attached to the EGF-receptors is not too large for FRET to occur. This means that for the experiments done at an environmental temperature of 37°C, a different explanation should be found for the fact that no decrease in anisotropy is found after stimulation with EGF.

11 References

- ¹Lakowicz, J.R. (1999), "Principles of Fluorescence Spectroscopy," Kluwer Academic/Plenum, New York.
- ²<http://www.bio.davidson.edu/courses/molbio/molstudents/spring2000/deeb/method.html>, accessed on 10-10-2012
- ³Lue, N., Popescu, G., Ikeda, T., Dasari, R. R., Badizadegan, K., and Feld, M. S. (2006), "Live cell refractometry using microfluidic devices," *Optics Letters*, 31, 2759–2761.
- ⁴Zhang, H., Berezov, A., Wang, Q., Zhang, G., Drebin, J., Murali, R. and Greene, M. I. (2007). "Review series ErbB receptors: from oncogenes to targeted cancer therapies," *Molecules*, 117(8), 2051-2058.
- ⁵Yarden, Y. and Sliwkowski, M. X. (2001), "Untangling the ErbB signalling network," *Nature reviews. Molecular cell biology*, 2(2), 127-137.
- ⁶Rimawi M.F., Shetty P.B., Weiss H.L., Schiff R., Osborne C.K., Chamness G.C., et al. (2010) "Epidermal growth factor receptor expression in breast cancer association with biologic phenotype and clinical outcomes," *Cancer*, 116, 1234-1242.
- ⁷Xue, C., Wyckoff, J., Liang, F., Sidani, M., Violini, S., Tsai, K.-L., Zhang, Z.-Y., et al. (2006). "Epidermal growth factor receptor overexpression results in increased tumor cell motility in vivo coordinately with enhanced intravasation and metastasis," *Cancer research*, 66(1), 192-197.
- ⁸Bae, J. H., Schlessinger, J. (2010), "Asymmetric tyrosine kinase arrangements in activation or autophosphorylation of receptor tyrosine kinases," *Molecules and Cells* 29(5), 443–448
- ⁹Leahy, B. D. J. (2004). "Structure and function of the epidermal growth factor (EGF/ErbB) family of receptors," *Advances*, 68, 1-27.
- ¹⁰Keating, E., Nohe, A., & Petersen, N. O. (2008), "Studies of distribution, location and dynamic properties of EGFR on the cell surface measured by image correlation spectroscopy," *European biophysics journal*, 37(4), 469-481.
- ¹¹Hofman, E. G., Bader, A. N., Voortman, J., Van den Heuvel, D. J., Sigismund, S., Verkleij, A. J., Gerritsen, H. C., et al. (2010), "Ligand-induced epidermal growth factor receptor (EGFR) oligomerization is kinase-dependent and enhances internalization," *The Journal of biological chemistry*, 285(50), 39481-39489.
- ¹²Nico van Belzen, N. van, Rijken, P.J., Hage W.J., Laat S.W. de, Verkleij A.J., Boonstra, J. (1988), "Direct visualization and quantitative analysis of epidermal growth factor-induced receptor clustering," *Journal of Cellular Physiology*, 134(3) 413-420.
- ¹³Bader, A. N., Hofman, E. G., Voortman, J., en Henegouwen, P. M. P. V. B. and Gerritsen, H. C. (2009), "Homo-FRET imaging enables quantification of protein cluster sizes with subcellular resolution." *Biophysical journal*, 97(9), 2613-2622.
- ¹⁴Kozer, N., Henderson, C., Jackson, J. T., Nice, E. C., Burgess, A. W. and Clayton, A. H. a. (2011), "Evidence for extended YFP-EGFR dimers in the absence of ligand on the surface of living cells," *Physical biology*, 8(6), 066002.

- ¹⁵Szabó, A., Horváth, G., Szöllosi, J., and Nagy, P. (2008), "Quantitative characterization of the large-scale association of ErbB1 and ErbB2 by flow cytometric homo-FRET measurements," *Biophysical journal*, 95(4), 2086-2096.
- ¹⁶Nagy, P., Claus, J., Jovin, T. M., and Arndt-Jovin, D. J. (2010), "Distribution of resting and ligand-bound ErbB1 and ErbB2 receptor tyrosine kinases in living cells using number and brightness analysis," *Proceedings of the National Academy of Sciences of the United States of America*, 107(38), 16524-9.
- ¹⁷Kozer, N., Kelly, M. P., Orchard, S., Burgess, A. W., Scott, A. M. and Clayton, A. H. A. (2011), "Differential and synergistic effects of epidermal growth factor receptor antibodies on unliganded ErbB dimers and oligomers," *Biochemistry*, 50(18), 3581-3590.
- ¹⁸Koushik, S. V., Blank, P. S., and Vogel, S. S. (2009), "Anomalous surplus energy transfer observed with multiple FRET acceptors," *PloS one*, 4(11), 8031.
- ¹⁹Luengo Hendriks, C.L., Vliet, L.J. van, Rieger B. and Ginkel, M. van (1999), "DIPimage: a scientific image processing toolbox for MATLAB, Pattern Recognition Group, Department of Applied Physics, Delft University of Technology, <http://www.ph.tn.tudelft.nl/DIPIlib>.
- ²⁰Squire, A., Verveer, P. J., Rocks, O. and Bastiaens, P. I. H. (2004), "Red-edge anisotropy microscopy enables dynamic imaging of homo-FRET between green fluorescent proteins in cells," *Journal of structural biology*, 147(1), 62-69.
- ²¹Ganguly, S., Clayton, A. H. A. and Chattopadhyay, A. (2011), "Organization of higher-order oligomers of the serotonin_{1A} receptor explored utilizing homo-FRET in live cells," *Biophysical journal*, 100(2), 361-368.
- ²²<http://www.invitrogen.com/site/us/en/home/support/Product-Technical-Resources/Product-Spectra.6380ph8.html>, accessed on 10-10-2012
- ²³Gautier, I., Tramier, M., Durieux, C., Coppey, J., Pansu, R. B., Nicolas, J. C., Kemnitz, K., et al. (2001), "Homo-FRET microscopy in living cells to measure monomer-dimer transition of GFP-tagged proteins," *Biophysical journal*, 80(6), 3000-3008.
- ²⁴Swaminathan, R., Hoang, C. P. and Verkman, a S. (1997), "Photobleaching recovery and anisotropy decay of green fluorescent protein GFP-S65T in solution and cells: cytoplasmic viscosity probed by green fluorescent protein translational and rotational diffusion," *Biophysical journal*, 72(4), 1900-1907.
- ²⁵Diamonti, a J., Guy, P. M., Ivanof, C., Wong, K., Sweeney, C. and Carraway, K. L. (2002), "An RBCC protein implicated in maintenance of steady-state neuregulin receptor levels," *Proceedings of the National Academy of Sciences of the United States of America*, 99(5), 2866-2871.
- ²⁶Kremers, G.-J., Gilbert, S. G., Cranfill, P. J., Davidson, M. W. and Piston, D. W. (2011), "Fluorescent proteins at a glance," *Journal of Cell Science*, 124(15), 2676-2676.
- ²⁷http://www.neb.com/nebecomm/tech_reference/gene_expression_cellular_analysis/SNAP_tag_technologies.asp#.UGrL2JgmSYE, accessed on 30-09-2012

²⁸Stöhr, A., (2008), PhD thesis, "Fluoreszenzgelöste Sonden für diagnostische und analytische anwendungen."

²⁹Glover, J. F., Irwin, J. T., Darbre, P. D., Glover, J. F., Irwin, J. T. and Darbre, P. D. (1988), "Interaction of Phenol Red with Estrogenic and Antiestrogenic Action on Growth of Human Breast Cancer Cells ZR-75-1 and T-47-D Interaction of Phenol Red with Estrogenic and Antiestrogenic Action on Growth of Human Breast Cancer Cells ZR-75-1 and T-47-D," *Cancer Research*, 48(13), 3693-3697.

³⁰Kancha, R. K., von Bubnoff, N., Peschel, C. and Duyster, J. (2009), "Functional analysis of epidermal growth factor receptor (EGFR) mutations and potential implications for EGFR targeted therapy," *Clinical cancer research: an official journal of the American Association for Cancer Research*, 15(2), 460-467.

³¹Song, G. J. and Hinkle, P. M. (2005), "Regulated dimerization of the thyrotropin-releasing hormone receptor affects receptor trafficking but not signaling," *Molecular endocrinology*, 19(11), 2859-2870.

³²Patel, D., Lahiji, A., Patel, S., Franklin, M., Jimenez, X., Hicklin, D. J. and Kang, X. (2007). "Monoclonal antibody cetuximab binds to and down-regulates constitutively activated epidermal growth factor receptor VIII on the cell surface," *Anticancer research*, 27(5), 3355-3366.

12 Appendix

This appendix covers the Matlab-functions that were used to calculate the calibrated anisotropy values from the parallel and perpendicular images.

The first function calculates the image alignment parameters from the two fluorescence intensity images of the beads recorded with two cameras. The second function is used to calculate a G-factor image that is used to measure correct anisotropy values. The last function calculates the calibrated parallel and perpendicular intensity images. From these images anisotropy images can be calculated.

```
% Function 1: image alignment
function [out] = imagealignment(data1,data2)

a = dip_image(data1);
b = dip_image(data2);

[zoom, trans, ang] = fmmatch(a,b);

[out,R] = find_affine_trans(a, b, [[zoom,zoom], trans, ang]); % calculate
image alignment factors

[data1out, R] = affine_trans(a,
[out(1,1),out(1,2)], [out(1,3),out(1,4)],out(1,5));

dip_image([b,data1out]) % check alignment
end

% Function 2: G-factor calculation
function [Gout Gout_filter] = dataprocsgfactor(imageloodr,imageevenw,
imageloodrback, imageevenwback, out, rref)

% background correction:

imageevenwbackcor = imageevenw - mean2(imageevenwback);
imageloodrbackcor = imageloodr - mean2(imageloodrback);

% image alignment of G-factor calibration images:

dipimageevenw = dip_image(imageevenwbackcor);
[dipimageevenwshift] = affine_trans(dipimageevenw,
[out(1,1),out(1,2)], [out(1,3),out(1,4)],out(1,5));
evenwshifted = dip_array(dipimageevenwshift);

% calculate and smooth G-factor image

Gout = (evenwshifted*(1-rref))./(imageloodrbackcor*(1+2*rref));
G = fspecial('gaussian',[8 8],3);
Gout_filter = imfilter(Gout,G,'same'); % smoothed G image

end
```

```

% Function 3: calculate anisotropy
function [anisotropy evenwshifted imageloodrbackcor] =
dataprocसानisotropy(imageloodr,imageevenw, imageloodrback, imageevenwback,
out,Gin)

% background correction and

imageevenwbackcor = imageevenw - mean2(imageevenwback);
imageloodrbackcor = Gin.*(imageloodr - mean2(imageloodrback));

% image alignment anisotropy measurement

dipimageevenw = dip_image(imageevenwbackcor);
[dipimageevenwshift, R] = affine_trans(dipimageevenw,
[out(1,1),out(1,2)], [out(1,3),out(1,4)],out(1,5));
evenwshifted = dip_array(dipimageevenwshift);

% calculate anisotropy image

anisotropy = (evenwshifted -
imageloodrbackcor)./(evenwshifted+2.*imageloodrbackcor);
end

```

Acknowledgements

For a year I worked on my graduation assignment in the NanoBioPhysics group. I want to thank my daily supervisor Peter Bosch for his help in getting acquainted with the fluorescence microscope setup and cell culturing protocols. I would also like to thank Hans Kanger and Peter Bosch for the discussions we had on my experiments and data and their feedback on my report. I also thank Vinod Subramaniam for letting me do this assignment in his group. I also want to thank Cees Otto for being the external committee member of my graduation committee. Also thanks to all other members of the NanoBioPhysics group that helped me with my work during my master assignment.

Finally I thank Jenny Ibach and Peter Verveer from the Max-Planck-Institut für Molekulare Physiologie in Dortmund for their feedback and Jenny for the used plasmid DNA.